



Norwegian University  
of Life Sciences

**Master's Thesis 2023 30 ECTS**  
Faculty of Science and Technology

# **Vibration performance of in situ cross-laminated timber (CLT) floors in medium-rise buildings**

**Simen Lysebo Hansen**  
Structural Engineering and Architecture

*The struggle itself toward the heights is enough to fill a man's heart. One must imagine Sisyphus happy.*

Albert Camus (1913–1960)

Nobel laureate in literature



# Acknowledgements

I am grateful for the invaluable support I have received from others, without which this thesis would not have been possible. Their assistance is truly appreciated.

I am tremendously grateful for the guidance and support of my primary supervisor, Professor Ebenezer Ussher. His contributions have been crucial to the completion of this thesis, from developing research questions to setting up testing sites and even in the writing process. Professor Ussher has always been available and willing to discuss my concerns, and I cannot thank him enough.

I would like to express my gratitude to Dr Angelo Aloisio, Dr Dag P. Pasca, and Professor Roberto Tomasi for attending our weekly meetings. Your valuable feedback and constructive criticism have been instrumental in driving the progress of my thesis. I appreciate the time and effort you have dedicated to this project and your willingness to provide answers to my inquiries. Thank you!

I would also like to express my gratitude to the individuals who provided me with various other forms of support throughout my thesis journey. Trond Fjeld Antonsen and the team at Ås High School for granting me access, Dr Xiaojun Gu for spending long nights and weekends assisting with testing, Håkon J. Ålerud of J.I Bygg for providing technical details, and Anette Juveli of RAAD for sharing detailed drawings and information. Your patience and generosity have been invaluable in helping me bring my thesis to fruition.

Ås, May, 2023

Simen Lysebo  
Hansen



## Summary

There is limited information regarding the vibration characteristics of CLT floor systems within superstructures. As designers utilise the excellent strength-to-mass ratio of CLT, they are often faced with a serviceability problem. Due to the relatively low mass-to-stiffness ratio, the system is prone to oscillation, and vibration becomes a major issue. In recent years, there have been a lot of efforts to establish guidelines for distinguishing between acceptable and unacceptable design. However, many of these guidelines do not consider the importance of non-bearing structures. This thesis utilises OMA to highlight how in-situ floors are affected by surrounding elements.

A comprehensive study was conducted on seven floors within Ås High School during the thesis project. In total thirteen distinct tests were carried out to gather field data, which was then analysed to determine modal characteristics. By determining modal characteristics, the effects of in-situ elements are thoroughly documented. Transfer of motion across non-bearing partitions is given special attention to explain detected mode shapes. The distribution of motion is documented through VDV and  $a_{rms}$  contour maps. An analytical component has been incorporated to assess the accuracy of the updated Eurocode 5 in calculating the fundamental natural frequency and root-mean-square acceleration.

The standing assumption that non-bearing partition walls can be ignored during design is challenged. Through detailed in-situ experiments, it becomes clear that they play an essential role in determining the modal characteristics of the floors. It has been found that partition walls have a significant impact on all modal characteristics. The configuration of surrounding partition walls especially impacts the fundamental mode shape. As the CLT floor system is integrated into the superstructure, its complexity rapidly increases, decreasing the number of identifiable modes. Distribution of motion across floors documented with VDV and  $a_{rms}$  is shown to follow low-frequency mode shapes. The consequence is that partition walls play an important role in determining critical acceleration spots. The revised EC5 underestimates the fundamental frequencies performance of the floors while overestimating its  $a_{rms}$  performance. This inaccuracy reduces its effectiveness in discriminating between acceptable and unacceptable design.



## Sammendrag

Det finnes begrenset med informasjon angående vibrasjonsegenskapene til CLT-gulvsystemer installert i konstruksjoner. Ingeniører som ønsker å anvende CLT sin utmerkede styrke til masse forhold støter ofte på et bruksgrensetilstand problem. På grunn av et relativt lavt forhold mellom masse og stivhet blir systemet lett satt i bevegelse og vibrasjoner blir et problem. Helt siden introduksjonen av CLT har det blitt arbeidet med å utforme retningslinjer som skiller mellom akseptabelt og ikke-akseptabelt design. De fleste av disse retningslinjene tar ikke hensyn til betydningen av ikke-bærende konstruksjoner. Denne avhandlingen anvender OMA for å belyse hvordan in-situ gulv blir påvirket av omkringliggende elementer.

Et omfattende studie har blitt utført på syv ulike gulv ved Ås videregående skole i løpet av prosjektperioden. Totalt ble tretten forskjellige tester utført for å samle inn felldata. Innhentede data ble analysert for å bestemme gulvenes vibrasjonsegenskaper og for grundig å dokumentere effekten av in-situ elementer. Overføring av bevegelse på tvers av ikke-bærende skillevegger er gitt spesiell oppmerksomhet for å forklare oppdaget modusformer. Fordelingen av bevegelse er dokumentert gjennom VDV og  $a_{rms}$  kon-turkart. En analytisk del er inkludert for å vurdere hvor nøyaktig oppdatert Eurokode 5 kan forutsi fundamental egenfrekvens og kvadratisk gjennomsnitt for akselerasjon.

Den aksepterte antagelsen om at ikke-bærende skillevegger kan ignoreres i design fasen utfordres. Gjennom detaljerte in-situ eksperimenter er det demonstrert at de har innflytelse på modale egenskaper. Spesielt er modusformen til den fundamentale egenfrekvensen påvirket av omkringliggende skillevegger.

Integrasjon av CLT-gulvsystemer i konstruksjoner øker raskt kompleksiteten, noe som reduserer antall identifiserbare modusformer. Fordeling av bevegelse på gulvet er vist til å følge lav frekvens modusformer via VDV og  $a_{rms}$ . Konsekvensen av dette er at skillevegger spiller en viktig rolle i å bestemme kritiske akselerasjonspunkter. Den reviderte EC5 systematisk undervurderer av gulvenes grunnfrekvenser, mens den overestimerer gulvenes akselerasjons egenskaper. En slik unøyaktigheten reduseres byggekodens egenskap til å skille mellom akseptabelt og ikke-akseptable design.





# Table of Contents

Acknowledgements . . . . .	iii
Summary . . . . .	v
Sammendrag . . . . .	vii
Table of Contents . . . . .	ix
List of Figures . . . . .	xiv
List of Tables . . . . .	xvi
List of Abbreviations and Symbols . . . . .	xvii
<b>1 Introduction</b>	<b>1</b>
1.1 Background . . . . .	1
1.2 Research questions and objectives . . . . .	2
1.3 Thesis outline . . . . .	2
1.4 Limitations . . . . .	3
<b>2 Theory</b>	<b>5</b>
2.1 Vibration response in structures . . . . .	5
2.1.1 Free oscillating system . . . . .	5
2.1.2 Damping . . . . .	6
2.1.3 Forced Damped Vibrations . . . . .	8
2.1.4 Resonant response . . . . .	9
2.1.5 Off-resonant response . . . . .	10
2.1.6 Discrete systems . . . . .	10
2.1.7 Continuous systems . . . . .	11
2.1.8 Global and local properties . . . . .	13
2.1.9 Mode shape for rectangle plates . . . . .	14
2.1.10 Acceleration . . . . .	14
2.2 Excitation from footfall . . . . .	15
2.2.1 Single person impact . . . . .	15
2.2.2 Group Impact . . . . .	17
2.2.3 Continuous forcing functions . . . . .	17
2.3 State-of-the-art . . . . .	19

2.3.1	Introduction . . . . .	19
2.3.2	Literature . . . . .	19
2.4	Codes and standards concerning floor vibration . . . . .	25
2.4.1	ISO 10137:2007 . . . . .	25
2.4.2	ISO 2631-1-1:1997 and ISO 2631-2:2003 . . . . .	25
2.4.3	British Standard BS 6472-1:2008 . . . . .	27
2.4.4	EC5-1-1 EN 1995-1-1:2004 . . . . .	29
2.4.5	EC5-1-1 prEn 1995 -1-1:20xx(E) . . . . .	30
2.5	Cross Laminated Timber . . . . .	32
2.6	Finite Element Software . . . . .	33
2.6.1	Modal Assurance Criterion . . . . .	34
2.7	Operational Modal Analysis . . . . .	34
<b>3</b>	<b>Methodology</b>	<b>37</b>
3.1	Field Tests . . . . .	37
3.1.1	Location . . . . .	37
3.1.2	Areas targeted for testing . . . . .	38
3.1.3	Floors . . . . .	43
3.1.4	Connections . . . . .	43
3.2	Experiment . . . . .	44
3.2.1	Equipment . . . . .	44
3.2.2	Set-up . . . . .	44
3.2.3	Excitation . . . . .	45
3.3	Signal Processing . . . . .	45
3.3.1	Artemis analytical tools . . . . .	46
3.3.2	Determination of modes . . . . .	47
3.3.3	Choosing results . . . . .	47
3.4	Time History Response . . . . .	47
3.5	Analytical results . . . . .	49
3.5.1	Current Eurocode 5 . . . . .	49
3.5.2	Purposed Eurocode 5 . . . . .	50
3.6	Modelling . . . . .	50
3.6.1	Numerical input . . . . .	51
3.6.2	Boundary conditions . . . . .	52
3.6.3	Evaluation of model . . . . .	52
<b>4</b>	<b>Results and discussion</b>	<b>53</b>
4.1	Modal Characteristics . . . . .	53
4.2	Influence of secondary structures . . . . .	64
4.3	Time history response . . . . .	66

4.4	The distribution of VDV . . . . .	70
4.5	Evaluation of analytical results . . . . .	74
4.6	SAP2000 FEM-model . . . . .	76
<b>5</b>	<b>General disucssion</b>	<b>79</b>
5.1	Modal Characteristics . . . . .	79
5.1.1	Detected modes of vibration . . . . .	79
5.1.2	Damping . . . . .	80
5.2	Influence of secondary structure . . . . .	81
5.3	Time history response . . . . .	82
5.4	The distribution of VDV . . . . .	83
5.5	Building codes . . . . .	83
5.6	FEM-modelling . . . . .	84
<b>6</b>	<b>Conclusions and further work</b>	<b>85</b>
	<b>References</b>	<b>87</b>
	<b>Appendix A Sensor grids with partition walls and cabinets</b>	<b>93</b>
	<b>Appendix B Specifications for technical equipment</b>	<b>99</b>
	<b>Appendix C All results calculated for section 4.4</b>	<b>101</b>



# List of Figures

2.1	Dynamic magnification factor for different damping ratios . . . . .	10
2.2	The responses of a system to different frequencies . . . . .	10
2.3	Difference between SDOF and MDOF system . . . . .	11
2.4	Mode shape of a simply supported beam . . . . .	12
2.5	Forcing functions for various activities. . . . .	16
2.6	A breakdown of the total force from aerobics into a series of harmonics through Fourier transformation . . . . .	18
2.7	Scale for evaluating rms-acceleration in joisted timber floors . . . . .	21
2.8	Resonance frequencies of human body organs . . . . .	24
2.9	Base curve for vertical rms-acceleration . . . . .	26
2.10	A human body's basicentric axes . . . . .	26
2.11	Flowchart for vibration verification using cEC5 . . . . .	29
2.12	Flowchart for vibration verification using prEC5 . . . . .	32
2.13	Overview of a 5-layer CLT with axis drawn on . . . . .	33
3.1	An overview map of the school and testing sites . . . . .	37
3.2	Picture of Ås High School . . . . .	38
3.3	Overview picture of 1F Public Area . . . . .	39
3.4	1F Public Area from the BIM-model . . . . .	39
3.5	Overview picture of 2F Multi Span . . . . .	40
3.6	The second level from the BIM-model . . . . .	40
3.7	Overview picture of 3F Classroom . . . . .	41
3.8	The third level from the BIM-model . . . . .	41
3.9	Overview picture of 3F Public Area . . . . .	42
3.10	3F Public Area from the BIM-model . . . . .	42
3.11	Cross-section of constructed floors, acoustic plates are not drawn on. . .	43
3.12	Connection between CLT-elements . . . . .	44
3.13	Connections between CLT and GLT470x585KLT160 . . . . .	44
3.14	Flowchart over data collection . . . . .	45
3.15	Frequency response function analysed with EFDD through Artemis . . .	46

3.16	Frequency response function analysed with SSI through Artemis . . . . .	47
3.17	Flowchart for estimating joint stiffness in FEM model . . . . .	52
4.1	The fundamental mode of 2F Multi Span H overlaid on structures . . . . .	64
4.2	The fundamental mode of 2F Multi Span 2 H overlaid on structures . . . . .	64
4.3	The fundamental mode of 3F Classroom H overlaid on structures . . . . .	65
4.4	The fundamental mode of 3F Multi Span H overlaid on structures . . . . .	65
4.5	The fundamental mode of 3F Single Span H W overlaid on structures . . . . .	66
4.6	The fundamental mode of 3F Single Span H overlaid on structures . . . . .	66
4.7	Histogram for 1F Public Area VDV . . . . .	71
4.8	Histogram of 2F Multi Span 2 H VDV . . . . .	71
4.9	Histogram of 3F Multi Span H VDV . . . . .	71
4.10	1F Public Area VDV-contour . . . . .	72
4.11	1F Public Area H $a_{rms}$ -contour . . . . .	72
4.12	2F Multi Span 2 H VDV-contour . . . . .	73
4.13	2F Multi Span 2 H $a_{rms}$ -contour . . . . .	73
4.14	3F Multi Span H VDV-contour . . . . .	73
4.15	3F Multi Span $a_{rms}$ -contour . . . . .	73
4.16	Empirical distribution of VDV . . . . .	74
5.1	Example of the resolution of the sensor grid . . . . .	79
5.2	Heel drops being performed at 1F Public Area . . . . .	82
A.1	Test setup for 1F Public Area . . . . .	94
A.2	Test setup for 2F Multi Span . . . . .	94
A.3	Test setup for 2F Multi Span 2 . . . . .	95
A.4	Test setup for 2F Single Span . . . . .	95
A.5	Test setup for 3F Public Area . . . . .	96
A.6	Test setup for 3F Multi Span . . . . .	96
A.7	Test setup for 3F Classroom . . . . .	97
A.8	Test setup for 3F Single Span . . . . .	97
A.9	Test setup for 3F Single Span Wall . . . . .	98
A.10	Test setup for 1F Public Area Walk . . . . .	98
C.1	Acceleration values for 1F Public Area H . . . . .	101
C.2	Acceleration values for 2F Multi Span v2 H . . . . .	102
C.3	Acceleration values for 3F Multi Span H . . . . .	103

# List of Tables

2.1	Recommended damping ratios for mass timber floor . . . . .	7
2.2	System definition from critical and viscous damping ratio . . . . .	8
2.3	Typical modes of rectangular plates with all sides supported . . . . .	14
2.4	Ratios between rms - and peak acceleration for different waveform . . . . .	15
2.5	Examples of expected walking frequencies depending on usage . . . . .	16
2.6	Recommended coordination factors $C(N)$ for $N$ number of people . . . . .	17
2.7	Probability of adverse commend for different VDV ranges . . . . .	28
2.8	Floor performance levels according to revised EC5 . . . . .	31
3.1	Material properties for Splitkon T22-lamella . . . . .	49
3.2	Summation of floors material properties . . . . .	50
3.3	Sintef calculated modulus . . . . .	51
3.4	Properties of SAP200 layered section . . . . .	51
4.1	Overview of selected tests cases for results and discussion section . . . . .	53
4.2	Modal Characteristics of 1F Public Area H . . . . .	54
4.3	Modal Characteristics of 2F Multi Span H . . . . .	55
4.4	Modal Characteristics of 2F Multi Span 2 H . . . . .	56
4.5	Modal Characteristics of 2F Single Span H . . . . .	57
4.6	Modal Characteristics of 3F Multi Span H . . . . .	58
4.7	Modal Characteristics of 3F Classroom H . . . . .	60
4.8	Modal Characteristics of 3F Single Span H . . . . .	61
4.9	Modal Characteristics of 3F Single Span H W . . . . .	62
4.10	Modal Characteristics of 3F Public Area H . . . . .	62
4.11	Overview of all EFDD and SSI-Merged frequencies and damping values derived from heel drop tests . . . . .	63
4.12	Time history from 1F Public Area . . . . .	67
4.13	Time history from 2F Multi Span . . . . .	68
4.14	Time history from 3F Classroom . . . . .	69
4.15	Time history from 3F Public Area . . . . .	70
4.16	Statistical analysis of VDV results for different floors . . . . .	71



4.17 Measured fundamental frequency compared with values calculated with cEC5 . . . . .	74
4.18 Measured fundamental frequency compared with values calculated with prEC5 . . . . .	75
4.19 Measured rms-acceleration compared with values calculated with prEC5 .	76
4.20 Simulated floor model in SAP2000 . . . . .	76
4.21 Results from iterative adjusting of joint stiffness. . . . .	77
5.1 Modal damping values found through testing . . . . .	80

# List of Abbreviations and Symbols

## Acronyms

AISC	American Institute of Steel Construction
BIM	Building Information Model
BIPM	Bureau international des poids et mesures
BSI	British Standard Institute
cEC5	Current NS-EN 1995 Eurocode 5: Design of timber structures
CEN	Comité Européen de Normalisation
CFDD	Curve-fit Frequency Domain Decomposition
CLT	Cross Laminated Timber
DMF	Dynamic Magnification Factor
EC	European Commission
ECDF	Empirical Cumulative Distribution Function
EFDD	Enchanted Frequency Domain Decomposition
EOM	Equation of motion
EWP	Engineered Wood Product
FDD	Frequency Domain Decomposition
FEA	Finite Element Analysis
FEM	Finite Element Model
GLT	Glue Laminated Timber
IPCC	Intergovernmental Panel on Climate Change
ISO	International Organization for Standardization
LVL	Laminated Veneer Lumber
MAC	Modal Assurance Criterion
MDOF	Multi Degrees of Freedom

MSF	Modal Separation Factor
NSB	National Standardisation Body
OMA	Operational Modal Analysis
prEC5	Purposed NS-EN 1995 Eurocode 5: Design of timber structures
rms	Root-mean-square acceleration
SDOF	Single Degree of Freedom
SLS	Serviceability Limit State
SPM	Steps per Minute
SSI	Stochastic Sub-space Identification
VDV	Vibration Dose Value

### Greek Symbols

$\alpha_{n,v}$	Numerical coefficient corresponding to the $n$ -harmonic, vertical direction
$\beta$	Frequency ratio
$\mu_n$	Maximum amplitude of $n$ -mode
$\mu_n(x)$	Unity normalised amplitude at position $x$
$\Omega$	Forcing frequency [ $Hz$ ]
$\omega$	Angular velocity [ $rad/s$ ]
$\omega_d$	Damped angular velocity [ $rad/s$ ]
$\omega_n$	Natural circular frequency [ $rad/s$ ]
$\phi$	Phase angle
$\phi_n$	Phase angle of $n$ -mode
$\phi_{n,v}$	Phase angle of the $n$ -harmonic, vertical direction
$\sigma_0$	Ohlsson's damping coefficient
$\zeta$	Damping ratio
$\{\phi_A\}$	Simulated displacement vector
$\{\phi_X\}$	Real measured displacement vector

### Other Mathematical Symbols

$y_p(t)$	Steady-state response [ $m$ ]
$\dot{y}(t)$	Velocity dependent on time [ $m/s$ ]

$\mathbf{C}\dot{\mathbf{y}}(t)$	Damping matrix for MDOF systems [ $Ns/m$ ]
$\mathbf{K}\dot{\mathbf{y}}(t)$	Stiffness matrix for MDOF systems [ $N/mm^2$ ]
$\mathbf{M}\ddot{\mathbf{y}}(t)$	Mass matrix for MDOF systems [ $kg$ ]
$a_i$	Acceleration [ $m/s^2$ ]
$a_{peak}$	Peak acceleration [ $m/s^2$ ]
$a_{rms}$	Root-mean-squared acceleration [ $m/s^2$ ]
$a_{w,rms}$	Frequency weighted root-mean-square acceleration [ $m/s^2$ ]
$c_{cr}$	Critical damping coefficient
$D_{n,h}$	Dynamic magnification factor for $h$ -mode
$E_0$	Modulus of elasticity parallel to the grain [ $N/mm^2$ ]
$E_{90}$	Modulus of elasticity perpendicular to the grain [ $N/mm^2$ ]
$E_{mean}$	Mean modulus of elasticity [ $N/mm^2$ ]
$F(t)_N$	Reduced total force according to ISO10137 [ $N$ ]
$F(x, t)$	Forcing function dependent on time and space
$F_0$	Excitation force [ $N$ ]
$F_d$	Damping force [ $N$ ]
$F_T$	Total force produced by a moving group [ $N$ ]
$F_v(t)$	Force produced by walking express in Fourier sets [ $N$ ]
$G_0$	Shear modules parallel to the grain [ $N/mm^2$ ]
$G_{90}$	Shear modules perpendicular to the grain [ $N/mm^2$ ]
$k_{res}$	Factor accounting for higher modes contribution to $a_{rms}$
$m(x, y)$	Distributed mass at specified point (x,y)
$M^*$	Modal mass [ $kg$ ]
$M_n$	Equivalent SDOF mass as n-mode modal mass [ $kg$ ]
$T_d$	Period of a damped oscillation [ $s$ ]
$T_n$	Period of a undamped oscillation [ $s$ ]
$t_{max}$	Time for maximum velocity [ $s$ ]
$u_n$	Maximum amplitude of n-mode
$v_m(x, y, t_{max})$	Velocity at specified point (x,y) at $t_{max}$
$w_n(x, t)$	Displacement at a given time and space
$y_h(t)$	Damped free vibration response [ $m$ ]
(t)	Acceleration dependent on time [ $m/s^2$ ]
a(x,t)	Acceleration at specified point (x,y)

c	Viscous damping coefficient [ $Ns/m$ ]
C(N)	Recommended coordination factor according to IOS10137
E	Modules of elasticity [ $N/mm^2$ ]
EI	Flexural rigidity [ $N/mm^3$ ]
F	Force [ $N$ ]
f	Frequency component of repetitive loading [ $Hz$ ]
G	Shear modules [ $N/mm^2$ ]
h	the $h$ -harmonic
I	Second movement of area [ $mm^4$ ]
k	Stiffness [ $n/mm$ ]
k	The number of harmonics that characterise the forcing function
KE	Kinetic energy [ $J$ ]
L	Total length [ $m$ ]
m	Mass [ $kg$ ]
n	The integer designating harmonics of the fundamental frequency
Q	Static load from a person walking [ $N$ ]
T	Period of a oscillation [ $s$ ]
t	time [ $s$ ]
w	Displacement of beam [ $m$ ]
x	Specified position
y(t)	Displacement dependent on time [ $m$ ]

# 1. Introduction

## 1.1 Background

Cross-laminated timber or CLT is a relatively new product in construction; it received its first European Technical Approval (ETA) in 2006 (Brandner, 2013). It has since seen wider adoption because of its more environmentally friendly profile compared to common construction materials like reinforced concrete (Hildebrandt et al., 2017). According to IPCC 2022, the use of steel and concrete in the construction industry worldwide produced 12  $GtCO_2$  in 2019, both directly and indirectly. The world's total emission was  $59 \pm 6.6$ , making steel and concrete responsible for between 22-18 % of the total world's emission (IPCC, 2022).

When possible, replacing reinforced concrete with CLT comes with a twofold reduction in  $CO_2$ . First is a less carbon-intensive production phase and less intrusive extraction processes. A CLT slab has a 75 % lower  $CO_2$  footprint than a similar slab of reinforced concrete (Oh et al., 2023). Second is wood's natural ability to extract  $CO_2$  from the air and store just the carbon atom. The amount of carbon stored in the wood varies between species but is usually in the 700-1000  $kg/m^3 CO_{2,eq}$  range (Dovetail, 2013).

As an engineered wood product, CLT has seen drastic improvements with time, achieving improved properties in air permeability, thermal energy and safety. Wood is also considered a sustainable material because of its recyclability, reusability and natural renewability. CLT's ability for prefabrication can lead to quicker construction, saving money and reducing inconvenience to nearby residents.(Bazli et al., 2022).

When designing CLT structures, the governing requirement is Serviceability Limit State or SLS (Hamm et al., 2010). CLT has a low modal mass-to-stiffness ratio, making it susceptible to oscillation. While this problem has a long research history, no definite evaluation criteria have been developed (Ebrahimpour and Sack, 2005) (Weckendorf et al., 2016). (Ussher et al., 2022).

If engineers want to design with minimal excess material and promote CLT in the building industry, the dynamic response in structural elements must be understood.

## 1.2 Research questions and objectives

Understanding the modal characteristics of CLT floor systems within a superstructure becomes increasingly important as the construction material sees increased adoption. Research and development have determined that the governing requirements are serviceability limit state. Further in-situ testing is needed to fully realize the benefits of engineered wood products. Currently, design criteria for timber floor vibrations are largely been formulated on the characteristics of isolated laboratory floors rather than real-world conditions.

This thesis will answer the following research questions:

1. How are non-bearing structures impacting the modal characteristics of a CLT floor system, are there changes to the natural frequencies, damping and mode shapes?
2. How is the distribution of motion across a CLT floor influenced by surrounding non-bearing structures?
3. Which of VDV and  $a_{rms}$  contour maps are best matched to the superposition of detected low-frequency mode shapes?

This thesis strives to contribute to existing floor vibration research by conducting detailed in-situ experiments. Its main scientific contributions are:

- The documentation of vibration characteristics of in-situ CLT floor systems.
- Data concerning the transfer of motion across non-bearing and bearing structures.
- A comparison between VDV and  $a_{rms}$  ability to represent the superposition of low-frequency modes.

## 1.3 Thesis outline

This thesis is outlined in standard IMRaD formatting with an added chapter for theory.

### *Chapter 2: Theory of vibrations*

The chapter introduces the theory of vibration, a state-of-the-art survey and an overview of building codes. The theory of vibration is centred around the different forms of excitation and how the medium for vibration reacts to them. State-of-the-art is a literature review of the current research into floor vibrations. Building codes and standards covered are ISO 10137, ISO 2631 and current and revised Eurocode 5. An introduction to CLT, FEM-modelling and OMA is also included to support chapter 3.

*Chapter 3:Methodology*

The chapter outlines the various techniques and tools the thesis utilises to gather and analyse data. It also gives an overview of the sites used for field testing. The structure used in the chapter is followed in chapter 4 and 5 so that the reader can easily navigate.

*Chapter 4:Results*

The chapter presents the various results procured through methods described in chapter 3. Under each result is a discussion of that specific result and its broader meaning for the thesis. The decision to include discussion in the result chapter was made since a large number of results are presented.

*Chapter 5:General discussion*

The chapter contains a general discussion of results gathered across all tests, presenting general findings and discussing their importance.

*Chapter 6:Conclusions and further work*

The chapter is a synthesised version of chapter 4 and 5 summarising the conclusions into bullet points. Recommendations for further research are also included in the chapter.

## 1.4 Limitations

As stated in the introduction, the science of floor vibration is highly complex, especially in newer materials like CLT and complex in-situ environments. Limitations must be imposed on the thesis so that work can be completed in the allotted time. While a general theory of vibrations is presented, only CLT gets attention as a medium. Only vibrations created by human structure interaction were considered, and only in the vertical direction. The effects of floor vibrations were only assessed in terms of human discomfort without considering any potential long-term harm to structures, machines, or processes.

Since the amount of testing possible was constrained by time, a decision was made to perform a detailed measurement in a single structure instead of a series of different structures. Only measuring one building limits the possibility of drawing broad conclusions across different buildings.





## 2. Theory

This chapter will outline the necessary theory for understanding the research questions, discussion and drawn conclusions. For a general understanding of vibration theory, it will rely on Chopra (Chopra, 2019). For floor-specific and other technical background details, Smith and Weckendorf are used (Smith et al., 2007) (Weckendorf, 2009). Other works are cited and used regarding specific standardisation, wood-specific theory and other details. Floor vibration is a complex mathematical and empirical problem, so the focus will be narrow. Only walking and running are given attention as excitation force, wood is the only specific medium and only SLS consequences are considered.

### 2.1 Vibration response in structures

#### 2.1.1 Free oscillating system

A system undergoes vibrations after being disturbed from its static equilibrium position by an initial displacement or external force (Chopra, 2019). The disturbance will create a simple harmonic oscillation as the system returns to its equilibrant force position should damping be a part of the system. If no damping is assumed, the system will continue to vibrate constantly, and the vibration is classified as free undamped oscillation. A free undamped oscillating system is impossible in practice but forms the basis for understanding the theory of vibration. According to D'Alembert's principle, a dynamic problem can be solved statically at any specific time. The sum of all forces is equal to zero by the introduction of an inertia force upholding a dynamic equilibrium (Crépel, 2005). The system can be expressed mathematically through Eqs (2.1) and (2.2).

$$F = -ky(t) \tag{2.1}$$

$$F = m\ddot{y}(t) \tag{2.2}$$

*Hooke's law* Eq (2.1) is applicable when the system remains linear-elastic and shows that created force is proportional to the system's displacement and stiffness. The created

force is a restoring force acting opposite to the displacement and brings the system back to equilibrium. The force is created by system properties like tension, compression, and shear or global properties like gravity (Pain, 2005). *Newton's second law of motion* Eq (2.2) related the created restoring force to acceleration. If the equations are set as equal one develops an Equation of Motion (EOM) (2.3a).

$$m\ddot{y}(t) + ky(t) = 0 \quad (2.3a)$$

$$\ddot{y}(t) = -\frac{k}{m}y(t) \quad (2.3b)$$

$$\ddot{y}(t) = -\omega_n^2 y(t) \quad (2.3c)$$

The system's natural frequencies are critical when determining a system's response to an external excitation and should be the first step. The relationship between excitation and fundamental natural frequency is further explored in section 2.1.4. Factor  $\omega$  is therefore often expressed in a simplified form; see Eq (2.4).

$$\omega_n = \sqrt{\frac{k}{m}} \quad (2.4)$$

The frequency is expressed in hertz [Hz], its SI-Unit for most practical applications (BIPM, 2019) . A transformation is necessary to translate between the different notations. Since hertz represents the number of cycles per second, the relationship between  $\omega$  and  $f$  is represented through Eq (2.5). The time between peaks, commonly called period, is also often used in vibration analysis and is expressed in Eq (2.6).

$$f = \frac{\omega_n}{2\pi} \quad (2.5)$$

$$T = \frac{1}{f} = \frac{2\pi}{\omega_n} \quad (2.6)$$

## 2.1.2 Damping

Free undamped oscillating systems form the basis of vibration theory, even when all real-world structures have some levels of damping. Damping is the dissipation of energy in a system undergoing vibrations. It enables the decay of motion and restores the structure to its original equilibrium position (Chopra, 2019). It is the conversion of mechanical energy to another form inaccessible for vibration (Mårtensson and Crocetti, 2022). In ex-situ experiments, the main source of damping is thermal effects from repeated elastic strain and internal friction. In the real world, a wide range of different mechanisms contribute to a total damping effect. Since accounting for each source individually is

impractical, an idealised *equivalent viscous damping* is often developed. Damping differs from mass and stiffness in that it is an inherent property of the system that can not be calculated with dimensions. To develop a viscous damping coefficient  $c$ , vibration experiments are necessary. The value is, therefore empirical and it is common to apply a generalised value in the design phase (Chopra, 2019). Empirically developed damping for mass timber floors is presented in Table 2.1

**Table 2.1:** Recommended damping ratios for mass timber floor(Wood Works, 2023)

Damping Category	Damping ratio ( $\zeta$ )	Range
Lightly	1-2%	Completely bare mass timber floors to mass timber floors with concrete topping and furniture.
Moderately	2-4 %	TCC or CLT slabs with floating concrete and furniture to floors designed with mechanical systems and raised or floating floor layers.
Heavily	4-5 %	Represents the higher end of damping introduced through design and includes the addition of partition walls, suspended ceilings, etc.
Explicit control	5%+	It is common for mass timber floors to have at most 5 % without explicit damping control. Higher damping requires the introduction of tools like a tuned mass damper.

Damping influences the rate of decay in a free-vibrating system and the magnitude of the amplitude if the system experiences forced vibrations. Eq (2.7) is applicable in a linear-elastic system and is used to calculate the damping force. The force is proportional to the system's velocity and always acts in the opposite direction.

$$F_d = -c\dot{y}(t) \quad (2.7)$$

Adding Eq (2.7) to the equation of motion developed in Eq (2.3a) gives the EOM for a damped oscillating system. Eq (2.8a) gives the displacement of a linear-elastic idealised system with no external force. A common algebraic transformation is normalising with the mass and expressing the viscous damping coefficient with damping ratio and fundamental natural frequency. The result of these transformations are shown in Eq (2.8b) and is achieved with Eqs (2.9a) and (2.9b)

$$m\ddot{y}(t) + c\dot{y}(t) + ky(t) = 0 \quad (2.8a)$$

$$\ddot{y}(t) + 2\zeta\omega_n\dot{y}(t) + \omega_n^2y(t) = 0 \quad (2.8b)$$

$$\zeta = \frac{c}{2m\omega_n} = \frac{c}{c_{cr}} \quad (2.9a)$$

$$c_{cr} = 2m\omega_n = 2\sqrt{km} = \frac{2k}{m} \quad (2.9b)$$

Factor  $c_{cr}$ , critical damping, is the dividing line between an oscillating and non-oscillating system. The smallest value of damping that would prohibit oscillatory behaviour. It is individual for every system and used to classify the type of damping inherent in the system. Table 2.2 show how to classify a system in regard to the relationship between viscous damping and critical damping. Buildings typically have a damping ratio of less than 10 %. This thesis is therefore primarily concerned with underdamped systems (Chopra, 2019)(Jarnerö et al., 2015).

**Table 2.2:** System definition from critical and viscous damping ratio

Category	Criteria	Description
Underdamped system	$c \leq c_{cr}$	Oscillation occurs until damping has dissipated all energy
Overdamped systems	$c \geq c_{cr}$	After an initial displacement the motion exponentially travels toward equilibrium position
Critically damped system	$c = c_{cr}$	The decay of the oscillation happens at the fastest possible rate.

The introduction of damping to the system will affect the angular velocity and reduce it with a factor. Eq (2.10) shows the conversion of natural angular velocity to damped angular velocity. As a consequence, the period between peaks will be reduced.

$$\omega_D = \omega_n \sqrt{1 - \zeta^2} \quad (2.10)$$

How to develop a general solution for the free damped vibrations equation developed in Eq (2.8a) can be found in literature, only the final step is presented in Eq (2.11) . Factor A and B are constants that need to be determined through initial know conditions (Chopra, 2019).

$$y(t) = e^{-\zeta\omega_n t} (A \cos \omega_D t + B \sin \omega_D t) \quad (2.11)$$

### 2.1.3 Forced Damped Vibrations

Previous equations of motions developed assumed no external force after the first initial displacement. The introduction of a harmonic excitation force to a damped oscillating system produces forced damped vibrations. The vibrations can be expressed with Eq (2.12), the harmonic excitation represented as  $F_0 \sin(\Omega t)$ .

$$m\ddot{y}(t) + c\dot{y}(t) + k(t) = F_0 \sin(\Omega t) \quad (2.12)$$

Any solution to Eq (2.12) will contain a homogeneous solution and a particular solution while the solution is inhomogeneous. The homogeneous solution is transient and will over time decay exponentially and become negligible. The particular solution is steady-state and exists as long as the system is excited by the external force. With time the transient response will decay to a point where only the steady-state response remains,

but the biggest deformations happen while the transient response still exists (Chopra, 2019).

$$y(t) = \underbrace{y_h(t)}_{\text{Damped free vibration response}} + \underbrace{y_p(t)}_{\text{Steady-state response}} \quad (2.13)$$

### 2.1.4 Resonant response

Evaluating displacement is done through the dynamic magnification factor, sometimes called the dynamic response factor. DMF is the ratio between the peak amplitude induced by vibrations and the static amplitude created by a load. Response induced in each mode of vibration is governed by Eq (2.14), which is part of the particular solution Eq (2.16).

$$D_{n,h} = \frac{h^2 \beta^2}{\sqrt{(1 - h^2 \beta_n^2)^2 + (2h\zeta\beta_n)^2}} \quad (2.14)$$

The ratio between the forcing function  $\Omega$  and natural frequencies of the system  $\omega$  is the deciding factor for when resonance occurs. As the frequency ratio  $\beta$  defined in Eq (2.15) approaches 1 the dynamic magnification factor increases exponentially. Since  $\beta$  is the ratio between forcing frequency and natural frequency, a ratio of 1 means the two frequencies converge.

$$\beta = \frac{\Omega}{\omega} \quad (2.15)$$

Figure 2.1 is a graphical overview of the interaction between dynamic magnification factor and frequency ratio. Since structures have a low damping ratio, controlling the frequency ratio is essential to avoid large deformations (Chopra, 2019). As the frequency ratio converges to 1 there is a spike in the dynamic magnification factor constrained by the damping ratio. If the damping ratio  $\zeta$  is equal to 0 and the frequency ratio  $\beta$  equals 1 a discontinuity is created (Gil-Martín et al., 2012).

Substituting Eqs (2.11) and (2.16) into Eq (2.13) gives the final total response. Displacement at any time is a combination of the transient response and steady-state response, expressed in Eq (2.17)

$$y_p(t) = \frac{F_0}{k} \cdot D_{n,h} \sin(\Omega t - \phi) \quad (2.16)$$

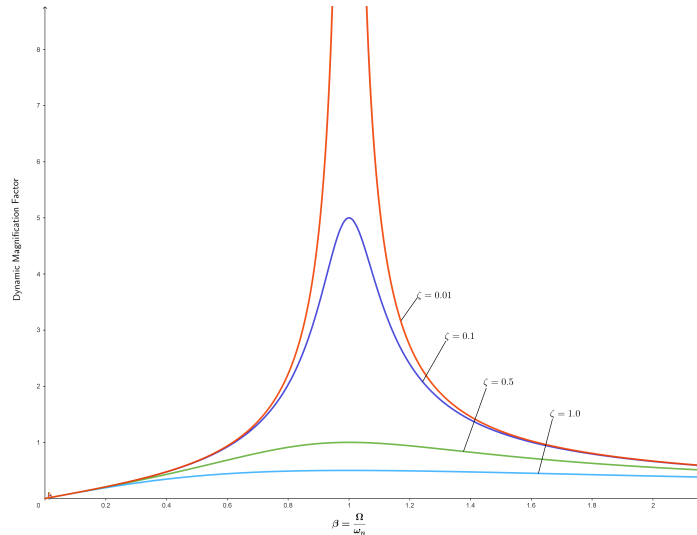


**Figure 2.1:** Dynamic magnification factor for different damping ratios

$$y(t) = e^{-\zeta\omega_n t} (A \cos \omega_D t + B \sin \omega_D t) + \frac{F_0}{k} \cdot D_{n,h} \sin(\Omega t - \phi) \quad (2.17)$$

### 2.1.5 Off-resonant response

A vibration system can have different steady-state responses depending on the excitation frequency. Figure 2.2 is an example of a system exposed to a range of different frequencies. Each peak is a resonance response as explored through Figure 2.1 and corresponds with different natural frequencies in the system. Between each peak an off-resonant response occurs, and while smaller than the peaks it is not insignificant.

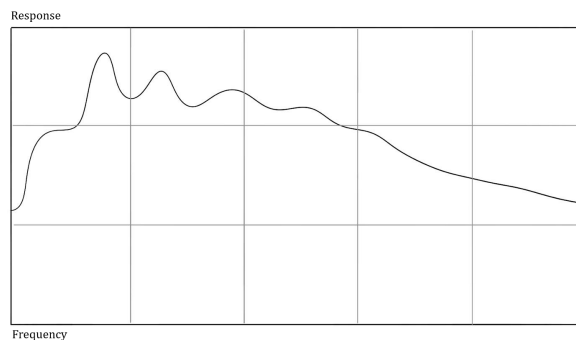


**Figure 2.2:** The responses of a system to different frequencies

### 2.1.6 Discrete systems

A vibration problem is usually centred around the motion of masses. Vibration models are therefore categorised as either discrete or continuous systems. In a discrete vibration system, each mass moves independently from other masses. A discrete model consists

of point masses, springs and dampers, each linked in a matrix. Acceleration, velocity and displacement stemming from external forces are determined by solving the matrix equations (Smith et al., 2007).

Single degree of freedom systems (SDOF) is the simplest form of a discrete system with only one mass. Formulas and methods for solving the system are discussed in previous sections 2.1.1 to 2.1.5. Real structures have more than one degree of freedom and are therefore classified as Multiple degrees of freedom systems (MDOF). MDOF is vastly more complex to analyse than SDOF, but they are linked together since the linear superposition of several SDOF characteristics represents an MDOF system (Ewins, 1984). A visual representation of the difference between an SDOF system and an MDOF system is provided in Figure 2.3

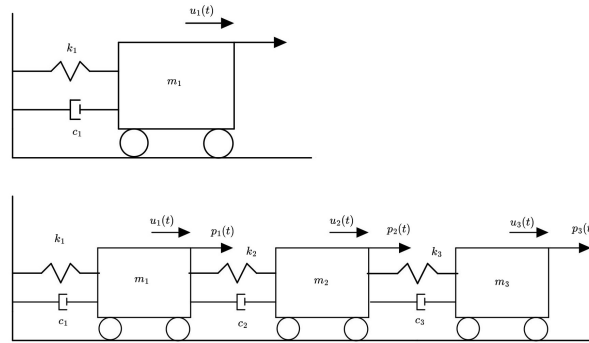


**Figure 2.3:** Difference between SDOF and MDOF system

Eq (2.18) express an MDOF with an  $n$ -degree of freedom through vectors assembled in a matrix formation. Further manipulation and solutions to the system fall outside of this thesis.

$$\mathbf{M}\ddot{\mathbf{y}}(t) + \mathbf{C}\dot{\mathbf{y}}(t) + \mathbf{K}\mathbf{y}(t) = \mathbf{f}(t) \quad (2.18)$$

### 2.1.7 Continuous systems

Unlike a discrete system where each mass is considered independently, a continuous system has all considered masses linked. Beams and floor structures under bending fall under this classification. Continuous systems can be solved either through the integration of continuous functions or discretisation with Finite Element Analysis (FEA). Eq (2.19) is the governing continuous function for a beam in bending. It connects the system's properties (stiffness, mass) to the system's behaviour (displacement, velocity and acceleration) at a specified point in time and space.

$$m \frac{\partial^2 w}{\partial t^2} + EI \frac{\partial^4 w}{\partial x^4} = F(x, t) \quad (2.19)$$



### Mode shapes

Figure 2.2 display that every system has a multiple of natural frequencies higher than the fundamental frequency. Each of these frequencies corresponds to a mode of vibration in the continuous system. The simplest mode shape corresponds to the fundamental frequency and is called the first mode. Each subsequent mode adds a half-sine wave to the deformation. Figure 2.4 visually represents mode shapes one to three for a simply supported beam. Each mode has been normalised with a non-dimensional amplitude of 1 (Smith et al., 2007).

Eq (2.20) is the mathematical expression for developing mode shapes of a uniform beam. The function lets one decide the  $n$ -th mode shape at a specified  $x$ -position.

$$\mu_n(x) = \sin \frac{n\pi x}{L} \quad (2.20)$$

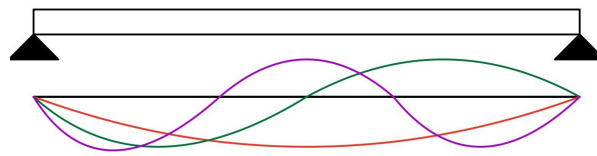


**Figure 2.4:** Mode shape of a simply supported beam

### Modal superposition

Eq (2.21) expresses a uniform beam's response to a sinusoidal forcing function. Each mode is a part of the total displacement of the system, however determining actual displacement is possible by superimposing all modes. Theoretically, an infinite number of modes exist. Depending on the system, the significance falls sequentially and only the first couple of modes are necessary.

$$w_n(x, t) = \sum_{n=1}^{\infty} u_n \sin 2\pi ft + \psi_n \sin \frac{n\pi x}{L} \quad (2.21)$$

### Modal mass

Modal mass is the amount of mass involved in a mode shape and corresponds to the amount of kinetic energy in the system. In expressing a continuous system as a series of discrete SDOF systems the point mass considered is the modal mass. Determining the modal mass for each is necessary and possible by the equation for maximum kinetic energy. Eq (2.22) correlates the kinetic energy needed to move an SDOF-system and a continuous system. A large modal mass means more kinetic energy is needed to excite the mode and is a method for analysing how much the mode will contribute to overall displacement. Element comprised of wood has a relatively low modal mass compared

with concrete, reducing the necessary energy. From a reduction in energy, it follows that the system is easier to excite and will experience more vibration problems (Smith et al., 2007).

$$KE = \frac{1}{2} M_n \nu_n(t_{max})^2 = \frac{1}{2} \int_{x_{min}}^{x_{max}} \int_{y_{min}}^{y_{max}} \nu_n(x, y, t_{max})^2 m(x, y) dy dx \quad (2.22)$$

### 2.1.8 Global and local properties

When solving a vibration problem the modal frequencies and viscous damping coefficient are the global properties, valid at any point in the system. A mode shape corresponding to a modal frequency reflects a relative deflection and might be impacted by local properties. Total displacement is the superposition of all mode shapes, but when the excitation frequency is close to a natural frequency the corresponding mode shape will dominate the final results. Random excitation randomises the contribution from each mode shape (Døssing, 1988).

Buildings are lightly damped and one can expect normal modes to occur. Normal modes have a phase angle  $\phi$  at either  $0^\circ$  or  $180^\circ$ , meaning movement is either in-phase or out-of-phase (Chopra, 2019). All sinusoidal waves will also travel through a fixed nodal point at the end and start of the building. Complex modes are different in that any phase angle  $\phi$  is possible and there is no fixed nodal point. Complex modes occur in structures with high localised damping (Døssing, 1988).

The phase angle measures the response lag between displacement and excitation force. It can be evaluated with Eq(2.23) and depends on the ratio between excitation frequency and fundamental natural frequency.

$$\tan(\phi) = \frac{2\zeta\beta}{1 - \beta^2} \quad (2.23)$$

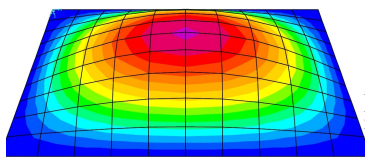
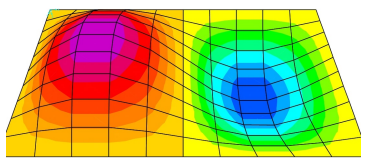
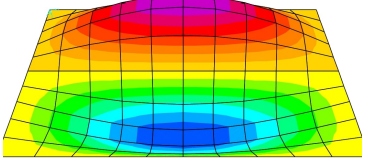
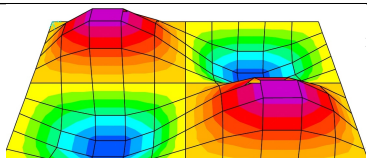
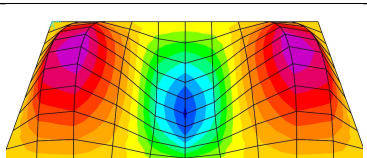
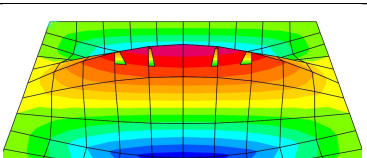
- $\phi \ll 1$  means  $\phi$  approaches  $0^\circ$  and displacement follow applied force, this means it is in-phase.
- $\phi \gg 1$  means  $\phi$  approaches  $180^\circ$  and displacement is opposite the applied force, this means it is out-of-phase.
- $\phi = 1$  means  $\phi$  is  $90^\circ$  and max displacement occurs when the forcing function equals zeros.

### 2.1.9 Mode shape for rectangle plates

Mode shapes described in previous sections and shown in Figure 2.4 rely on a simply supported beam to describe the theory. Floors primarily resemble plates and have mode shapes in both transverse and longitudinal directions. There are 21 different boundary configurations for a plate, each with its governing equation. Presented in Leissa are 20 different equations for approximating each mode shape. For a rectangle plate the node lines will be straight, running through the centre of the plate between opposite edges. Mode shapes for rectangular plates can not share the same frequency, but there is a possibility for shared frequency in square plates (Leissa, 1969). Node lines can be seen in Figure 2.3 as the straight lines not displaced by the mode.

In order to accurately simulate mode shapes individual stiffness should be applied to each orthogonal direction rather than calculating one equal stiffness. This produces more accurate mode shapes and frequencies (AISC, 2016).

**Table 2.3:** Typical modes of rectangular plates with all sides supported

Mode 1,1	Mode 2,1	Mode 1,2
		
Mode 2,2	Mode 3,1	Mode 1,3
		

### 2.1.10 Acceleration

A common value for evaluating vibration levels is the acceleration of the floor. Per definition, acceleration is the second differential of displacement with respect to time. Eq (2.24) is derived from Eq (2.21) and represents acceleration for a simply-supported beam (Smith et al., 2007).



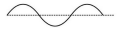
$$a(x, t) = \sum_{n=1}^{\infty} -4\pi^2 f_n^2 u_n \sin(2\pi f_n t + \phi_n) \sin\left(\frac{n\pi x}{L}\right) \quad (2.24)$$

Acceleration is often represented either through its peak or root-mean-square value. Peak acceleration or  $a_{peak}$  is the largest acceleration the system experiences, but time is not a factor. Root-mean-square acceleration or  $a_{rms}$  indicate how long a system is

experiencing an amount of acceleration (Smith et al., 2007). Figure 2.4 gives a graphical overview of different acceleration forms, and Eq (2.25) provides the standard way of calculating rms-acceleration. A more advanced method for calculating rms-acceleration is done by applying a weight for different frequencies creating weighted root-mean-square acceleration  $a_{w,rms}$ . This is covered more in section 2.4.2.

$$a_{rms} = \sqrt{\frac{1}{n} \sum_{i=1}^n (a_i)^2} \quad (2.25)$$

**Table 2.4:** Ratios between rms - and peak acceleration for different waveforms, inspired by (Smith et al., 2007)

Waveform signal	$a_{peak}$ to $a_{rms}$ ratio
	$\sqrt{2}$
	$\sqrt{3}$
	1

## 2.2 Excitation from footfall

Humans affect floors and create vibrations through the motion of their bodies. Either acting alone as a single point load or a group of people acting as a distributed load (ISO, 2007). Walking can be presented as a quasi-static or dynamic load depending on the situation and the fundamental frequency of the affected medium (Smith et al., 2007).

### 2.2.1 Single person impact

Excitation through walking takes the form of a forcing function comprised of three distinct parts; load application, period of rest and push-off. Figure 2.5 details the forcing function produced by different forms of walking/running. In the figures, one can see a sharp increase as the person applies the load and starts the step. After the load application follows a period of rest as the person transitions from heel to toe. The final part consists of the person applying an additional part as they push off the ground. While different activities produce different forcing functions, one should also expect different forcing functions from each individual person (Park et al., 2021). A certain level of generalisation and assumption is needed when producing models, thus empirical measurements might be necessary (ISO, 2007).

Predicting the consequences of the forcing function relies on knowing the natural frequency of the system it impacts. A theoretical forcing function which decays in 1s will produce different reactions when applied to mediums with different natural frequencies.

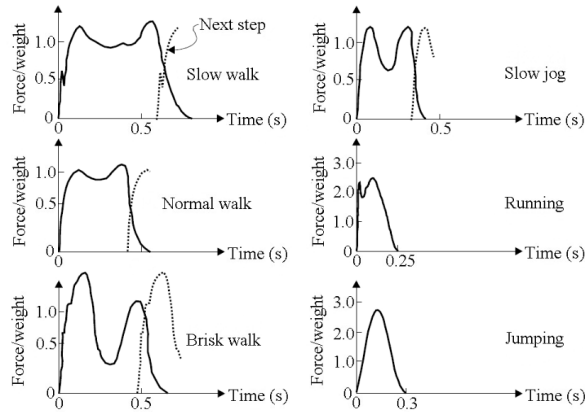


**Figure 2.5:** Forcing functions for various activities. (Wheeler, 1982), found in (Pavic and Reynolds, 2002)

A 1Hz system would give a large reaction when exposed to the excitation, while a 0.01Hz and 100Hz system would give a small reaction. The 0.01Hz system would not react fast enough to produce a reaction and for the 100Hz system, the load would resemble a quasi-static load (Smith et al., 2007). Determining the natural frequencies of a system is therefore the first step when evaluating a vibration problem; see Eq (2.4).

The frequency of the forcing function correlates to the time between each step, often expressed as step per minute (SPM). AISC Design Guide 11 give guidance on expected frequency for different types of walking, these are outlined in Table 2.5. The frequency varies between 1.25Hz to 2.1Hz depending on the persons walking pace. The pace is assumed to be governed by the area’s function and level of furniture (AISC, 2016). ISO 10137 applies a larger spectrum of frequencies between 1.2Hz to 2.4Hz but gives no guidance on which to expect. Both design guides apply a max value of 4Hz when the person is running but disagree on the lower bound. AISC states that running starts at 1.6Hz while ISO applies a higher value of 2Hz (AISC, 2016)(ISO, 2007).

Attention should also be applied to the person’s stride length and weight. Stride length governs the needed amount of steps to cross the considered area. Since the floor needs a certain number of steps to reach full resonance steady-state, limiting the number can stop full resonance from occurring. Weight linearly correlates to the dynamic force applied by the walker (Wood Works, 2023).

**Table 2.5:** Examples of expected walking frequencies depending on usage (AISC, 2016)

Characteristics	Very Slow	Slow	Moderate	Fast
Walking Frequency	1.25	1.6	1.85	2.1
Steps per minute	75	95	110	125
Potential Occupancies	Technical production	Furnished areas	Schools and office area	Transitory areas

### 2.2.2 Group Impact

A dynamic load produced by a group depends on the total weight, the density of the group distributed on the floor area and the level of coordination between participants (ISO, 2007). The standard assumes that groups are representative of the general population and that a certain level of variability exists depending on the complexity of the activity and skill of participants. Eq (2.26) together with a reduction value from Table 2.6 give a simplified way of determining group impact. If a group is smaller than 50 persons, a value of 1 should be used.

$$F(t)_N = F(t) \cdot C(N) \quad (2.26)$$

**Table 2.6:** Recommended coordination factors  $C(N)$  for  $N$  number of people (ISO, 2007)

Coordination	High	Medium	Low
1st harmonic	0.80	0.67	0.50
2nd harmonics	0.67	0.50	0.40
3rd harmoinc	0.50	0.40	0.30

### 2.2.3 Continuous forcing functions

Footfall, as seen in Figure 2.5 is a highly complex function and will vary significantly between people. Walking is the rhythmic continuation of a footfall, either during or after the existing step depending on the activity. The complexity of the function makes it necessary to break it down to determine the overall response.

The original complex continuous forcing function is decomposed into a series of simple sinusoidal waves. This collection of sinusoidal waves is called a Fourier Series and the superposition of every wave will form an exact representation of the original function. In a Fourier Series, there are an infinite amount of sine waves, the addition of each additional wave increases the convergence and leads to a better approximation. Each sinusoidal wave has its own associated amplitude, phase shift and frequency.

The frequency will always be a multiple of the fundamental frequency of the original continuous forcing function, therefore each sinusoidal wave in a Fourier series is a harmonic. The existence of harmonics is more important than the processes of creating them when understanding vibrations in floor structures. For this reason, the process will not be outlined figure but Figure 2.6 is a graphical representation of the first four harmonics of low-level aerobics.

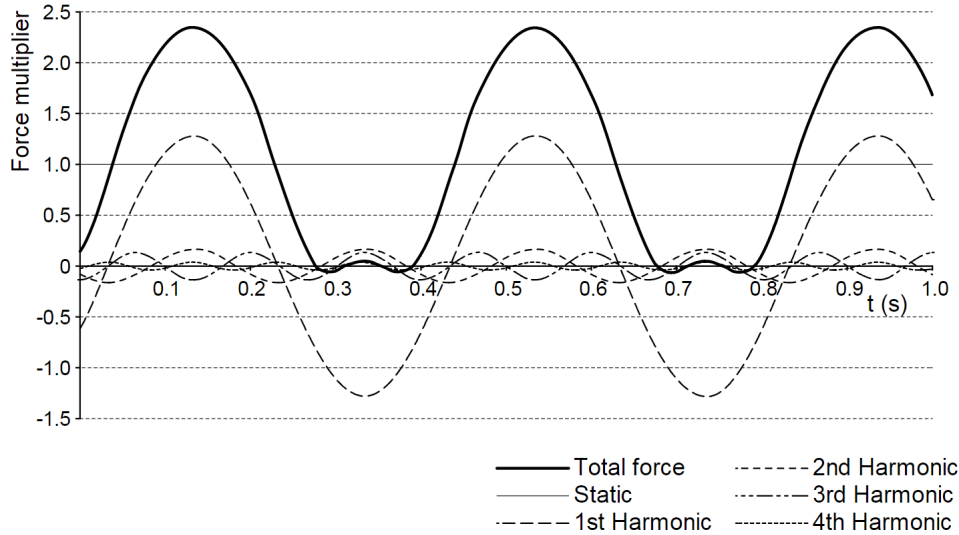


**Figure 2.6:** A breakdown of the total force from aerobics into a series of harmonics through Fourier transformation (Smith et al., 2007)

In Figure 2.6 harmonic one to four is shown together with the total force. For each subsequent harmonic, there is a decrease in amplitude and an increase in frequency. Most of the energy is concentrated in the first couple of harmonics, but there is still some energy in the higher harmonics. If there was no energy at higher levels, the total force should have fallen to zero between peaks and been a perfect half-sine wave.

Floor designers are commonly concerned with harmonics up to and including the fourth harmonic of the continuous forcing function created by walking (Wood Works, 2023). The classification of high-frequency floors is derived from this design principle and is given if the fundamental frequency of the floor is higher than the fourth harmonic (Smith et al., 2007). A low-frequency floor is one with a fundamental natural frequency lower than the fourth harmonic. This makes the classification of floors dependent on each person's walking frequency, the limit is therefore often given as a range. ISO 10137 applies a limit between 8-10 Hz (ISO, 2007).

If the floor is classified as a high-frequency floor, it is assumed that energy from one footstep had dissipated before the next step. For modelling purposes, it is acceptable to assume the forcing function as a series of independent load applications. The continuous forcing function can therefore be expressed as a series of impulse loads if the underlying assumption is met (Smith et al., 2007).

Equation (2.27) gives a Fourier series of a person walking across a 3m long platform for the vertical direction (ISO, 2007).

$$F_v(t) = Q \left( 1 + \sum_{n=1}^k \alpha_{n,v} \sin(2\pi n f t + \phi_{n,v}) \right) \quad (2.27)$$

## 2.3 State-of-the-art

### 2.3.1 Introduction

State-of-the-art will give an overview of vibration literature covering; human susceptibility to vibrations, how parameters influence floor performance and behaviour, and how to evaluate floor performance. Vibration research has uncovered several important factors to consider when analysing floor structures. The lack of a single decided criterion highlights the complexity of the problem and the development of several vibration design guidelines.

### 2.3.2 Literature

Reiher and Meister studied the difference between steady-state and transient vibrations on human susceptibility to the vibration of floor surfaces. In 1931 they showed that test persons developed a perception threshold after five minutes of exposure to a sinusoidal oscillation (Reiher and Meiste, 1931). The threshold was constant vibration velocity and the product of amplitude and frequency. Variation in acceleration over time became more influential as the vibrations grew stronger. Study of 1932 showed that for transient vibrations the decay process had no significant effect if the damping decrement was greater than 0.1 (Reiher and Meister, 1932). A damping decrement of 0.1 equals a damping ratio  $\zeta$  of 16 %, which most wood floor structures fall under (Wood Works, 2023). Therefore, this thesis will research transient responses created by heel drop and steady-state derived by walking.

Lenzen conducted vibration research on composite steel joist-concrete slab floors (Lenzen, 1933). He determined that the most significant factor was damping, while amplitude and frequency showed an insignificant effect. A human would not perceive it if only five cycles were necessary to dampen the vibration to a negligible level. After twelve cycles, humans would perceive the transient vibration as similar to a steady-state.

Ohlsson conducted several experiments on joisted timber and steel floors, trying to link human subjectivity to system properties (Ohlsson, 1982). Positive design choices discovered were reductions of spans and installation of ceilings underneath the floors. Creating excitation with heel drop and measuring impact response from test subjects showed that anti-symmetrical modes were a major factor in annoyance levels. The different resonances generated were interacting, and modes higher than fundamental played a significant role in human annoyance levels.

Accounting for only the fundamental mode was insufficient, and Ohlsson recommended a 5 Hz spacing between adjacent natural frequencies. Interaction between modes of vi-



bration was dependent on the damping coefficient, growing in severity if a high vibration amplitude remained for a period after the impact. Especially magnitude of velocity was affected by higher first-order modes.

Ohlsson created four different perception cases for discussing floor vibration. Each distinction gives a clear method for classifying the situation. The classification reflects the subjective nature of human perception in different settings.

**The first distinction** concerns the source of excitation, whether it is self-generated or externally generated. If self-generated vibration is sensed as *springiness* and an unacceptable floor is *springy*. Externally generated vibrations are created by other people walking and are sensed by a person standing, sitting or lying. This should be categorised as *footfall-induced vibrations* and unacceptable floors are *easily excited*

**The second distinction** classifies the floor either as lightly or heavily damped. Unlike the common practice in structural dynamics, Ohlsson argued for the use of the damping coefficient over the damping ratio. Ohlsson theorised that a measure for constant decay rate with respect to time would be more efficient. Ohlsson referenced Lenzen's work on cycles but argues that time and not cycles govern perception. The limit purposed was  $\sigma_0 = 0.4Hz$  where  $\sigma_0$  is defined in Eq (2.28). With a  $\sigma_0 = 0.4Hz$  the amplitude created by a step would be reduced by 75% before the next step.

$$\sigma_0 = \frac{c}{c_{cr}} \cdot f \quad (2.28)$$

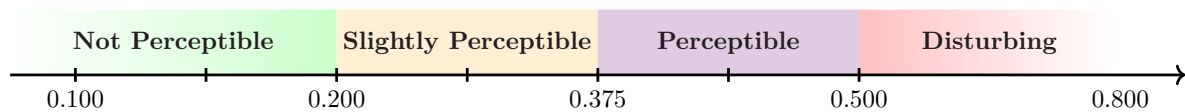
**The third distinction** separates *mono-frequency floors* from *multi-frequency floors*. If a single mode of vibration dominates the dynamic response, it is mono-frequency. If multiple modes are needed to determine the total response, it is multi-frequency.

**The fourth distinction** describes the interaction between human presence and the floor. If the presence of a human body significantly changes modal properties, such as mass and damping, the floor would be considered *light-weight floors*. *Heavy floors* experience insignificant changes when exposed to a human body. Whether human presence changes modal properties is mainly governed by the modal mass of each mode.

Concluding, Ohlsson comments on how to improve the vibration performance of floor structures. Improving continuous dynamic loading problems is achieved by increasing modal stiffness and damping ratio. For transient impulsive loading, an increase in modal mass and damping ratio is recommended. Increasing damping and stiffness will typically be positive and can never be harmful. An increase in mass has the possibility of reducing the resonant frequency; see Eq (2.4). Determining the forcing function is therefore critical when deciding how to improve the design.

Chui tested 6 different joisted wood floors with varied acceptability ratings to categorise them through  $a_{rms}$  (Chui, 1987). Excitation was created through heel drops at the centre of the floors. The person creating the excitation was also responsible for reporting the evaluation afterwards. Floors measured all had an rms-acceleration response between 0.1-0.8  $m/s^2$ , which was subdivided into a scale. The evaluation scale is shown in Table 2.7 and can be used to judge pure  $a_{rms}$ . Chui highlighted the difficulty of creating a scale and also suggested a hard limit of 0.45  $m/s^2$  frequency-weighted  $a_{w,rms}$

**Figure 2.7:** Scale for evaluating rms-acceleration in joisted timber floors, inspired by (Chui, 1987)



Alvis et al. performed several tests comparing human perception to several different values derived from vibration measurements (Alvis et al., 2001). Values included peak acceleration, root-mean-square acceleration, filtered peak acceleration and fundamental frequency. No single parameter was correlated to human perception of vibration. Alvis concluded that a possible source was the local properties of the system and that different floor location was more susceptible to contributions from higher modes. The floor must therefore be rated by testing several different floor areas, making FEM analysis preferable to hand calculations.

Ljunggren et al. 2007 studied the effect of different frequencies in the presence of an additional second constant frequency (Ljunggren et al., 2007). The first study was concerned with determining a threshold for single-frequency vibration. Results showed that sensitivity was the inverse of frequency, meaning higher frequency resulted in lower sensitivity and annoyance. The threshold values developed were approximately 1.6 times as great as those in ISO 10137. The second study adds a constant 8 Hz frequency with different amplitudes. Subjects became more sensitive as frequencies got closer in range, confirming earlier studies. Sensitivity was drastically lower for lower frequencies. Ljunggrens lowest frequency was 10 Hz and was easier to detect when paired with a base signal than alone. The third study examined the annoyance of dual sinusoidal vibrations and found as a general rule that annoyance increased when the amplitude of the second frequency increased but decreased if the frequency became higher.

In his appended paper to his doctoral thesis, Ljunggren studied perception from simulated multiple frequency floor vibrations (Ljunggren, 2006). The study concluded with 3 general rules. An increase in vibration amplitude follows an increase in annoyance. If amplitude remains constant, an increase in frequencies results in higher acceptance. Sensitivity depends on the number of participating frequencies and the spacing between

them. The exception to rule number two is when the fundamental and second frequency is spaced close together. If a 2 Hz spacing is assumed, the annoyance level remains the same independent of a change in frequency. This constant annoyance level is because a beating phenomenon makes up a huge part of the final signal and dominates the perception compared to just frequencies.

Glisovic and Stevanovic specifically research the contribution of closely spaced frequencies, also called modal clustering (Glišović and Stevanovic, 2010). Orthotropic materials were more susceptible to the phenomenon and consequently saw increases in amplitudes from the interaction between modes. An increase in amplitude follows an increase in velocity and acceleration. A parametric study was conducted with both ex-situ and in-situ test setups. The measured values were different natural frequencies,  $a_{rms}$  in accordance with ISO 2361-2 and  $MSF$  expressed in Eq (2.29). The study showed that the fundamental frequency was determined by stiffness in the span direction and the magnitude of the dynamic response was determined by the total mass in the system. The ratio between stiffness in different orthogonal directions determined spacing between adjacent frequencies.

$$MSF_n = \frac{f_{n+1}}{f_n} \quad (2.29)$$

Hamm et al. conducted vibration measurements in around fifty real-life buildings and on a hundred different floors (Hamm et al., 2010). The expected frequency was calculated using DIN 1052 (DIN, 2008) and compared to experimental results. For almost all cases, the calculated frequency was lower than the measured one. The study could also not find any significant correlation between subjective evaluation and either measured or calculated frequency. The difference between measured and calculated frequency was concluded to stem from a wrong assumption in the code. Bearings for in-situ floors behaved like a torsional spring instead of the assumed pin end. The partition wall ignored in the code also provided additional stiffness to the system, which according to Ohlsson is always positive (Ohlsson, 1982)

Weckendorf et al. analysed how architectural and construction detailing affected floor vibration performance in constructed buildings (Weckendorf et al., 2014). In-situ experiments were conducted at different floor heights in an empty apartment building in Canada. Along the joist mode shapes were approximately half-sine waves, meaning the joist end could be simulated as simple hinge support. Between joist and structural elements, there is no deliberate continuity. Across joist more complex mode shapes was found, with complexity increasing with the order of the mode. The difference in along-joist and across-joist was attributed to the difference in flexural rigidity for different

directions.

Vibration transfer between areas with different transient roles happens through high-order modes around 60 Hz. Therefore, vibration transfer between areas is not likely to be perceived by occupants. No significant difference was found between levels, but it was only verified in a four-story building. Separation walls can be disregarded when defining effective span and floor width. Only structural boundaries should be accounted for when designing.

Jarnerö et al. studied the change in vibration properties of a floor element during different construction phases (Jarnerö et al., 2015). Starting with controlled experiments in the laboratory and ending in a fully complete eight-story building. The installation of the floor element into the structure was shown to alter dynamic properties significantly. The damping ratio was affected more than natural frequencies. Measured in-situ damping was on average 6 %, a considerable difference from the 1.4 -1.8 average damping ratios measured in the laboratory. 39 % of damping was contributed to the floor element installation in a superstructure, another 12 % was contributed from finishes and partition walls. Natural frequencies increased, especially with the installation of partition walls that increased stiffness.

The largest increases in higher modal damping ratios were observed in modes shapes that actuated the support underneath. Mode shapes also became increasingly more complex as the supporting conditions changed and screws and elastic interlayers were introduced. These elements function as local dampers and create an uneven damping distribution.

Much of Jarnerö's work is corroborated by Homb's doctoral thesis where similar experiments were carried out (Homb, 2005).

Weckendorf et al. 2016 conducted operational modal analysis on different floor elements ex-situ and determined system properties like modal frequencies, damping and mode shapes (Weckendorf et al., 2016). The testing was done on 5-ply and 7-ply CLT elements categorised as heavy-weight according to Ohlsson's definition. Results showed an increased risk for modal clustering as the width-to-span ratio increased or additional plates were added to the CLT element along the width. Operating with an assumed 1m width and not accounting for floor plans would therefore result in unreliable calculations. Testing on timber bearing support also resulted in higher modal clustering than steel support. This was explained by timber's lower stiffness compared to steel making the support more flexible. Damping was significantly impacted by human presence on the floor, but the impact varied on the position taken. An increase in damping for a specific mode was shown to be dependent on the person's position relative to the nodes of mode

shapes. A person has the greatest influence when standing almost at the centre of the floor, where no mode shape has a node. First order mode saw the sharpest increase in damping, over 300 %, when the person was positioned at the centre of the floor.

Kawzra et al. performed an extensive study of a CLT slab in an outdoor tent with 651 surface points measured (Kawzra et al., 2021). A large number of sensor points allowed the detection of local properties. From testing a large number of higher modes were found, but only seven were unambiguous. All identified modal properties exhibit slight variation dependent on environmental factors, this increased the complexity of the mode shape. A FEM model developed stressed the need for accurate material properties and boundary conditions to get the necessary accuracy. Low natural frequency computed modes consistently were in disagreement with experimental modes. Asymmetry created by the placement of a shaker were most extensive for the second mode, for sequential modes the symmetry increased.

Ussher et al. 2022 examined the difficulty of predicting dynamic response in lightweight timber floors (Ussher et al., 2022). The basis of the study was experimental data collected on well-defined CLT slabs, from this a FEM model was constructed to simulate more complex slab systems. Several parameters were examined for their ability to discriminate between acceptable and unacceptable floor designs.  $VDV$ ,  $a_{peak}$  and  $v_{peak}$  proved desirable design criteria, but the ability of  $a_{rms}$  was less clear. The different parameters were accurately predicted when only a single element was considered. For multiple elements connected together, higher modes than the fundamental were needed. Ussher argues that studies conducted on only a single strip of CLT have an inherent fault when trying to extrapolate to a system of connected CLT strips. Frequency range limits were examined based on cEC5 use of a cut-off at 40 Hz. It was shown that increasing the cut-off impacted all parameters and increased the number of modes covered.

Duarte researched vibration influence on human perception in 2006 and collected an overview of the resonance frequencies in the human body (Duarte and Pereira, 2006). While her research was conducted at much higher frequencies than a floor element would experience, Figure 2.8 is still relevant for discussion. Much vibration research on floors have documented vibration levels around 8 Hz, and several human body part can resonate at this frequency.

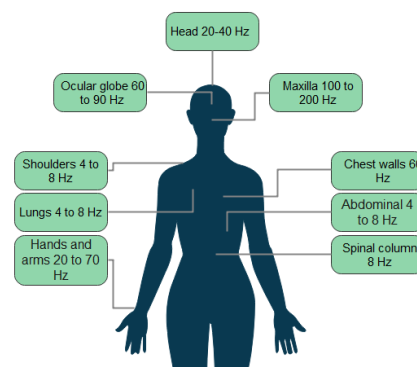


**Figure 2.8:** Resonance frequencies of human body organs

## 2.4 Codes and standards concerning floor vibration

### 2.4.1 ISO 10137:2007

ISO 10137 *Bases for design of structures - Serviceability of buildings and walkways against vibrations* guide how to evaluate serviceability problems created by vibrations (ISO, 2007). The standard only covers buildings and assumes linear response to loads. Not covered are bridges meant for vehicular traffic or pedestrian traffic, nor vibration created by machinery.

The procedure for measuring vibration is given in ISO 8041, but general guidelines are given in ISO 10137 (ISO, 2017). The standard gives definitions of different vibration phenomena, sources and dynamic properties such that vibration problems can clearly be described and compared. Integration and differentiation make it possible to derive either acceleration, velocity or displacement from each other, but measuring the desired value directly is recommended.

Serviceability criterion and variability should be decided in the design phase, and certain non-destructive situations that exceed criteria must be expected. Chosen criteria depend on the most sensitive or chosen receiver; human occupants, building contents or building structure. Each receiver group is given its own classification system in the standard breaking it down further.

Further analysis can be conducted using annex A to D, annex E provides information on mitigation methods. Annex C is of particular importance since it gives guidance on different vibration criteria. Acceleration criteria are based on a withdrawn version of ISO 2631-2 and are expressed in Figure 2.9. The curve should be calibrated using Tabel C.1 in the same section in accordance with the suitable application. Figure 2.9 shows that human sensitivity is greatest in the 4-to-8 spectra, corroborating Figure 2.8.

### 2.4.2 ISO 2631-1-1:1997 and ISO 2631-2:2003

ISO 2631-1 *Mechanical vibration and shock - Evaluation of human exposure to whole-body vibration - General requirements* scope is the transmission of motion to the human body from supporting surfaces (ISO, 1997). It gives guidance on how to combine principal factors and determine if vibration levels are acceptable.

In measuring vibration, the standard recommends measuring the surface between the transmission medium and the body. Three different definitions of principal areas are given in Figure 2.10.

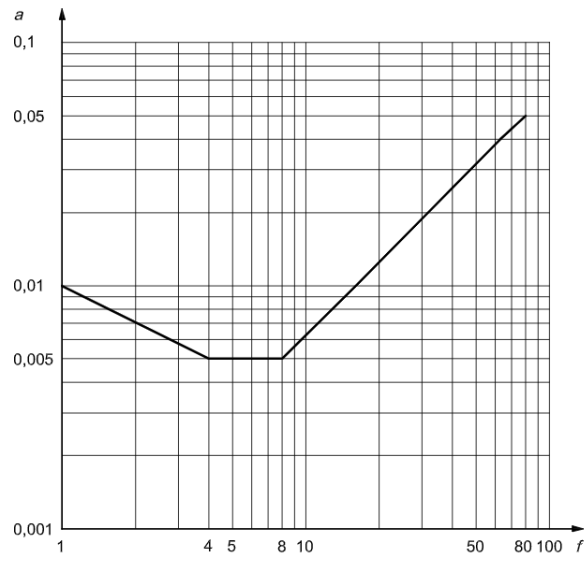


Figure 2.9: Base curve for vertical rms-acceleration (ISO, 2007)

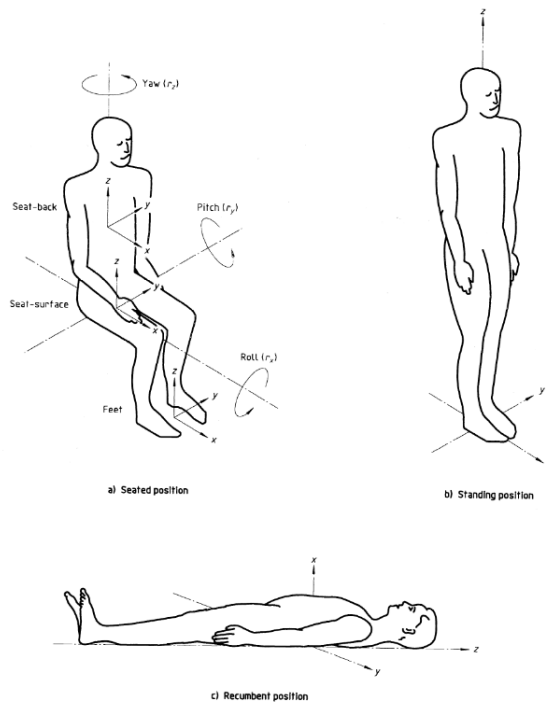


Figure 1 — Basicentric axes of the human body

Figure 2.10: A human body's basicentric axes (ISO, 1997)

Depending on which basicentric axes are chosen, the standard provides the method for frequency weighting the acceleration after a narrow or one-third octave band is applied to the signal. Frequency-weighted acceleration forms the basis of VDV and  $a_{w,rms}$ . Users of the standard are encouraged to show both unweighted and weighted rms-acceleration, in accordance with Eqs (2.30) and (2.25)

$$a_{w,rms} = \left[ \frac{1}{T} \int_0^T a_w^2(t) dt \right]^{\frac{1}{2}} \quad (2.30)$$

Vibration dose value (VDV) is given attention since peaks are more important when utilising power to the fourth instead of power to the second. For VDV the standard provides Eq (2.31), but no attention is given to recommending acceptable VDV levels. BS 6472 and ISO 10137 build on the concept and give recommendations with a table from a redacted version of ISO 2631 (BSI, 2008)(ISO, 2007)

$$VDV = \left[ \int_0^T [a_w(t)]^4 dt \right]^{\frac{1}{4}} \quad (2.31)$$

ISO 2631-2 *Mechanical vibration and shock - Evaluation of human exposure to whole-body vibration - Vibrations in buildings* are built upon part 1 with more attention given to building (ISO, 2003). It gives an overview of important factors to consider when reporting on vibrations. What is the nature of the excitation source, and when does excitation occur? Which types of vibrations are created, and for how long are the occupants exposed to them? Are associated phenomena like structure-borne noise, airborne noise, induced rattling and visual effects created? Associated phenomena are of vital importance since they make complaints more likely, but are hard to incorporate into an equation.

Annex A in the standard also defines frequency weighting when the occupant's posture is undefined. ISO 2631-2 differs from ISO 2631-1, which differentiates between different postures.

### 2.4.3 British Standard BS 6472-1:2008

BS 6472 *Guide to evaluation of human exposure to vibration in buildings Part 1: Vibration sources other than blasting* builds on ISO with some crucial differences (BSI, 2008).

It has its own system for weighting frequencies and employs geocentric coordinates instead of the basicentric axes shown in ISO 10137. Guidance is given on weighted peak



acceleration, depending on one's sensitivity a person would notice a peak between 0.01 to  $0.02 \text{ m} \cdot \text{s}^{-2}$ .

VDV is given more attention in the British standard than other parameters and is the primary evaluation method. The equation is the same as in ISO 2631-1 Eq (2.31), but the frequency weighting differs. BS 6472 also give guidance on expected levels of adverse comment; see Table 2.7. Recommended values are corroborated by ISO 10137 with slight differences (ISO, 2007).

**Table 2.7:** Probability of adverse comment for different VDV ranges

<b>Probability of adverse comments</b>	<b>Office buildings 8 h day</b>	<b>Office buildings 16 h day</b>
Low	0.2-0.4	0.4-0.8
Possible	0.4-0.8	0.8-1.6
Probable	0.8-1.6	1.6-3.2

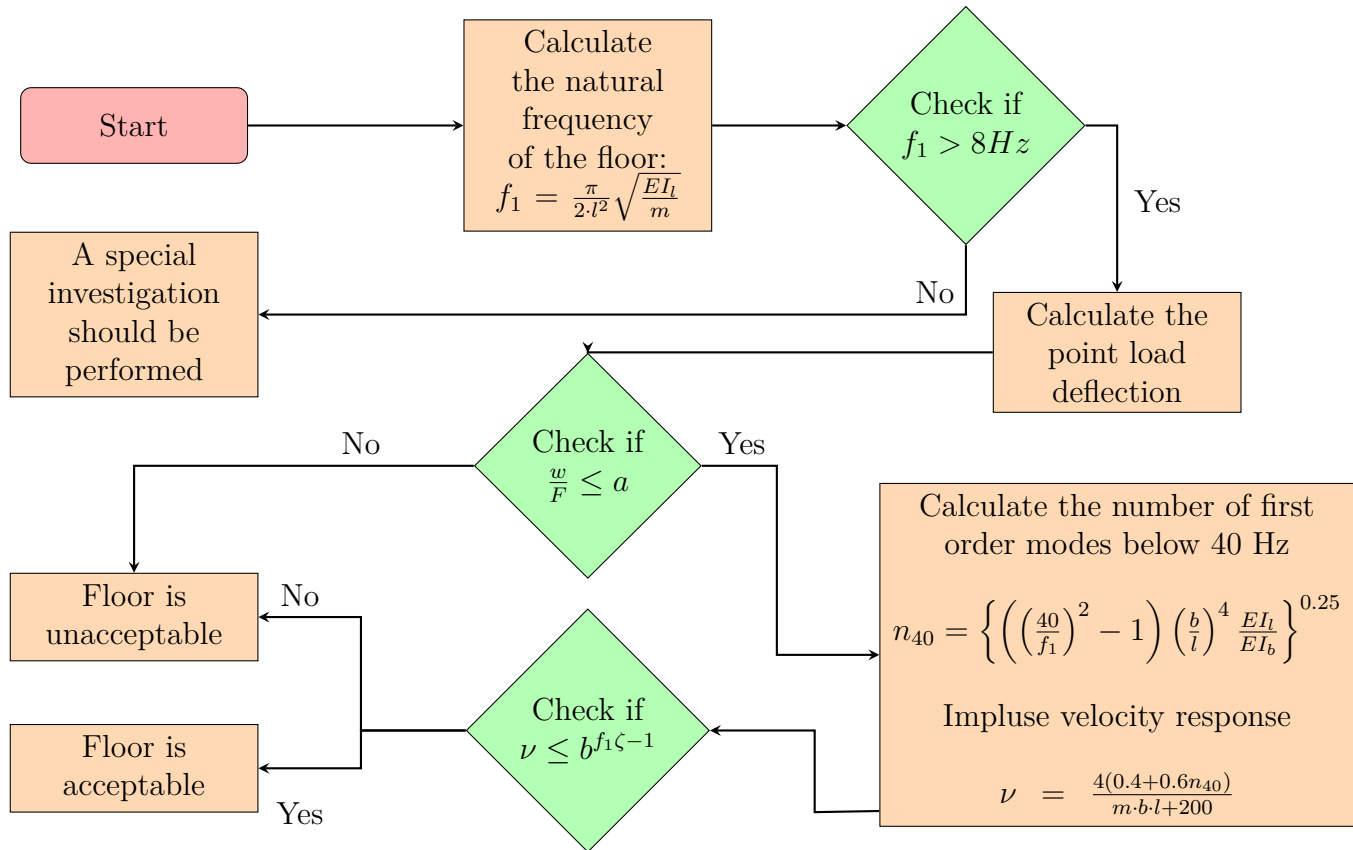


**Figure 2.11:** Flowchart for vibration verification using cEC5, inspired by (Schirén and Swahn, 2019)

#### 2.4.4 EC5-1-1 EN 1995-1-1:2004

The current Eurocode 5 (cEC5) has one criterion for verifying the method and two criteria for evaluating the acceptability of floor vibrations (CEN, 2010). Figure 2.11 provides an overview of using the code (Schirén and Swahn, 2019). The guidelines only apply if the fundamental natural frequency is above 8 Hz. A special investigation must be performed if it is below, but a process has never been included in the code. Acceptability is judged on unit impulse velocity response  $b$  and point load deflection  $a$ . The Norwegian Annex gives no value for  $a$  for spans greater than 4.5 metres and no guidance for  $b$  (Standards Norway, 2010). cEC5 provides guidance for acceptable ranges for both  $a$  and  $b$ .

The fundamental frequency is dependent on longitudinal bending stiffness  $(EI)_L$  [ $Nm^2/m$ ], the mass of the floor  $m$  [ $kg/m^2$ ] and span length  $l$  [ $m$ ]. When controlling stiffness, the maximum instantaneous vertical deflection  $w$  [ $mm$ ] is divided by the force  $F$  [ $kN$ ]. Impulse velocity response is decided by the width  $b$  [ $m$ ], length  $l$ , mass  $m$  and the number of first-order modes below 40 Hz defined as  $n_{40}$ . A first-order mode is a mode parallel to the joists with the shape of a half-sine wave (Ussher et al., 2017). When controlling velocity criterion  $b$  damping ratio  $\zeta$  of 1 % is often assumed.

### 2.4.5 EC5-1-1 prEn 1995 -1-1:20xx(E)

Through mandates M/466 and M/515, the European Commission has given CEN the order to amend and extend the current EC5 (EC, 2010)(EC, 2012). The process has been ongoing since 2010 and has a deadline in 2026 when the standard is distributed to the National standardisation body (NSB) (EC, 2023).

Revised Eurocode 5 introduces seven different levels for floor performance. Level I would be the best performance, VI the lowest acceptable, and VII is unacceptable. One criterion verifies the method, and three criteria evaluate the floor's vibration performance. The floor needs a fundamental natural frequency higher or equal to 4.5 Hz for the method to be applicable. Performance criteria are stiffness  $w_{1kN}$ , acceleration  $a_{rms}$  and velocity  $v_{rms}$ . The lowest-performing criterion governs the final performance prediction if the method is applicable. Criteria and levels can be seen in Table 2.8 and Figure 2.12 gives a brief overview of how to use the code.

Deflection criteria remain from cEC5, but are renamed to stiffness criteria and are denoted as  $w_{1kN}$ . Factors for calculating the deflection are  $F$  a 1 kN point load, length of the floor  $l$  [m], effective width of the floor  $b_{eff}$  [m], mass of floor  $m$  [kg/m<sup>2</sup>] and longitudinal bending stiffness  $(EI)_L$  [Nm<sup>2</sup>/m]. The effective width is defined in Eq (2.32a), and the criterion for stiffness is given in Table 2.8. Parameter  $w_{lim}$  should be calculated when  $w_{lim,max} > 0.5$  in accordance with Eq (2.32b). Multipliers  $k_{e,1}$  and  $k_{e,2}$  account for double spans and transversal stiffness  $EI_T$  [Nm<sup>2</sup>/m] when calculating fundamental frequency.

$$B_{eff} = \min \left\{ 0.95L \left( \frac{EI_T}{EI_L} \right)^{0.25}; B \right\} \quad (2.32a)$$

$$\begin{aligned} w_{lim} &= w_{lim,max} && \text{when } w_{lim,max} \leq 0.5 \\ 0.5 \leq w_{lim} &= \frac{150R}{L} \leq && \text{when } w_{lim,max} > 0.5 \end{aligned} \quad (2.32b)$$

Determination of expected  $a_{rms}$  is dependent on  $k_{res}$  which accounts for higher modes and is calculated with Eq (2.33a),  $\mu$  which represents resonant buildup and is assumed to be 0.4,  $F_h$  is the assumed vertical force for a person walking set to 50 N,  $\zeta$  is damping ratio chosen from section 9.3.1(3) and modal mass  $M^*$  [kg] calculated with Eq (2.33b)

$$k_{res} = \max \left\{ 0.192 \left( \frac{B}{L} \right) \left( \frac{EI_L}{EI_T} \right)^{0.25}; 1 \right\} \quad (2.33a)$$

$$M^* = \frac{mLB}{4} \quad (2.33b)$$

Criterion  $v_{rms}$  is determined by multiplying total peak velocity with a reduction factor. Total peak velocity is found through Eqs (2.34a) to (2.34e). Impulse mean velocity in Eq (2.34a) is a ratio between walking frequency  $f_w$  [Hz] and fundamental frequency  $f_1$  [Hz] adjusted by certain factors. Peak velocity is the ratio between impulse mean velocity and modal mass of the floor. An assumed average weight of a person is added to the modal mass, and the ratio is reduced by a factor  $k_{red} = 0.7$ . Factor  $k_{imp}$  accounts for the impact of higher modes, similar to  $k_{res}$ . Peak total velocity is the product of peak velocity and  $k_{imp}$ . Final rms-velocity is calculated with the formula in Figure 2.12 with a factor  $\eta$  calculated with Eq (2.34e).

$$I_m = \frac{42f_w^{1.43}}{f_1^{1.3}} \quad (2.34a)$$

$$v_{1,peak} = k_{red} \frac{I_m}{(M^* + 70kg)} \quad (2.34b)$$

$$k_{imp} = \max \left\{ 0.48 \left( \frac{B}{L} \right) \left( \frac{EI_L}{EI_T} \right)^{0.25} ; 1 \right\} \quad (2.34c)$$

$$v_{tot,peak} = k_{imp} v_{1,peak} \quad (2.34d)$$

$$\begin{aligned} \eta &= 1.35 - 0.4k_{imp} \quad \text{when } 1 \leq k_{imp} \leq 1.9 \text{ else } \eta = 0.59 \text{ for joisted floors} \\ \eta &= 1.35 - 0.4k_{imp} \quad \text{when } 1 \leq k_{imp} \leq 1.7 \text{ else } \eta = 0.67 \text{ for all other floors} \end{aligned} \quad (2.34e)$$

**Table 2.8:** Floor performance levels according to revised EC5

Criteria	Floor performance levels						
	I	II	III	IV	V	VI	VII
Frequency criteria $f_1$ [Hz] $\leq$	4.5						
Upper stiffness criteria for all floors [mm]	0.25	0.5	1	1.5	2	-	
Stiffness criteria for all floors [mm]	$w_{lim}$ calculated with Formula 9.30						
Response factor R	4	8	12	24	36	48	-
Acceleration criteria $a_{rms}$ [m/s <sup>2</sup> ] $\leq$	0.005 R						
Velocity criteria $v_{rms}$ [m/s <sup>2</sup> ] $\leq$	0.0001 R						

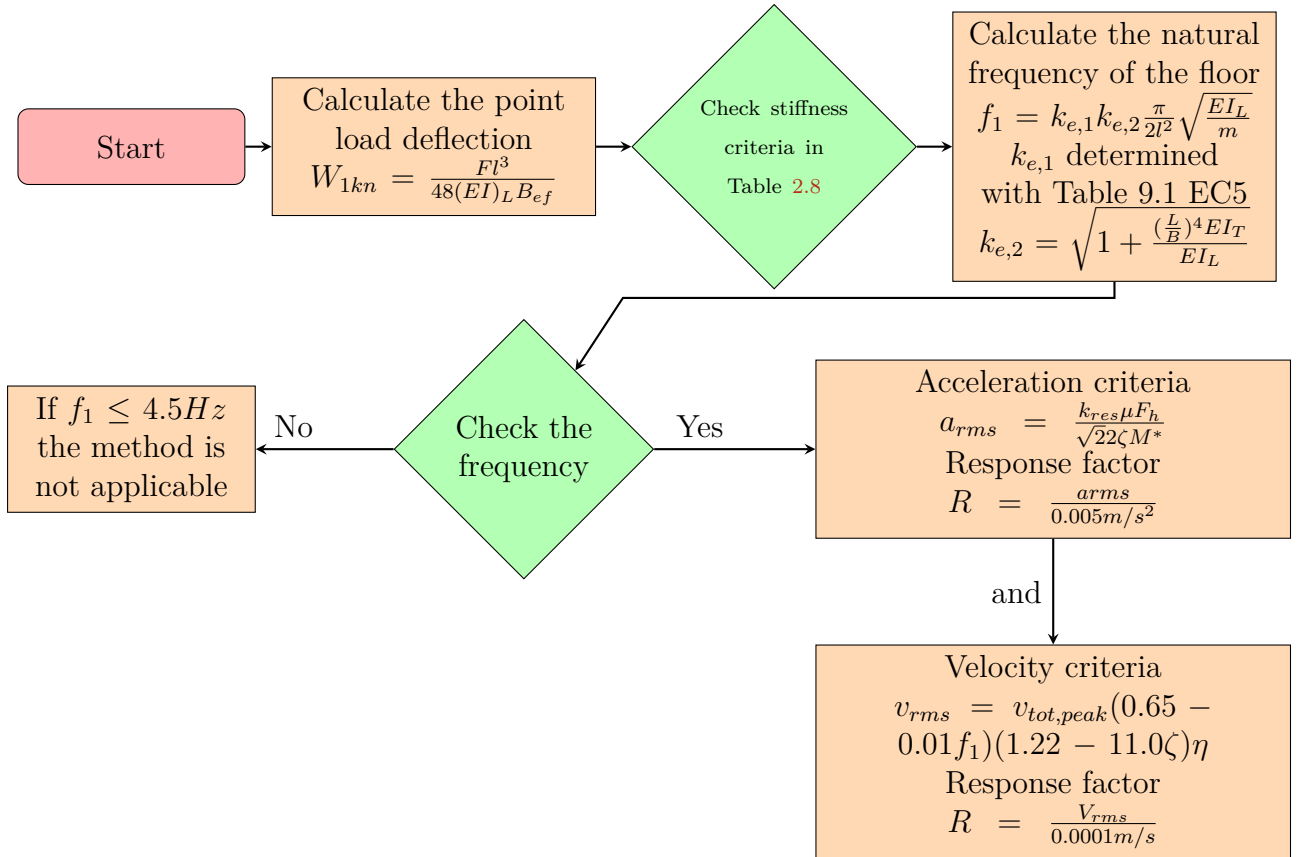


Figure 2.12: Flowchart for vibration verification using prEC5

## 2.5 Cross Laminated Timber

CLT is an engineered wood product (EWP) for load-bearing purposes. It is constructed with a minimum of 3 board layers, where each is rotated  $90^\circ$  in comparison to neighbouring board layers. As a building material, it achieves great strength in both in-plane directions. By alternating the direction of the grain, it utilises wood's inherent strengths in a better way. The technic evens out strengths and weaknesses since wood is strongest parallel to the grain and weakest perpendicular to the grain. Board layers are often connected by glue or screws, sometimes each board is also glued together internally in the layer (Markus Wallner-Nova, 2014). A board layer can also be called a lamella.

Like wood generally, CLT has one strong ( $0^\circ$ ) and one weak ( $90^\circ$ ) in-plane axis. CLT behaves as an orthotropic plate with different properties in the three orthogonal directions. The  $0^\circ$  as the most robust direction is in the direction of the top lamella since CLT usually is constructed with an odd number of layers. The relationship between the strong and weak axis is relatively high with  $E_0/E_{90} \approx 30$ . Since the ratio between the strong and weak axis is so high, the transverse weak axis is for simplicity often ignored in design (Brandner et al., 2016)

Proholz volume 2 provides information on estimating the effective bending stiffness of

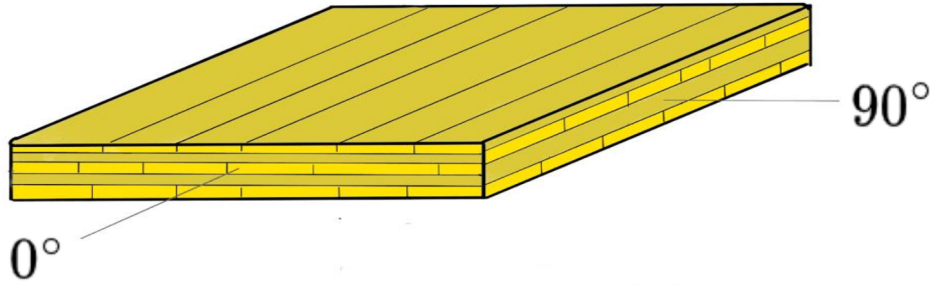


**Figure 2.13:** Overview of a 5-layer CLT with axis drawn on, inspired by (Markus Wallner-Nova, 2014).

CLT plates (Markus Wallner-Nova, 2018). For a 5-layer CLT with an assumed width of 1m, the bending stiffness can be calculated with Eqs (2.35a) and (2.35b). The equations disregard the contribution from perpendicular lamella.

$$EI_{CLT,0} = E_{mean,0} \cdot 10^6 \left( 3 \cdot \frac{1 \cdot t_i^3}{12} + t_i \cdot b \cdot (2 \cdot t_i)^2 + t_i \cdot b \cdot (-2 \cdot t_i)^2 \right) \quad (2.35a)$$

$$EI_{CLT,90} = E_{mean,0} \cdot 10^6 \left( 2 \cdot \frac{1 \cdot t_i^3}{12} + t_i \cdot b \cdot (t_i)^2 + t_i \cdot b \cdot (-t_i)^2 \right) \quad (2.35b)$$

A method was developed by Aranha in 2016 to estimate the elastic modulus and shear modules in CLT-materials (Aranha, 2016). Aranha's method supports FEM-modelling in programs not designed with predefined CLT materials, like SAP2000.

## 2.6 Finite Element Software

An example of FEM-based software is SAP2000, a design tool with a multitude of different analytical options and a wide range of integrated design codes (Computers and Structures, 2017). The program can be considered general-purpose civil-engineering software. Integrated building codes make it easy to produce reports and make necessary design changes (Habibullah, 2023). Modelling can be done in 2D or 3D with increasingly more complex geometry. Nonlinear and dynamic consideration analyses are available along with FEA.

Modelling can be done at a global or local scope, meaning every part can be given different values. Some options available for modelling are shell, multi-layered shell, isometric materials, springs and dampers. More options are available if necessary, like cables and curved members.

Vibration analysis can be modelled as steady-state and transient. Steady-state often assume the only load applied is stationary and often is the self-weight of the structure. For transient response, load application must be specified in time and space. Each load

application can have an applied time history to simulate walking or rotatory machinery. Dynamic analysis includes *response spectrum* for acceleration and maximum response, *steady-state* for fatigue behaviour dependent on specified damping and *time history* for deformation.

Mesh in SAP2000 is assigned through manual input or an automatic default tool. Compared with other FEM software, the automatic mesh tool provided in SAP2000 is limited. It lacks sophisticated algorithms to handle mesh critical areas (Animas et al., 2016). The mesh used is therefore *coarse*, limiting the accuracy the program can provide.

SAP2000 has been previously used for modelling the vibration of floor vibrations (Pasca et al., 2021). It has also been used for other modal analyses like the dynamic behaviour of buildings (Beskhyroun et al., 2020) and identification of material properties (Yanik et al., 2020).

### 2.6.1 Modal Assurance Criterion

When evaluating a FEM model created in a simulation program, the Modal Assurance Criterion (MAC) is a valuable tool (Pastor et al., 2012). It compares the real measured floor element and the simulated values quantitatively. The comparison is between the normalised scalar product of real and simulated model vectors. One value is calculated between each mode in a matrix arrangement. Eq (2.36) is a typical formula for calculating MAC values, but others are available should they fit a project better.

$$MAC(r, q) = \frac{|\{\phi_A\}_r^T \{\phi_X\}_q|}{(\{\phi_A\}_r^T \{\phi_A\}_r)(\{\phi_X\}_q^T \{\phi_X\}_q)} \quad (2.36)$$

MAC always falls between no consistent representation 0 and consistent representation 1. What corresponds to a good enough MAC value falls upon each project to decide.

## 2.7 Operational Modal Analysis

Operational Modal Analysis (OMA) is an alternative to mobility-based modal analysis. The advantage of OMA is its ability to gather accurate modal identification without artificial excitation. Vibration data is gathered from the construction under operating conditions, alleviating the need for an initial excitation. Civil-engineered structures like buildings and bridges are assumed to experience stochastic input forces. This makes OMA ideal for modal identification since it can operate without knowing the excitation force. A founding assumption is that excitation force is stochastic and can be separated from deterministic signals. Examples of elements superimposing deterministic signals on the building are ventilation systems and generators (Jacobsen et al., 2007). The lack of

known inputs while a strength can also lead to confusing excitation characteristics with the dynamic response. No control over inputs makes detecting closely spaced modes or exciting specific modes hard. (Rainieri and Fabbrocino, 2014).

OMA is a driver in the development of structural health monitoring (SHM), providing engineers with real-time information about changes to material properties and geometry (Saidin et al., 2022). It is quickly growing as a preferred analytical tool since testing is non-destructive, bears little cost and does not disturb normal usage. The drawback is that very sensitive, low-noise equipment is needed to measure the small amplitudes accurately. (Rainieri and Fabbrocino, 2014).





# 3. Methodology

The methodology outlines the different techniques and tools used to gather data from fields test and the processing of that data into results. The section structure is repeated in both chapter 4 and 5 to make navigation easy for the reader. Methods used draw on the theory from the previous chapter 2.

## 3.1 Field Tests

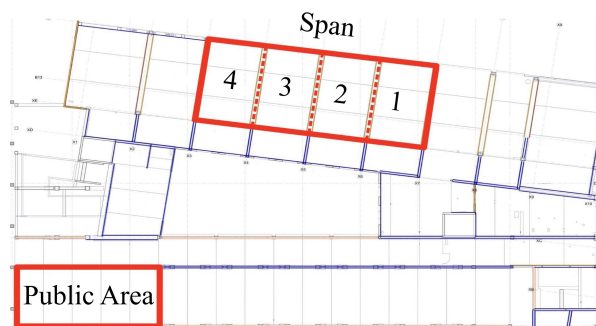


**Figure 3.1:** An overview map of the school and testing sites

### 3.1.1 Location

All tests performed in this thesis were conducted on floors in a newly built block of Ås High School; see Figure 3.2. The building started in 2020 and finished fourteen months later. The construction houses students in health care, language, and special education at different levels. This new block is connected to the school’s existing auditorium, facilitating easy student access. Construction was ordered by Viken county municipality and a variety of Norwegian companies handled the building process. A detailed overview of contracts can be found in (Trunmo, 2021).

Acoustic reports and observations on location indicate a certain level of technical equipment connected to ceilings along with acoustic plates. These elements were not modelled individually but added as an additional spread-out weight. Testing was conducted at night or on weekends when the students were away to limit the background noise. Un-

fortunately, the background noise could not be eliminated entirely as a certain amount of traffic was nearby and is perceivable at the higher end of the spectrum. Especially during winter months in Norway when snowploughs drove by at regular intervals.

Students have been complaining about vibrations on certain floors of the building since it opened for use. Excitation caused by footfalls on the floors results in a high level of movement followed by audible and or visual cues. Different equipment will shake and produce noise, and structural noises can be heard. The reason for the performance is still under investigation and no measurement for improving performance has been installed.



**Figure 3.2:** Picture of Ås High School (orientation corresponds to spans seen in the BIM-model for different levels)

### 3.1.2 Areas targeted for testing

#### 1F Public Area

Test 1F Public Area was performed in a common area meant to provide students with a place for mingling. The area is relatively large with sparse furniture, allowing for movement. Figure 3.3 presents the area as it is every day for occupants, while 3.4 is from the BIM model used in construction. The floor has a 6m span (outer lamina of CLT span parallel in 6m) and a width of 11.5m. CLT200mm was used in construction, and the cross-section is the same as Figure 3.11 without the presence of any partition walls. Supporting the floor is one GLT380x360 with a 103x200 cutout in the top corner allowing for the floor to rest, and a HSQ204 S344 around a PL10x170 on the other side. Steel can be differentiated as red in Figure 3.4. A railing of LVL 35mm thick runs around the edges, it is mounted atop the floor.



**Figure 3.3:** Overview picture of 1F Public Area

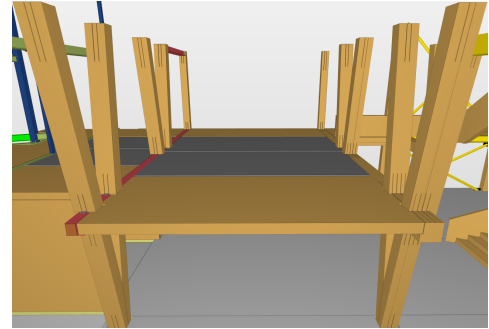


**Figure 3.4:** 1F Public Area from the BIM-model

## 2F Multi Span and Single Span

Healthcare students occupy second-floor classrooms and have a large degree of materials and shelves simulating real work environments. Each classroom is designed to accommodate a relatively low number of students and more furniture than standard classrooms. Each room is approximately 10m wide and 8m long. On the short edges, there are partition walls dividing each classroom. A corridor and a facade with windows board the long edges. The classrooms are separated from the corridor by glass partition walls.

Classroom 2F Multi Span is the only classroom with two spans in the same room with no separation wall in between; see Figure 3.5. The two spans are the last two spans starting on the left in Figure 3.6 and correspond to spans 4 and 3 in Figure 3.1. All classrooms use the same CLT with 160mm thickness with cross-section shown in Figure 3.11. Partitions walls are mounted directly on top of the CLT floors to reduce flank transmission of sound. Beams running under the floor are GLT470x585 with 107x160 cuts on both sides, allowing for the CLT to rest on top; see Figure 3.13. The beam in front of the two middle spans is not directly connected to the floor, only providing stiffness to the bracing. All spans are therefore two sides supported by a beam and free on both short sides. Facade walls are placed on top of the floors and are of unknown thickness. 2F Single Span is in the neighbouring classroom of 2F Multi Span and is the first span from the left in Figure 3.6. It corresponds to span 1 In Figure 3.1



**Figure 3.5:** Overview picture of 2F Multi Span

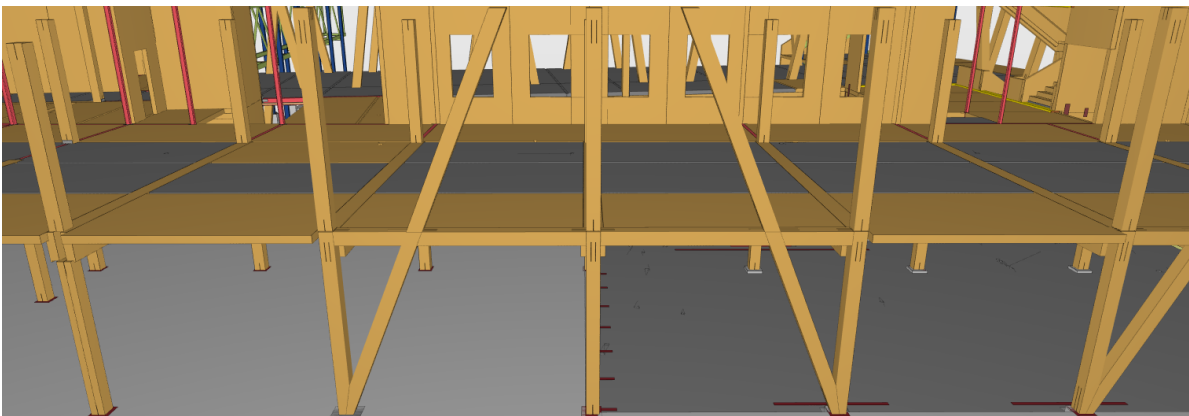


**Figure 3.6:** The second level from the BIM-model

### 3F Multi Span

Third-floor classrooms are reserved for language studies and have more desks and chairs than second-floor classrooms. The rooms are also much more bare and produce fewer audible and visual cues. 3F classrooms were slightly smaller, approximately 9m in width and 8m in length. An overview of one classroom can be seen in Figure 3.7. Figure 3.8 present all spans on the third floor. The floor construction is the same as 2F Multi Span, and the same beams are used. The floor is two sides supported since the beam seen running in front is not connected to the floor. Facade walls are placed on top of the floors, but the thickness and weight are unknown. 3F Multi Span corresponds to

span 4 and 3, 3F Single Span Wall is span also span 3 and 3F Single Span is span 2 in Figure 3.1



**Figure 3.7:** Overview picture of 3F Classroom

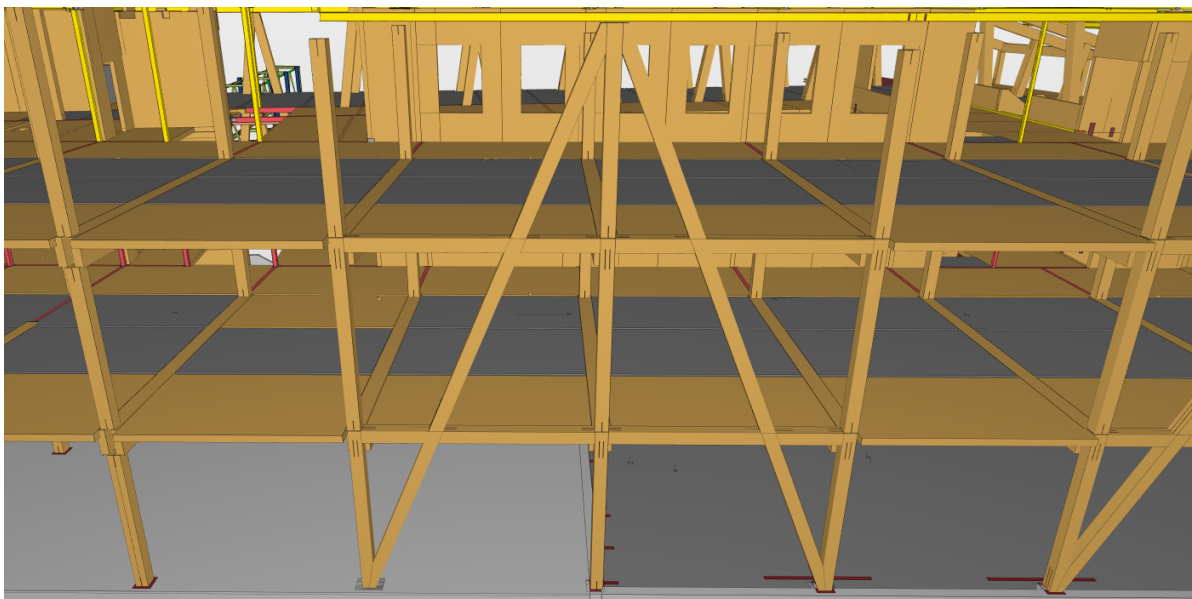


**Figure 3.8:** The third level from the BIM-model

### 3F Public Area

1F and 3F Public Area have the same geometry and placement at different heights in the building. CLT160mm was used in the floor's cross-section, unlike the 200mm used 1F Public Area. The reason for the difference is unknown. Three book cabinets are placed on the floors, adding a sizeable additional point load. There was no way of accurately determining the weight of the cabinets since they were filled with a random selection of books; see Figure 3.9. The area is slightly larger than 1F Public Area, with a length of 12m and a width of 6m. From the BIM model, three different beams support the floor elements, all running perpendicular to the span. On the left side is a GLT190x540 with a 107x160 cutout, and on the right side is an HSQ224 S355 marked with red and GLT 280x540 the rest of the way. Figure 3.10 show the BIM model of the area with the steel beam present on the right.



**Figure 3.9:** Overview picture of 3F Public Area

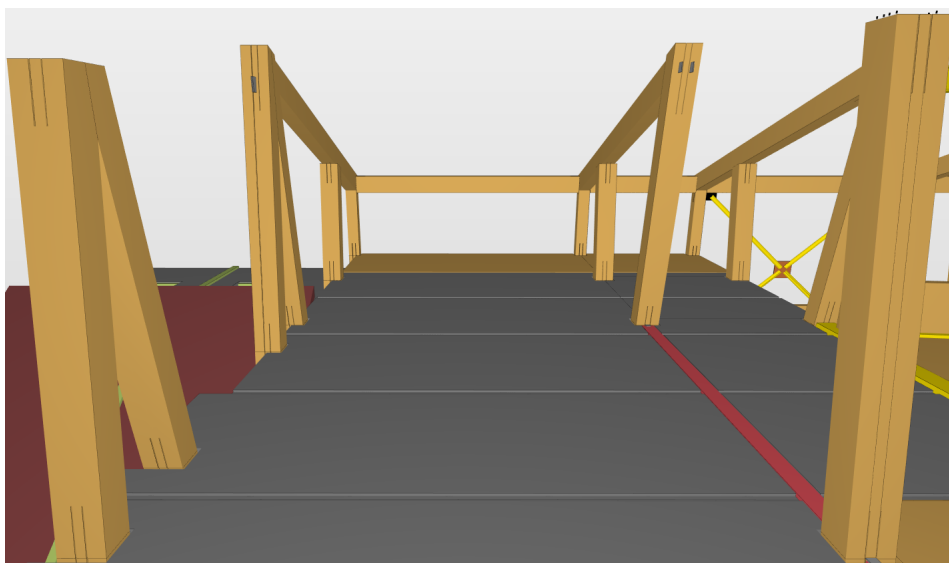


**Figure 3.10:** 3F Public Area from the BIM-model

### 3.1.3 Floors

All floors are constructed as a CLT slab with a floating top layer, a cross-section is provided in Figure 3.11 and material dimensions in Table 3.2. The construction of partition walls varies as room utilisation changes, but are mainly constructed with: 2x12.5mm gypsum, 100 mm staggered wood frame filled with isolation and 2x12.5 gypsum. According to the Norwegian Firecode, each classroom must have partition walls capable of resisting fire for 60 minutes (EI60) (Dibk, 2023). A robust construction can therefore be assumed.

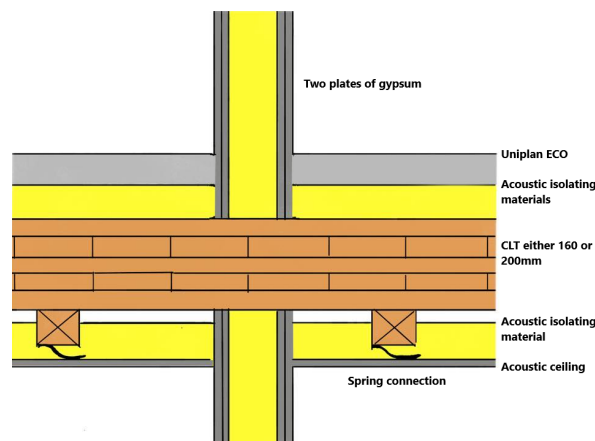


**Figure 3.11:** Cross-section of constructed floors, acoustic plates are not drawn on (The wall in the middle is a typical separation wall running from top to bottom).

### 3.1.4 Connections

Detail drawing of the connections used for construction can be seen in Figure 3.12 and 3.13. There is no common width on each CLT element, but they are never more than 3m in width. Between each plate of CLT, a plate-to-plate connection is constructed with a 120mm single surface spline board held in place with nails. Further reading on these kinds of connections can be found in the CLT Handbook U.S edition (Mohammad et al., 2013). The edge of every CLT element is placed inside a cut-out section in the supporting GLT beam, and then angled VGZ screws are used to secure the connection.



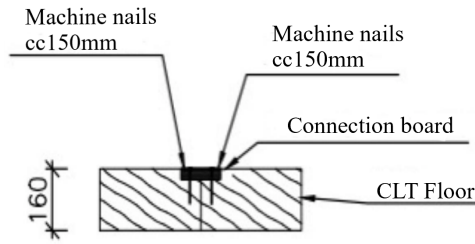


**Figure 3.12:** Connection between CLT-elements

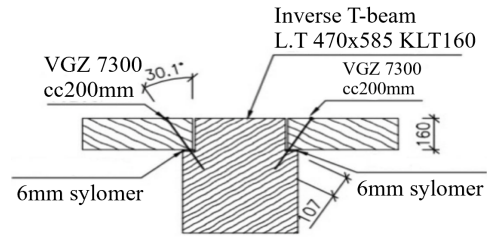


**Figure 3.13:** Connections between CLT and GLT470x585KLT160

## 3.2 Experiment

### 3.2.1 Equipment

Annex B gives a technical description for all equipment used in testing. The employment of equipment was assisted by a laboratory technician with extensive experience in vibration measurement. Figure 3.14 gives a flowchart for data collection. A total of 10 sensors collected data from the floor following an excitation. Sensors were connected to the data logger through cables, and a certain degree of cable management was necessary to minimise contact. Minimising was not possible in all situations, but overall contact was limited. The sensor signal was run through a signal conditioner, and a data logger collected the data and provided it to the PC where it was monitored. Data was captured at 200 Hz, meaning a Nyquist frequency of 100 Hz (Brandt and Ahlin, 2010). Tests were set to run for a total of 2 minutes.

### 3.2.2 Set-up

During testing, the amount of furniture was minimised in order not to have interference from other elements. A grid structure was developed to achieve a good resolution for each mode shape of the floors, as seen in Annex A. Of the 10 sensors available 2 were stationary, and 8 were roving. The 8 roving sensors would move across the floor in rows, and the 2 stationary sensors acted as references.

Dimensions for a particular floor were either taken from a wall or the centre of a beam and made into a grid. Sensors were placed at every intersecting line of the grid, each roving sensor representing a degree of freedom. A slight deviation of placement from the idealised grid where allowed. The standard configuration was 8 sensors in each row, moving across the floor. Reference sensors were placed in areas with a significant motion to avoid a mode node. All sensors were connected to the floor with double-sided tape. The tape was the preferred method since it would not damage the floor.

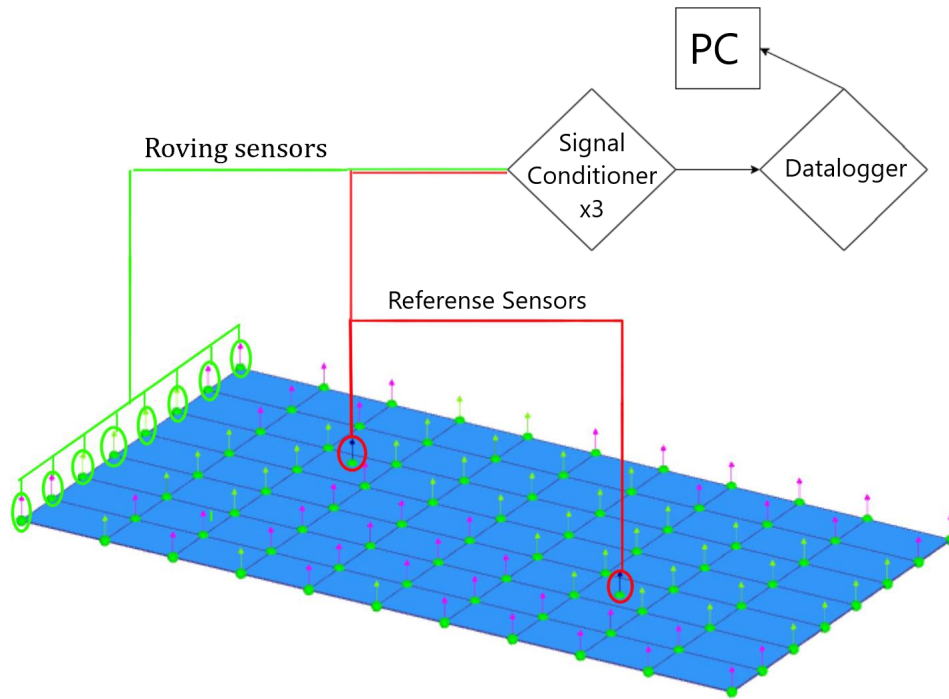


**Figure 3.14:** Flowchart over data collection

### 3.2.3 Excitation

All floors were assumed heavy-weight in accordance with Ohlsson's classification (Ohlsson, 1982). Since human presence was negligible, excitation was created by a human standing on the floor and exerting heel drops as broadband excitation with the person weighing 74 kg. Before every test the floor was examined to mark a sensitive area, heel drops were then be performed at that mark. The action was performed every 10 seconds for 2 minutes, except for the last drop that occurred after 5 seconds so it could be captured in the 2-minute interval. A 2 minutes interval was chosen to capture the possible resonant build-up and ensure an adequate sample size.

Some floors were excited by walking in an attempt to discover more modes. Walking was performed in three different ways; one-person walking, two-person walking in-phase and two-person walking out-of-phase. Tests were performed for the same 2 minutes, and no set rhythm was imposed on the walking. Unlike heel drop, walking was performed at random across the floor area.

## 3.3 Signal Processing

All sensor data were processed and analysed through the commercial software Artemis Modal Pro. The program allows for easy access to different analytical options and graphical representations of displacement. From these options, Stochastic Subspace

Identification (SSI) and Enchanted Frequency Domain Decomposition (EFDD) were used to determine natural frequencies, mode shapes and damping. Curve-fit Frequency Domain Decomposition (CFDD) was only used to determine damping in the system. FDD methods utilise Fourier transformation to transform time domain into frequency domain for spectral density. To determine mode shapes and damping, an inverse Fourier transformation brings it back to time domain. SSI fits time-domain raw data to a parametric model, minimising deviation between the two (Brincker and Andersen, 2006).

### 3.3.1 Artemis analytical tools

FDD is the basis for EFDD/CFDD and was introduced in 2000 in the original paper *Modal Identification from Ambient Responses using Frequency Domain Decomposition*. The method utilises Singular Value Decomposition to decompose the spectral density function matrix. The results of the operation are a series of SDOFs that each represent different modes (Brincker et al., 2000).

EFDD builds upon FDD by adding a model estimation layer. Spectral Bell functions are created through SDOF identified by FDD. MAC values are calculated between a reference vector from FDD and a singular vector created at a frequency. This action is performed on both sides of the reference vector and stops when additional frequencies result in MAC values lower than a specified value (Solutions, 2023b). An example of modes picked with EFDD can be seen in Figure 3.15

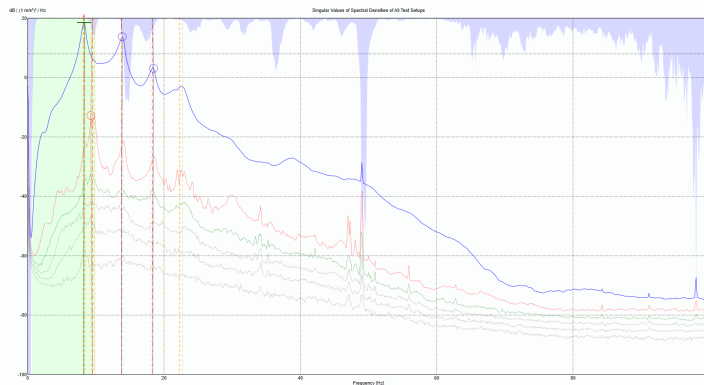


**Figure 3.15:** Frequency response function analysed with EFDD through Artemis

CFDD works on the same principle as EFDD but estimates the natural frequency and damping with curve-fitting. SDOF Spectral Bell is fitted through frequency domain least-squares estimation (Solutions, 2023a).

SSI Unweighted Principal Component Merged (SSI-UPC) is the chosen SSI form. Weighting in SSI is through two different weight matrices, which in this case both equal the unity matrix adding no weight. The method works best for modes with similar energy

levels and small state space dimensions that can be used (Solutions, 2023d)(Solutions, 2023c). Figure 3.16 shows an example of modes picked with SSI-UPC.

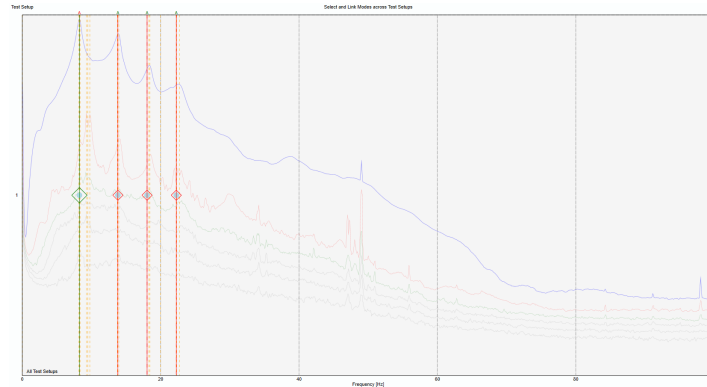


**Figure 3.16:** Frequency response function analysed with SSI through Artemis

Further reading on the analytical methods is available through citation. All analysis is handled through Artemis with no modification to standard analytical choices.

### 3.3.2 Determination of modes

Determination of modes was ideally done through automatic mode estimation allowing the program to determine clear modes. All automatically determined modes were evaluated visually to ensure they were not noise modes. After the automatic estimated modes were discovered, the frequency domain was inspected, and additional possible modes were manually picked out and inspected. If modes with similar frequencies were found, the one with the lowest complexity was prioritised.

### 3.3.3 Choosing results

In total, 22 different tests were performed on various floors. From this selection, only 13 tests are presented in the thesis. Results are discarded if they were duplicates of the same test set-ups, or if the signal was unclear with no clearly defined boundary conditions.

## 3.4 Time History Response

All sensors gather acceleration information, and this raw acceleration data was processed for some floors. The acceleration values included a contribution for all modes. Three different forms of accelerations were calculated;  $a_{peak}$ ,  $a_{rms}$  or VDV. For detailed information concerning the difference between them consult section 2.1.10. Peak acceleration is the largest acceleration the sensor experience.  $a_{rms}$  applies a time factor, showing how much acceleration a sensor is experiencing over a given time. VDV is frequency-weighted

$a_{rms}$  to the power of four, massively increasing the difference between large and small values. All data were uploaded to Excel, where it was less time-consuming to apply Eq (2.25) to determine  $a_{rms}$  and search for the maximum absolute value determining peak response. The difference between rms - and peak acceleration is shown in figure 2.4.

VDV requires  $a_{w,rms}$  and was handled through a MatLab script built around ISO 2631-1 (ISO, 1997). The script automatically processes time history and acceleration into VDV by weighting the acceleration in accordance with ISO 2631-1 (ISO, 1997). Frequency weighting  $W_k$  was used since the standard recommends it for comfort in the z-direction.

The addition of the mean value in VDV is not covered in any standard. Therefore two approaches were applied to differentiate between comfort and floor performance. VDV presented in section 4.3 keeps the mean since it increases the VDV slightly overall. Mean was removed from the VDV presented in section 4.4 to isolate floor performance. Removing means neglected the gravitational contribution and focused on acceleration created by excitation. The variance between removing and keeping the mean is minimal.

ISO 2631-1 gives guidance on how to combine VDV received over time depending on how many times the vibration event occurs, Eq (3.1a). All VDV presented in this thesis are the dose produced by the 2 minutes of excitation. In section 4.3, a parameter  $i$  is calculated to reflect the number of 2-minute events necessary to override a 0.4 VDV limit. Eq (3.1b) is developed utilising the BS 6472(BSI, 2008) instead of ISO 2631-1 but is principally the same.

$$VDV_{total} = \left( \sum_i VDV_i^4 \right)^{\frac{1}{4}} \quad (3.1a)$$

$$i = e^{\frac{\ln\left(\frac{VDV_{limit}}{VDV}\right)}{0.25}} \quad (3.1b)$$

The same process was repeated for sensors across the floor after running the script on reference sensors. All calculated  $a_{rms}$ ,  $a_{rms}$  and VDV values can be found in Annex C. Calculated VDV values were analysed with a standard Excel tool to find the max, mean, average, standard deviation, kurtosis and skewness. Matlab was used to create graphical representations of the data. Contour plots were created using the `countourtf`-command in Matlab (Mathworks, 2023c). The `ecdf` command (Mathworks, 2023b) created the empirical distribution function. The `histfit` command created histograms with fitted curves after the data was processed through the `boxcox`-command (Mathworks, 2023d). Box-Cox transformation is a statistical transformation to normalise a data set(Mathworks, 2023a).

## 3.5 Analytical results

### 3.5.1 Current Eurocode 5

The current Eurocode 5 was designed for joisted timber floors, neglecting the transversal flexural rigidity and the ratio between span and width. CLT floor system as EWPs has great strength, allowing long spans without underlying joists. The considerable transversal and longitudinal strength of the element is presented in section 2.13. All spans had their fundamental frequency calculated with cEC5 so its accuracy in predicting the fundamental frequency could be determined. The calculated fundamental frequency could then be compared with the lowest frequency measured for that span. Verification was only performed for the fundamental frequency as it could be verified with empirical data. From the current Eurocode 5, the fundamental frequency where calculated using the formula presented in Figure 2.11. The formula is repeated underneath in Eq (3.2). Stiffness was calculated in accordance with proHolz recommended Eq (2.35a) and Eq (2.35b).

$$f_1 = \frac{\pi}{2 \cdot l^2} \sqrt{\frac{EI_l}{m}} \quad (3.2)$$

Material data was collected from Sintef certification of Splitkon products in Table 3.1 (Sintef, 2022). For CLT160mm each layer was assumed 32mm thick and for CLT200mm layer 1-3-5 was assumed 40mm thick. These cross-sections are the standard design provided by Splitkon, and no mention of costume arrangement was found in the documentation. All layers were assumed T22 in accordance with delivery information provided by the contractor. A summation of mass and bending stiffness for each layer in the cross-section of the floor is shown in Table 3.2.

**Table 3.1:** Material properties for Splitkon T22-lamella

Mechanical Properties		T22 lamella
		$N/mm^2$
Young's modulus tension	$E_{0,mean}$	13 000
	$E_{90,mean}$	430
Shear modulus	$G_{0,mean}$	810
	$G_{90,mean}$	81
<b>Density</b>		$kg/m^3$
Mean density	$\rho_m$	470
Characterisitic density	$\rho_k$	390

**Table 3.2:** Summation of floors material properties

Layers	Properties				
	Thickness (mm)	Density ( $kg/m^3$ )	Weight ( $kg/m^2$ )	$(EI)_l$ ( $Nm^2/m$ )	$(EI)_t$ ( $Nm^2/m$ )
Vinyl	5	120	0.6		
Concrete	60	2120	127.2		
Acoustic mat	50	15	0.75		
CLT 160	160	470	75.2	$2.9 \cdot 10^6$	$7.6 \cdot 10^5$
CLT 200	200	470	94	$5.48 \cdot 10^6$	$1.15 \cdot 10^5$
Technical			20.4		
Acoustic plates			15.3		
Total with 160mm			239.45		
Total with 200mm			258.25		

### 3.5.2 Purposed Eurocode 5

The revisions in prEC5 on vibrations seek to expand the code to include more than just joisted timber floors. An analysis was conducted to assess the effectiveness of revised Eurocode 5 on CLT floors in predicting the fundamental natural frequency and rms-acceleration. These values were chosen since they could be verified with field data.

The calculations follow Figure 2.12 with the floors categorised as CLT slabs with a floating floor layer ( $\zeta = 0.04$ ). All material properties are the same as used for current Eurocode 5; see Table 3.2. The equations needed to find the fundamental natural frequency and rms-acceleration are presented in Figure 2.12. They are also repeated underneath as Eqs (3.3) and (3.4). The additional formulas needed to perform the calculations are provided in section 2.4.5. The  $k_{kres}$ -factor accounts for the contribution of higher modes on  $a_{rms}$ , but was never higher than 1 for all floors. Meaning no adjustments were deemed necessary in order to account for higher modes of vibrations.

$$f_1 = k_{e,1}k_{e,2} \cdot \frac{\pi}{2l^2} \sqrt{\frac{EI_L}{m}} \quad (3.3)$$

$$a_{rms} = \frac{k_{res}\mu F_h}{\sqrt{22\zeta M^*}} \quad (3.4)$$

## 3.6 Modelling

A FEM model of 1F Public Area was designed in SAP2000, a program described in section 2.6. A constructed model that corresponds well with real-life measurement would allow for additional analysis. No calibration programs were available, limiting the possibility to update the model and construct an accurate simulation.

### 3.6.1 Numerical input


Since SAP2000 does not provide timber materials as a predefined choice, all material parameters had to be manually defined. Sintef certification contains calculated Young's modulus and shear modulus for the 5% and 50% fractile. The 50%-fractile was chosen since it was more likely to correspond to real strength than 5%, and shear modules were only provided for the 50%. Table 3.3 gives an overview of the calculated parameters and their axis. The length and width of the modelled floor were 11.5m long and 6m in width, the same as 1F Public Area. The area was chosen since the highest number of modes could be detected there. The mesh applied corresponds to the grid created for measurement, with the short side divided into 8 points and the long side into 11 points. Such a *coarse* grid limits the accuracy but was deemed adequate for a simple structure.

**Table 3.3:** Sintef calculated modulus

Fractile	E-modul for bending		Shear modul		
	Bending about axis		Bending about axis		
	Y (strong)	X (weak)	XZ (strong)	YZ (weak)	XY (rolling)
50% (160mm)	10284	2392	112	62	756
5 % (160mm)	6882	1602	-	-	-
50% (200mm)	10997	1757	126	50	761
5 % (200mm)	7369	1176	-	-	-

The area section in SAP2000 was modelled as a layered section with all sections from the floor. Table 3.4 gives all strength parameters, density, and thickness. Density and thickness were taken from Table 3.2 for most materials. Technical, vinyl and acoustic plates were combined into one technical layer with a thickness of 100mm to calculate density. All materials except CLT were assumed to have no bending strength.

**Table 3.4:** Properties of SAP200 layered section

Layer	Technical	Concrete	Acoustic	CLT	Model
Density $kg/m^3$	3.63	2120	15	470	
Thickness mm	100	60	5	200	
$E_y$ $N/mm^2$	-	-	-	10997	
$E_x$ $N/mm^2$	-	-	-	1757	
$E_z$ $N/mm^2$	-	-	-	1500	
$G_{xy}$ $N/mm^2$	-	-	-	761	
$G_{xz}$ $N/mm^2$	-	-	-	126	
$G_{yz}$ $N/mm^2$	-	-	-	50	



### 3.6.2 Boundary conditions

Boundary conditions were in the generated Artemis model shown not to be fixed, and significant movement could be seen. It was hypothesised that by modelling each joint along the area as a spring in the z-direction and fixing the x-and-y direction it would be possible to calibrate the spring with Hooke's Law.

Calibration with Eq 2.1 relied on the displacement provided by Artemis. Starting with an assumed spring stiffness of  $10 \text{ kN/mm}$  and dividing simulated force on real displacement, a more accurate  $k$  could be found. The process could then be repeated a number of times, sequentially providing a value closer to the actual stiffness.

The work was performed manually, and ten cycles were performed. For each cycle, the simulated force was divided on the real-life displacement. All editing was done through interactive database editing, a feature in SAP2000 allowing easy editing of a large number of joints.

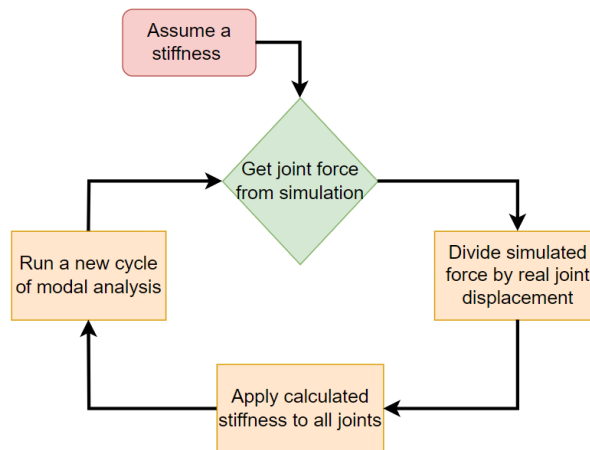


**Figure 3.17:** Flowchart for estimating joint stiffness in FEM model

### 3.6.3 Evaluation of model

Three criteria were checked to see the model's performance with each cycle. First is the difference in frequencies for all modes. The assumed stiffness could be verified by comparing the frequency found during the experiment with the simulated value. The total absolute difference between joint and sensor displacement was calculated to control how well the method for calibrating spring stiffness worked. Only displacement from edge sensors and joint were considered. Since there were no calibration programs available, a high MAC for higher modes was not anticipated.

## 4. Results and discussion

This chapter presents all results derived from the analytical tools in the methodology. For consistency, the results are presented with the same structure as the previous chapter. Results and discussions are combined enabling explanation and interpretation of figures and tables as they are presented. The first section describes various modal characteristics. The second section explores the influence of partition walls on the fundamental mode shape. The third and fourth sections show the distribution of acceleration at different points on the floors. The fifth section highlights the difference between calculated and measured values. Lastly, results from a FEM model of 1F Public Area are presented.

The naming schema for all results will be Floor Number - Area description - Test repetition - Excitation action. Table 4.1 has an overview of all tests performed and in which section they are used.

**Table 4.1:** Overview of selected tests cases for results and discussion section

Test identification	Modal Characteristics	Influence of secondary structures	Acceleration	VDV	Building Codes
1F Public Area H	•		•	•	•
1F Public Area W	•		•		•
2F Multi Span H	•	•			
2F Multi Span 2 H	•	•	•	•	•
2F Multi Span W			•		•
3F Single Span H	•	•			•
3F Single Span H W	•	•			
3F Multi Span H	•	•		•	
3F Multi Span W					
3F Classroom H	•	•			•
3F Classroom W			•		
3F Classroom W 2P			•		
3F Public Area H	•		•		•

*Notes: 3F Single Span H W denotes a single span with a wall atop, and 3F Classroom W 2P denotes a test with two people walking.*

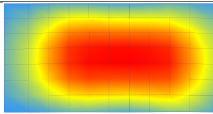
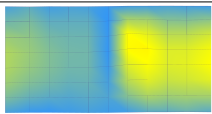
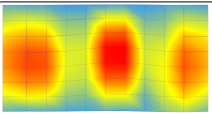
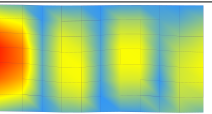
### 4.1 Modal Characteristics

Results of modal characteristics include a number of tables detailing the findings gathered from in-situ vibration of floors at Ås High School. All results are procured from Artemis Modal with the analytical OMA tool described in sections 2.7 and 3.3. The

mode shapes are always found with EFDD to be consistent across several tests. Frequencies and modes complexity are detected using EFDD and SSI-UPC Merged. Damping is found with previous methods but also includes results from CFDD. Discussion concerning damping and CFDD is presented in chapter 5 as they are better discussed in general than specific.

In the presentation of mode shapes similar areas share the same orientation, allowing for better comparison between them. *Public Area* always has the width along the x-axis and span along the y-axis. *Multi Span* and *Classroom* have spans along the x-axis and width on the y-axis. *Single Span* are orientated at an angle with span being the shorter side and width being the longer side of the rectangle. Description of all areas are presented in section 3.1.2 and will not be repeated in this section. The transversal direction is parallel to the width and the longitudinal direction is parallel to the span. The transversal direction is the same as the weak axis of CLT with other layers being perpendicular to it.

**Table 4.2:** Modal Characteristics of 1F Public Area H

Mode	1 <sup>th</sup>	2 <sup>th</sup>	3 <sup>th</sup>	4 <sup>th</sup>
Figure				
EFDD Frequency [Hz]	8.239	9.493	13.754	18.317
EFDD Complexity [%]	1.614	9.469	13.5	70.513
Mode separation [Hz]	-	1.254	4.261	4.463
SSI Frequency [Hz]	8.256	-	13.818	18.033
SSI Complexity [%]	0.682	-	1.292	6.98
EFDD Damping [%]	3.725	2.466	3.579	2.173
CFDD Damping [%]	2.51	1.372	2.006	1.184
SSI Damping [%]	3.975	-	2.688	2.928

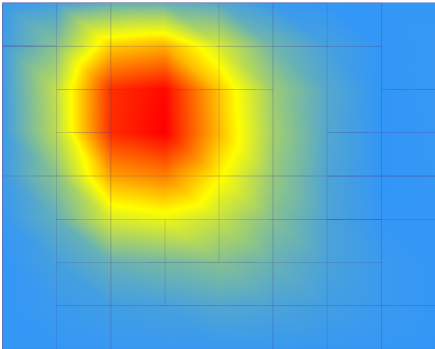
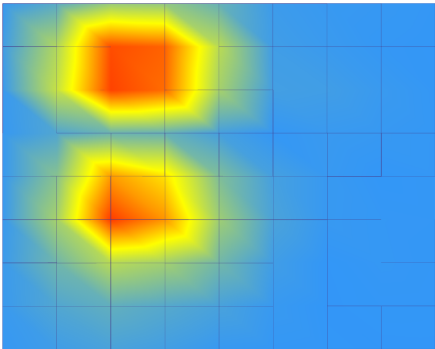
1F Public Area H was the only area where up to four mode shapes could be unambiguously detected. The clear mode shapes seen in Table 4.2 are likely the result of fewer local properties. Common local properties for the school are partition walls and point loads. 1F Public Area has in comparison with other areas much fewer local properties, which is reflected in reduced complexity. All mode shapes are behaving like four or three-side supported slabs, even when no supporting beam could be found on the shorter sides. The left side should receive an additional stiffness from the LVL railing running on top of it, producing a clamping effect. No element providing additional stiffness could be found on the right side.

The second mode shape has a relatively low complexity, but unclear presented mode shape. From observing the result in Artemis it seems that reference sensors were placed at the anti-nodes for the second mode. Reference sensors are not connected to the grid providing the graphical representation, only working in comparison with the roving sensors. Therefore when the reference sensor is experiencing a large movement relative

to roving sensors the mode shape gets less pronounced. Other tests performed in the area with different sensor placements show a much clearer shape for the second mode.

EFDD and SSI discovered similar natural frequencies for the floor, but SSI did not detect the second mode. EFDD has a much larger degree of complexity than SSI, growing quickly for each subsequent mode. Even with a complexity of 70.5 % for EFDD the mode shape could be clearly discerned.

**Table 4.3:** Modal Characteristics of 2F Multi Span H

Mode	1 <sup>th</sup>	2 <sup>th</sup>
Figure		
EFDD Frequency [Hz]	13.387	17.383
EFDD Complexity [%]	8.371	30.529
Mode separation [Hz]	-	3.996
SSI Frequency [Hz]	13.329	18.089
SSI Complexity [%]	1.665	29.043
EFDD Damping [%]	5.477	-
CFDD Damping [%]	3.356	-
SSI Damping [%]	4.717	4.889

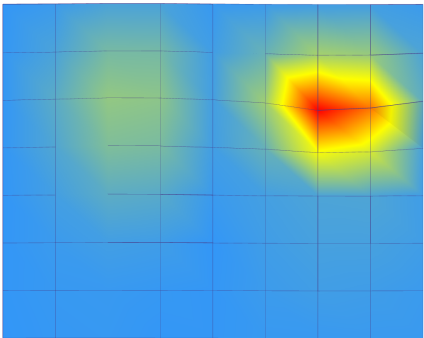
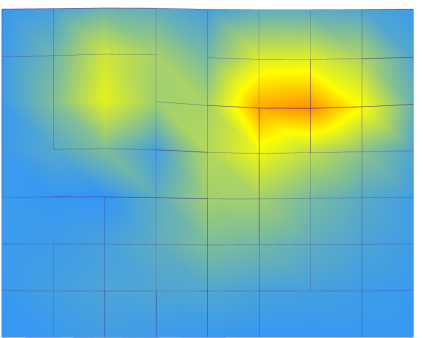
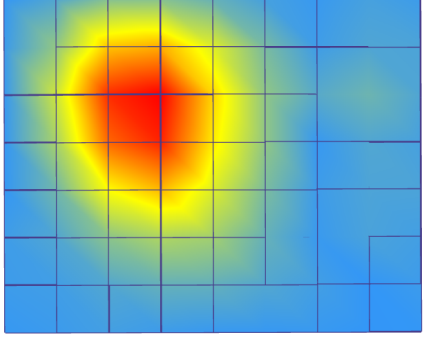
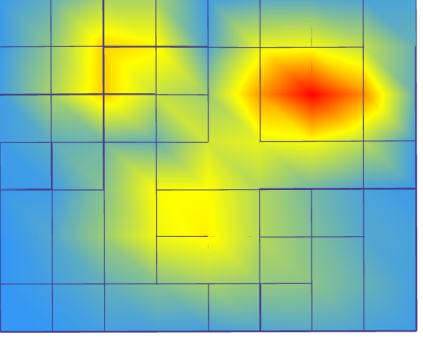
2F Multi Span H is the first of two different test setups for the same area. The area was the only place in the school where two spans are inside the same room. From the results, only two modes are included in Table 4.3 since higher modes could not be verified. While the area has no partition walls on top there are several underneath in a complex arrangement. These are likely providing local properties increasing complexity and creating complex mode shapes. All heel drops were performed in the top left side area. The location of the fundamental mode shape in the same area could be a combination of the floor plan and the excitation spot. This is discussed further in section 4.2, but the presence of partition walls distorts normal modes into complex shapes.

Discerning support beams from the mode shape is proven unreliable. There are three beams running underneath along the y-axis, two on the sides and one in the middle. No beams are running along the x-axis. Both the first and second modes are seeing movement across the middle beam and mode shapes are constrained moving down. Since the mode shape can not be discerned from knowing only beam placement, it is likely a combination of beams and partition walls are responsible.

The natural frequencies are considerably higher than other similar areas like 3F Multi Span and 3F Classroom. As the mass can be assumed to be similar the floor must receive

an additional stiffness. Partition walls are the most likely contributor since floor levels were found to play an insignificant role (Weckendorf et al., 2014). The complexity of 2F Multi Span H is lower than for 3F Multi Span H, even when the amount of partition walls is higher. Since all other factors than partition walls are similar, it seems like complexity is not directly correlated to the number of partition walls. Other factors like configuration, excitation, construction, etc must also play a role.

**Table 4.4:** Modal Characteristics of 2F Multi Span 2 H

Mode	1 <sup>th</sup>	2 <sup>th</sup>
Figure EFDD		
Figure SSI-Merged		
EFDD Frequency [Hz]	13.919	18.55
EFDD Complexity [%]	83.402	96.632
Mode separation [Hz]	-	4.631
SSI Frequency [Hz]	13.253	18.024
SSI Complexity [%]	10.624	34.189
EFDD Damping [%]	3.062	-
CFDD Damping [%]	-	-
SSI Damping [%]	3.828	9.616

2F Multi Span 2 H is an alternative version of the first version with a slightly different sensor grid setup. Results from the test presented in Table 4.4 were much more unclear than the first test. As the grid was mostly similar the difference must come from the change in excitation spot. The spot was moved from top left to top right in an attempt to excite the far right span. When using EFDD, mode shapes were not copied or mirrored. Instead, a highly localized mode was identified. Displacements were largely contained in a small area and the rest of the floor saw little movement. The second mode also changed direction, moving to the left instead of down.

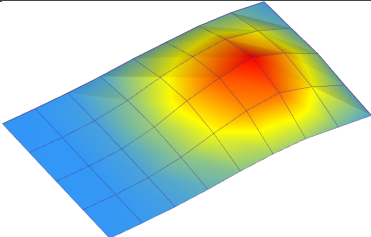
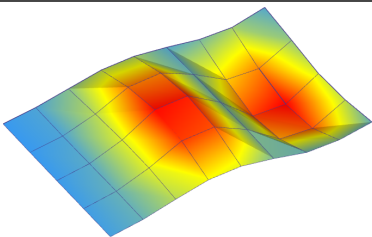
As the mode shapes were different from other results they were examined in detail. Mapping partition walls underneath show that displacement occurred almost on top of

them. As no other floors displayed this behaviour the modes shapes found with SSI-UPC Merged were also included. The fundamental mode shape with SSI was more similar to 2F Multi Span H. The second mode is still showing some differences. EFDD is most likely presenting a faulty result and will be ignored in further discussion. The reason why EFDD is so dissimilar to SSI is unknown and is not presented in other results.

The two versions of 2F Multi Span sharing the same fundamental mode shape indicate that placement of the first mode is a consequence of the system, not where excitation is created. Excitation was performed in two different spans, but fundamental mode shapes kept their shape.

Between 2F Multi Span H first and section version the natural frequencies is mostly similar, but there is some difference. The largest difference is the complexity of the mode shape, it being vastly greater for the second version. The large complexity of EFDD might be a reason for the difference in presented mode shapes. SSI is showing a complexity lower than EFDD, but is still much greater than in the first version

**Table 4.5:** Modal Characteristics of 2F Single Span H

Mode	1 <sup>th</sup>	2 <sup>th</sup>
Figure		
EFDD Frequency [Hz]	9.912	15.144
EFDD Complexity [%]	8.494	16.328
Mode separation [Hz]	-	5.232
SSI Frequency [Hz]	9.928	15.348
SSI Complexity [%]	7.52	2.448
EFDD Damping [%]	3.011	4.039
CFDD Damping [%]	2.193	2.174
SSI Damping [%]	2.817	4.427

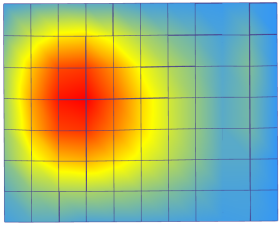
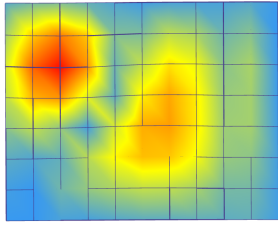
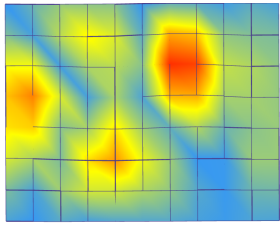
2F Single span is a single span between two columns in the classroom neighbouring 2F Multi Span. The site was chosen as a comparison to 3F Single Span and because it was highly susceptible to vibration. Participants in the experiment described the area as the section most severely impacted. Since higher modes were unclear only the first and second modes are included in Table 4.3. The shapes are similar to the ones detected in 2F Multi Span H.

Low vibration performance could not be discerned from modal characteristics. The span has a fundamental frequency above 8 Hz and good modal separation between the first and second (Ohlsson, 1982)(Ljunggren, 2006). An explanation of the perceived vibration

level being so high compared to other areas was the presence of kitchen cabinets. The cabinets were filled with kitchenware producing significant audible cues.

The mode shapes are largely contained within a single span contradicting all other results. Examination of floor plans shows that classrooms on the first floor are around 6m. The 5m span of 2F Single Span is placed inside this 6m long classroom. The first-floor plan is mirrored underneath, meaning the left side of 2F Multi Span and 2F Single Span correspond.

**Table 4.6:** Modal Characteristics of 3F Multi Span H

Mode	1 <sup>th</sup>	2 <sup>th</sup>	3 <sup>th</sup>
Figure			
EFDD Frequency [Hz]	7.903	11.718	18.848
EFDD Complexity [%]	17.666	36.791	86.192
Mode separation [Hz]	-	3.815	7.130
SSI Frequency [Hz]	7.849	11.655	12.779
SSI Complexity [%]	1.029	9.47	23.671
EFDD Damping [%]	2.896	3.523	-
CFDD Damping [%]	1.904	1.948	-
SSI Damping [%]	2.635	7.488	4.781

3F Multi Span H was performed across two spans in different classrooms. A partition wall was placed atop the second span, separating the two rooms. The difference between 2F and 3F Multi Span is the floor level and placement of partition walls. From mode shapes in Table 4.6, much more of the floor is actuated by the heel drop. Both spans saw a significant degree of movement even when excitation occurred in the left side span. While more mode shapes were detected for 3F Multi Span H than 2F Multi Span H, the detected shapes are more ambiguous. This is reflected in the higher complexity even when the floor plan has fewer partition walls.

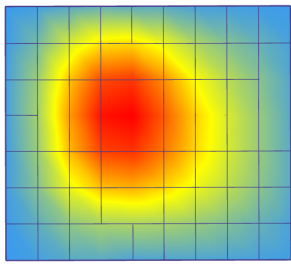
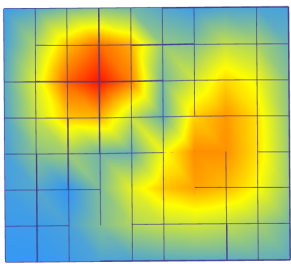
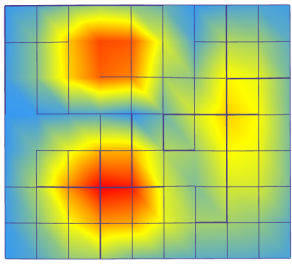
Mode shapes indicate that the transfer of motion between the two classrooms is hindered to a certain degree, but how much is not possible to determine. On the right of the floor, there is an interaction between the partition wall and beam. The area oscillates at a higher frequency than the rest of the floor. When utilising prEC5 to calculate fundamental frequency, the  $k_{e,1}$  factor accounts for multiple spans. It increases as the relationship between the longest and shortest span increases (CEN, 2023). The increase in frequency for the floor area could be explained by it being a smaller span and the partition wall acting as a pseudo-boundary condition.

Comparing 3F and 2F Multi Span H, the natural frequencies and damping values are lower on the third floor. All else being equal, the likely source of the difference is

partition walls. 3F Multi Span H natural frequency for the third mode is not matching between SSI and EFDD, a discrepancy of 6 Hz. The discrepancy is followed up on in 3F classroom H and seems to be EFDD and SSI detecting different modes.



**Table 4.7:** Modal Characteristics of 3F Classroom H

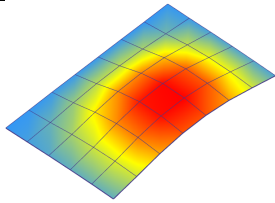
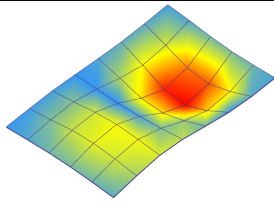
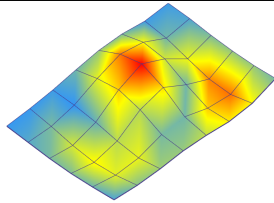
Mode	1 <sup>th</sup>	2 <sup>th</sup>	3 <sup>th</sup>
Figure			
EFDD Frequency [Hz]	7.893	11.718	13.477
EFDD Complexity [%]	1.285	45.864	32.868
Mode separation [Hz]	-	3.825	1.759
SSI Frequency [Hz]	7.842	11.457	12.79
SSI Complexity [%]	0.268	11.622	27.895
EFDD Damping [%]	3.403	3.067	-
CFDD Damping [%]	2.147	1.616	-
SSI Damping [%]	2.546	4.565	2.554

3F Classroom H was performed on an area corresponding with 3F Multi Span H, but partition walls of the classroom are used as boundaries instead of beams. The right side of shapes presented in Table 4.7 corresponds to the partition wall in 3F Multi Span. The first mode has its anti-node in the centre of the floor, actuating the whole room in its motion. Detected natural frequencies for the first and second modes match the previous test, but the third mode deviates.

The third mode in the table differs from that in Table 4.6. The third mode displays another shape more similar to the second mode seen in 2F Multi Span H. The frequency has also fallen for EFDD, matching that of SSI, unlike in 3F Multi Span H where EFDD was higher than SSI. It is likely that third mode shown in the table is different from the third mode shown in Table 4.7. A transversal second mode for the first span is possible. These are not detected in other multi-span tests without interference from partition walls but can be seen in single-span tests.

The degree of complexity for a mode shape moves independently from each other. We are seeing a reduction in complexity for the first mode and an increase in the second mode. The first mode has the lowest complexity of all classroom tests. The second mode has the second highest complexity, with only 2F Multi Span 2 H being higher. No comparison is drawn between third modes since they are most likely unrelated.

**Table 4.8:** Modal Characteristics of 3F Single Span H

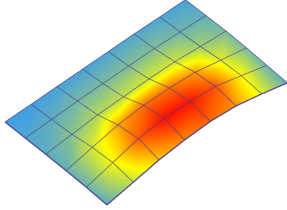
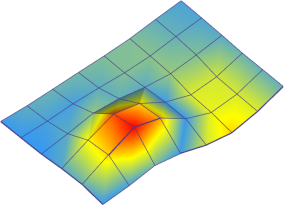
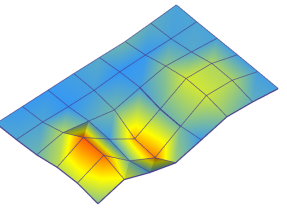
Mode	1 <sup>th</sup>	2 <sup>th</sup>	3 <sup>th</sup>
Figure			
EFDD Frequency [Hz]	8.808	14.335	19.923
EFDD Complexity [%]	17.159	42.272	78.608
Mode separation [Hz]	-	5.527	5.588
SSI Frequency [Hz]	8.691	-	20.231
SSI Complexity [%]	1.284	-	34.08
EFDD Damping [%]	5.476	4.462	2.1
CFDD Damping [%]	3.038	2.487	1.027
SSI Damping [%]	5.488	-	3.842

3F Single Span was performed in the classroom opposite to the 3F Multi Span and 3F classroom. It has the same construction and geometry as 2F Single Span and 3F Single Span with a wall. Comparison between 3F Single Span with and without wall are discussed for Table 4.9. Comparing mode shapes between Table 4.8 and 2F Single Span H, we see similar shapes for the first and second modes. The difference between the 2F and 3F Single Span is that a higher percentage of the floor is actuated. The shape is going edge to edge instead of stopping before reaching the corridor edge, both reaching the facade edge. Observing the floor plan, this is the result of partition walls. The distance from the window to the corridor is 5.75m on the first floor and 8m on the second and third floors.

Corroborating discussion on 2F Single Span H the first mode shape is not contained within the beams, meaning the containment seen on the second floor is likely to stem from the partition wall under it. The second mode is contained within the single span, similar to what is seen in Table 4.7. The long left side is likely a stable boundary because the partition wall runs atop and underneath. Both the second and third mode is transversal, indicating lower stiffness in the direction perpendicular to the CLT outer layers.

For 3F Single Span H, the EFDD and SSI mostly agree on natural frequencies. The single span is experiencing higher natural frequencies than 3F Multi Span. The reason for the discrepancy is unknown since the relationship between mass and stiffness should be the same. Single span on the second floor had significantly higher natural frequencies, likely caused by the proximity of partition walls to beams on both sides.

**Table 4.9:** Modal Characteristics of 3F Single Span H W

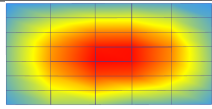
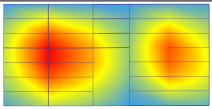
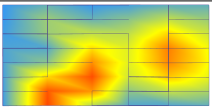
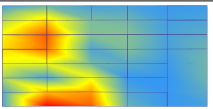
Mode	1 <sup>th</sup>	2 <sup>th</sup>	3 <sup>th</sup>
Figure			
EFDD Frequency [Hz]	11.57	18.529	27.211
EFDD Complexity [%]	19.654	49.557	98.538
Mode separation [Hz]	-	6.959	8.682
SSI Frequency [Hz]	10.746	21.243	-
SSI Complexity [%]	4.575	38.248	-
EFDD Damping [%]	6.106	2.014	2.89
CFDD Damping [%]	3.338	2.363	1.735
SSI Damping [%]	7.303	6.554	-

3F Single Span H W highlights the influence of partition walls placed on top of the floor slab. A direct comparison can be drawn between Table 4.9 and other single-span tests. The mode shapes have been rotated 180° to better compare it to 3F Single Span. The fixed boundary seen in both tests is the same, meaning for 3 Single Span W the facade is at the bottom and the corridor on top.

The shapes corroborate previous discussions concerning the importance of partition walls in creating boundary conditions. Influence from the partition wall can be observed in all mode shapes. It restricts the transfer of motion and compresses the mode shapes to the right side. Excitation was created on both sides of the partition wall, but motion mainly occurs on the largest section. The action only slightly increases the complexity of the mode shape but massively increases the natural frequencies.

Damping has increased across the board, except for EFDD damping second mode. The reason it is decreasing by more than 50 % is unknown. However, it highlights the complexity of the phenomena of damping.

**Table 4.10:** Modal Characteristics of 3F Public Area H

Mode	1 <sup>th</sup>	2 <sup>th</sup>	3 <sup>th</sup>	4 <sup>th</sup>
Figure				
EFDD Frequency [Hz]	6.194	7.286	9.185	12.05
EFDD Complexity [%]	27.096	11.257	43.241	37.973
Mode separation [Hz]	-	1.092	1.899	2.865
SSI Frequency [Hz]	6.073	7.192	-	11.915
SSI Complexity [%]	4.859	1.018	-	32.305
EFDD Damping [%]	3.39	2.702	1.601	3.258
CFDD Damping [%]	1.571	1.463	-	1.285
SSI Damping [%]	4.543	2.137	-	7.163

3F Public Area shares the same placement at a different level and 6m span with 1F Public Area. The floor only has 160mm CLT compared to the 200mm CLT in 1F Public Area, meaning lower flexural rigidity. On top there are also placed a series of heavy

cabinets providing considerable point loads. With a reduced stiffness and increased mass, the lower natural frequencies seen in Table 4.10 were expected. Natural frequencies for higher modes have also dropped, reducing the frequency separation between all modes.

The shapes for the first and second modes are increasingly complex but still unambiguously in shape. Higher modes see a much more complex shape and display the presence of a heavy weight on the right side. This is unlike the results seen in Kawzra, where the higher modes were more resistant to added weight (Kawzra et al., 2021). EFDD and SSI predict very similar natural frequencies for the systems.

Damping values between EFDD and SSI are very different for all modes. Comparing values between 1F Public Area and 3F Public Area it may be seen that there is no consistent increase or decrease in damping values. The first mode damping is higher for SSI, but lower for EFDD. Similar back and forth is shown for all four modes, highlighting the difficulty of drawing conclusions on damping on a test-to-test basis.

**Table 4.11:** Overview of all EFDD and SSI-Merged frequencies and damping values derived from heel drop tests

OMA Tool	Test	$F_1$	$D_1$	$F_2$	$D_2$	$F_3$	$D_3$	$F_4$	$D_4$	Modal damping
EFDD	1F Public Area H	8.239	3.725	9.493	2.466	13.754	3.579	18.317	2.173	2.99
SSI-Merged		8.256	3.975	-	-	13.818	2.688	18.033	2.928	3.20
EFDD	2F Multi Span H	13.387	5.477	17.383	-	-	-	-	-	5.48
SSI-Merged		13.329	4.717	18.089	4.889	-	-	-	-	4.80
EFDD	2F Multi Span 2H	13.919	3.062	18.55	-	-	-	-	-	3.06
SSI-Merged		13.253	3.828	18.024	9.616	-	-	-	-	6.72
EFDD	2F Single Span H	9.912	3.011	15.144	4.039	-	-	-	-	3.53
SSI-Merged		9.928	2.817	15.348	4.427	-	-	-	-	3.62
EFDD	3F Multi Span H	7.903	2.896	11.718	3.523	18.848	-	-	-	3.21
SSI-Merged		7.849	2.6635	11.655	7.488	12.779	4.781	-	-	4.98
EFDD	3F Classroom H	7.893	3.403	11.718	3.067	13.477	-	-	-	3.24
SSI-Merged		7.842	2.546	11.457	4.565	12.79	2.554	-	-	3.22
EFDD	3F Single Span H	8.808	5.476	14.335	4.462	19.923	2.1	-	-	4.01
SSI-Merged		8.691	5.488	-	-	20.231	3.842	-	-	4.67
EFDD	3F Single Span H with wall	11.57	6.106	18.529	2.014	27.211	2.89	-	-	3.67
SSI-Merged		10.746	7.303	21.243	6.554	-	-	-	-	6.93
EFDD	3F Public Area H	6.194	3.39	7.286	2.702	9.185	1.601	12.05	3.258	2.74
SSI-Merged		6.073	4.543	7.192	2.137	-	-	11.915	7.163	4.61

Table 4.11 is a final presentation for all EFDD and SSI-Merged values presented in the section. Modal damping refers to the average damping of all identified modes.

## 4.2 Influence of secondary structures

To better understand the influence of non-bearing partition walls on the deformed shape, the fundamental mode shape of the selected area is presented overlaid on the floor plan. On the floor plan, both beams and partition walls are presented so the reader can see their contribution. Beams are represented by red lines, and partition walls with white lines. Only the first mode is explored, but conclusions for higher modes can be drawn by comparing mode shapes in section 4.1. 1F and 3F Public Area are omitted since they are affected by fewer partition walls and generally has less complex mode shapes

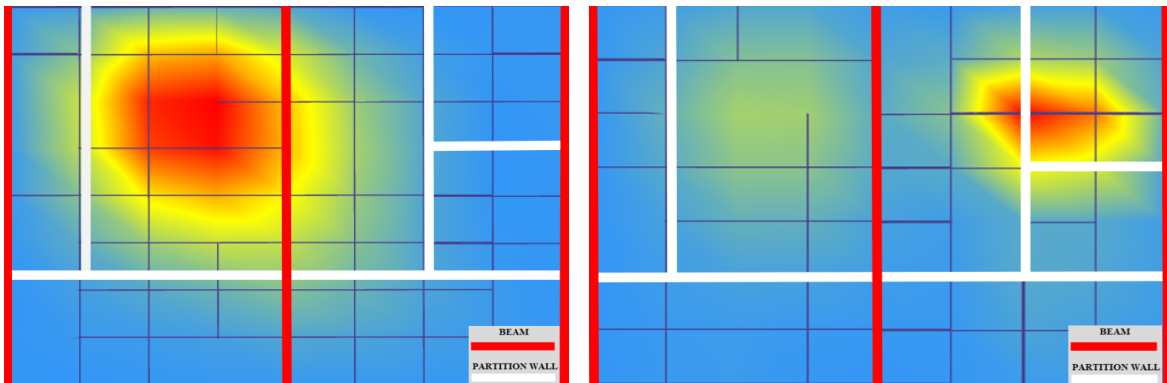


**Figure 4.1:** The fundamental mode of 2F Multi Span H overlaid on structures

**Figure 4.2:** The fundamental mode of 2F Multi Span 2 H overlaid on structures

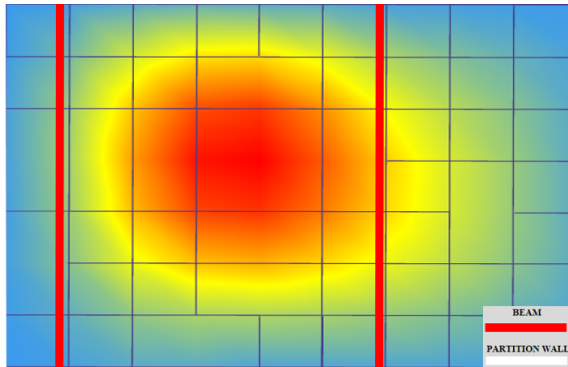
Figure 4.1 and Figure 4.2 shows how partition walls are affecting the mode shapes in 2F Multi Span H and 2F Multi Span 2 H. Since the two test covers the same area a direct comparison can be drawn.

In the first figure, excitation is primarily contained within a large rectangle created by partition walls and beams. Heel drops were performed approximately in the same area as the first mode can be seen. The horizontal wall marking the first-floor corridor provides a robust barrier against the downward motion. Containment on the left and right side is performed by either a partition wall or beam, but motion seems to move across the beam more than across the partition walls.

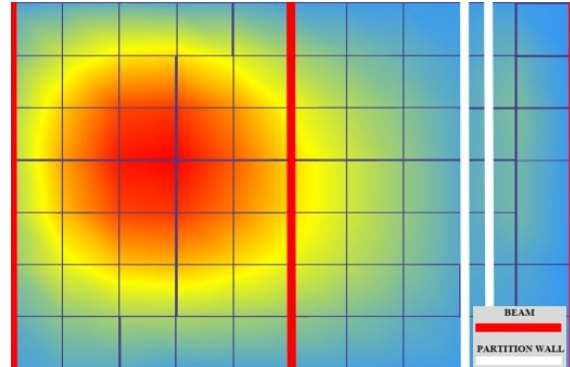
The difficulty of exciting the right side span is likely due to how the partition walls are configured. A combination of vertical and horizontal walls would provide a robust geometric shape with significant stiffness. From SSI mode shape in Figure 4.3 we can discern that the most extensive motion is occurring in the span not excited. The first mode's placement is a consequence of the system, not where excitation is created.

Figure 4.2 covering 2F Multi Span 2 H corroborate the decision of ignoring the mode

shape provided by EFDD. As discussed for Table 4.3 it is unlikely that the most extensive movement would occur right on top of the partition walls. The result is likely faulty, and the time-history-based SSI provides a better representation. SSI-Merged shows some movement in the top right rectangle, which is picked up by the VDV-contour in Figure 4.12. Therefore, some acceleration occurs in the top right but should not be the most affected area.



**Figure 4.3:** The fundamental mode of 3F Classroom H overlaid on structures

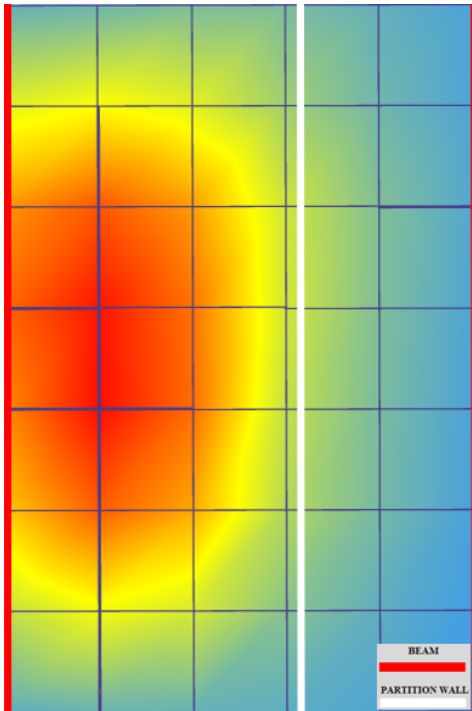


**Figure 4.4:** The fundamental mode of 3F Multi Span H overlaid on structures

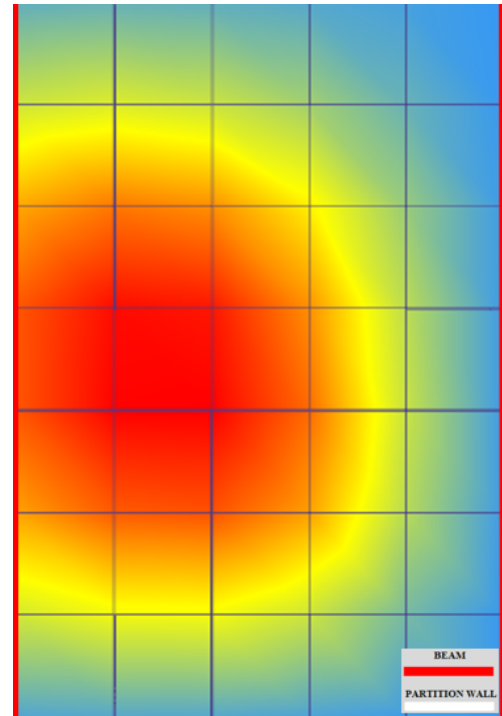
Figure 4.3 and 4.4 show the impact of partition walls and beams on mode shapes found for 3F Classroom and 3F Multi Span. While they do not directly correlate, they correspond to a high degree and can be compared.

Figure 4.3 goes from one partition wall to another, running over two beams. The lowest part of the mode shape is approximately 4m from the first wall and 5m from the other. Heel drops were performed in the left side span, but results from Tables 4.3 and 4.4 indicate that the fundamental mode shape is independent of the excitation spot. There is a noticeable difference in the amount of motion transferred across the left and right beams. As proximity to partition walls are the only difference, this is likely the source. The beam and partition wall interact, providing a combined stiffness dependent on the distance between them.

Figure 4.4 covers a 10m multi-span with beams every 5m. Two partition walls are placed close together on the far right side. The shape is unsurprisingly similar to the first figure, missing the far left part. A slight amplification in acceleration happens in the small span between the partition wall and the right side beam. The motion tapers off as it approaches the walls but creates a more significant motion on the other side again between the right beam and partition walls. This makes sense from Eq (2.33b) and Figure 2.12 if the partition wall forms a boundary condition and there is a smaller modal mass in the area compared to the rest of the floor.



**Figure 4.5:** The fundamental mode of 3F Single Span H W overlaid on structures



**Figure 4.6:** The fundamental mode of 3F Single Span H overlaid on structures

Figure 4.5 and 4.6 display the effect of placing a partition wall on top of a span. The two spans are next to each other with 3F Single Span H W being rotated 180°, meaning the fixed boundary seen in both matches. Partition walls shown in Figure 4.5 matches the walls in the right side span in Figure 4.4.

The partition wall effect on mode shapes is visible from the two figures. Partition walls form a clear boundary and hinder motion transfer between classrooms. Observing higher mode shapes in Table 4.9 the presence of the partition wall affects not only the first mode but also higher modes. These final figures corroborate results from other tests, showing the effect of the partition wall in restricting mode shapes and that interacting between beam and partition wall creates boundary conditions. The amplification of acceleration seen in Figure 4.4 is not seen repeated in Figure 4.9. There is no definitive reason for why the phenomenon is not repeated.

### 4.3 Time history response

To better understand how different points on the floor performed, acceleration measured by reference sensors is analysed. Reference sensors are ideal since they are placed with space in between them at the same tests. If roving sensors were used, a slight difference in excitation would be expected since different heel drops were measured.

Every table includes  $a_{rms}$ ,  $a_{peak}$  and VDV . Three different methods for evaluating vibration performance through acceleration. ISO 10137 and BS 6472 use VDV to categorise floor performance (ISO, 2007) (BSI, 2008). ISO 10137 also gives guidance on evaluating  $a_{rms}$ , and from the literature one could use Chui’s scale presented in Figure 2.7. The  $a_{rms}$  presented in prEC5 are for evaluating a calculated value and will therefore not be used to evaluate a measured value (CEN, 2023). Peak acceleration verification is not presented in this thesis but is discussed in literature (Han et al., 2009) and used in the AISC 11 (AISC, 2016). For this reason, discussion on  $a_{peak}$  will not include human sensitivity, only focusing on it as a physical value.

Every table includes acceleration data from reference sensors 1 and 2 when available if not only 1 is included. The first column is data from the heel drop test where excitation happens in a fixed place. The second column is data from one person walking around the floor. Both tests have the same time period of 2 minutes, but walking simulates steady-state and heel drop transient excitation. The precise location of reference sensors 1 and 2 can be found in annex A.

Under VDV is  $i$ , this symbolises the number of doses needed to override a  $VDV_{tot}$  limit of 0.4 and is calculated with Eq (3.1b).

**Table 4.12:** Time history from 1F Public Area

Test	1F Public Area Heel		1F Public Area Walk	
Sensor	Ref. 1	Ref. 2	Sensor 1	-
$a_{rms}$ [ $m/s^2$ ]	0.06999	0.07571	0.06794	-
$a_{peak}$ [ $m/s^2$ ]	0.44290	0.46410	0.15480	-
VDV [ $m/s^{-1.75}$ ]	0.3139	0.3088	0.08437	-
$i$	2.63	2.81	505.2	-

The acceleration measured by reference sensors on 1F Public Area is shown in Table 4.12. No walking was performed with the 1F Public Area H set-up, but an independent walking test was performed with sensor 1 in the centre.

All sensors experience similar  $a_{rms}$  with the highest value being only 11.4 % higher than the lowest. The lowest  $a_{rms}$  were found for walking representing steady-state, and higher values were measured for heel drop. The ratio was expected since the oscillation’s largest amplitude should be during the transient response (Chopra, 2019). Figure 2.5 also displays that walking has a lower force-to-weight ratio than jumping. Heel drops are more similar to jumping than walking and should produce a larger response.

The measured  $a_{peak}$  is considerably higher for heel drops than walking. However, internally in heel drop, there is little difference between Ref.1 and Ref.2. Largest peak acceleration from heel drop is 186 % higher than what was produced by walking. The



relationship between  $a_{rms}$  and  $a_{peak}$  for Ref.1 is 6.3, which is much larger than the relationship proposed in Table 2.4 corroborated by literature (Smith et al., 2007)(AISC, 2016).

VDV and  $i$  are similar between heel drop sensors, but heel drop is vastly higher than walking. This is a consequence of the higher peak values produced by transient excitation. Actions similar to heel drops are less likely to occur in a school but would only need to happen 2-3 times a day to be perceived as a problem. There is no chance of 1F Public Area W ever becoming a problem when evaluated through VDV.

**Table 4.13:** Time history from 2F Multi Span

Test	2F Multi Span 2 H		2F Multi Span 2 W	
Sensor	Ref. 1	Ref. 2	Ref. 1	Ref. 2
$a_{rms}$ [ $m/s^2$ ]	0.10851	0.06893	0.06798	0.07081
$a_{peak}$ [ $m/s^2$ ]	1.23800	0.26850	0.27500	0.18910
VDV [ $m/s^{-1.75}$ ]	0.7101	0.1156	0.06505	0.06741
$i$	0.10	143.4	1428.8	1239.8

For 2F Multi Span, heel drop and walking were performed on the same set-up. Therefore, reference sensors shown in Table 4.13 share the exact location. Readers can see the precise location of reference sensors in relation to partition walls in Annex A.

Similar to 1F Public Area  $a_{rms}$  are similar between heel drop and walking, with Ref.1 heel drop being an outlier. Such a large difference between two references for the same excitation is not found in any other tests, Ref.1 being 57.4 % higher than Ref.2. Observing the placement of Ref.1 in Figure 4.2, it was placed close to the anti-node of the fundamental mode. In comparison, Ref.2 was placed in a relatively undisturbed area. The relationship flips for the walking test, Ref.2 being higher than Ref.1. Since the difference is quite small this can be the result of random excitation. The effect of partition walls on the acceleration distribution is reduced when excitation is random.

Peak acceleration again has Ref.1 as an outlier, being 461 % higher than Ref.2. Stability of Ref.2 is also shown in that it experiences  $a_{peak}$  closer to walking. Ref.1 walking is also impacted by placement, but the difference is relatively smaller between Ref.1 and Ref.2 for walking. Ref.2 walking has measured a smaller peak but higher rms-acceleration. As a negative relationship is unsupported in theory, it is likely that a more significant share of the random walking happened close to it (AISC, 2016).

The presence of partition walls is shown in a more uneven distribution of VDV and  $i$ . Depending on the location, one can perform the heel drops 1 or 144 times before exceeding the limit. Walking produces a lower VDV on 2F Multi Span than 1F Public Area. Partition walls might contribute positively and reduce acceleration. The difference is somewhat exaggerated by VDV being to the power of four, making it better in discriminating (Ussher et al., 2022).

**Table 4.14:** Time history from 3F Classroom

Test	3F Classroom Heel		3F Classroom Walking 1P		3F Classroom Walking 2P	
	Ref. 1	Ref. 2	Ref. 1	Ref. 2	Ref. 1	Ref. 2
$a_{rms}$ [ $m/s^2$ ]	0.09382	0.10205	0.0714	0.07402	0.07767	0.07987
$a_{peak}$ [ $m/s^2$ ]	0.59060	0.74940	0.18060	0.11610	0.27660	0.26280
VDV [ $m/s^{-1.75}$ ]	0.3541	0.4693	0.07550	0.07054	0.16690	0.16360
$i$	1.62	0.52	787.7	1034	33	35.7

For 3F Classroom, two kinds of walking were performed: one person walking and two persons walking. The walking was limited to two lines along the length of the classroom. No rhythm was imposed, but the two persons walked out of phase with each other. Table 4.14 includes values from both walking tests and heel drop.

There is a difference of 29 % between heel drop and walking average  $a_{rms}$ , more significant than the difference seen for 1F Public Area. Different excitation produced similar rms-acceleration for both sensors, and adding an extra person to walking only slightly increased the rms-acceleration. Corroborating discussion for Table 4.13, some areas are experiencing an inverse relationship between  $a_{rms}$  and  $a_{peak}$ . The relationship only occurs for walking and is likely a result of a higher level of randomness.

Addition of an extra person walking increased peak acceleration between 53-125 %, a massive increase. While walking is a constant excitation, there is a more significant growth in the peak acceleration than in the measurement for overall acceleration  $a_{rms}$ .

VDV and  $i$  are also impacted by adding one more person walking. One more person walking increases VDV significantly, reducing the  $i$ . From Eq (2.26) and ISO 10137, we know that impact from multiple people can be summed to find total force (ISO, 2007). As the force increases, the acceleration must also increase, see Eq (2.12). The precise relationship between adding additional people and produced force has yet to be discovered. From theory, an unknown number of people walking should exceed one person's heel dropping. Knowing this relationship could contribute to easier testing as fewer people would be needed.

3F Public Area only has heel drop acceleration since no walking was performed there. Table 4.15 can only provide one type of acceleration. The area resembles 1F Public Area in that no partition walls are present. The floor's cross-section is slightly different with

**Table 4.15:** Time history from 3F Public Area

Test	3F Public Area Heel	
Sensor	Ref. 1	Ref. 2
$a_{rms}$ [ $m/s^2$ ]	0.07740	0.08814
$a_{peak}$ [ $m/s^2$ ]	0.30390	0.55900
VDV [ $m/s^{-1.75}$ ]	0.2172	0.3925
i	11.5	1

lower stiffness, and 3F Public Area has several heavy cabinets atop it. Ref.2 is placed in the cabinet area, and Ref.1 is in the open area, consult annex A for precise placement.

The difference in  $a_{rms}$  between Ref.1 and Ref.2 is relatively higher for 3F Public Area than 1F Public Area. Ref.2 is 14.3 % higher than Ref.1 the difference was 8 % at 1F Public Area. Being constructed with 160mm CLT instead of 200mm, the third-level floor has a lower modal mass than the first. Lower modal mass is reflected in it having higher  $a_{rms}$  than the heavier first level floors (Smith et al., 2007)(CEN, 2023).

There is a much more significant difference between  $a_{peak}$ , Ref.2 is experiencing a peak almost twice that of Ref.1. This difference was not found in 1F Public Area, which had almost identical peak acceleration for the two sensors. While differences in peak acceleration exist across the floors, Ref.2 being closer to the edge should have received the lowest amount. The presence of cabinets could lead to an alternative distribution of peak acceleration compared to 1F Public Area.

Peak acceleration seems to increase with the addition of a point load. Observing Eq (2.2), if the mass of the floor is constant, then the added force acting on it must increase acceleration. From D'Alembert's principle, the restoring force must grow proportionately to the added load (Crépel, 2005). Cabinets are, therefore, decreasing the floor's fundamental frequency through added mass and increasing the acceleration of an area as point loads.

## 4.4 The distribution of VDV

To better understand the distribution of VDV across different floors, all roving sensors for 1F Public Area H, 2F Multi Span 2 H, and 3F Multi Span H had VDV calculated and analysed. The previous section 4.3 used data from reference sensors, and the data is therefore not included. The analysis performed was chosen to highlight the uniformity or dissimilarity of acceleration at different areas and how they compare with discovered fundamental mode shapes. No walking tests were included since all mode shapes were found with heel drops.

**Table 4.16:** Statistical analysis of VDV results for different floors

Area	1F Public Area H	2F Multi Span 2 H	3F Multi Span H
Max VDV [ $m \cdot s^{-1.75}$ ]	0.5096	0.5256	0.8366
Mean VDV [ $m \cdot s^{-1.75}$ ]	0.2464	0.0839	0.2743
Median VDV [ $m \cdot s^{-1.75}$ ]	0.2511	0.0373	0.2217
STD.dev	0.1351	0.1222	0.1993
Kurtosis	-1.0799	5.6055	-0.4166
Skewness	-0.1114	2.4440	0.6885

Statistical analysis of the distribution is presented in Table 4.16. Max VDV for 1F Public Area H and 2F Multi Span 2 H is similar. This relationship is not shown in any other data and is most likely a coincidence produced by a low number of tests. The two floors have different cross-sections, span-length and amount of partition walls. 3F Multi Span H has the highest VDV value, higher than measured through reference sensors in Table 4.14. Evaluating max VDV with limits purposed by BS 6472 in Table 2.7 all floors are problem areas (BSI, 2008).

Supporting the conclusion that max VDV being similar is a coincidence is the difference between mean and median for 1F Public Area H and 2F Multi Span 2 H. The mean and median are much more similar between 1F Public Area H and 3F Multi Span H. 2F Multi Span 2 H in comparison has a much lower average value, reflecting containment of excitation in Figure 4.2.

3F Multi Span H has the highest standard deviation. However, only 2F Multi Span 2 H has a coefficient of variance above 1. 1F Public Area H and 3F Multi Span H can be considered low variance. 2F Multi Span 2 H also have much higher skewness and kurtosis. Indicating most values are similar, but some extreme values are vastly greater than the mean. The other areas have a lower kurtosis and skewness. Meaning that data are distributed more symmetrically and have longer tails than the normal distribution. A graphical representation for standard deviation, kurtosis and skewness can be seen in Figures 4.7 to 4.9.

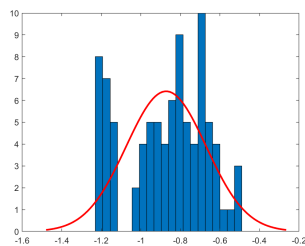


**Figure 4.7:**  
Histogram for  
1F Public Area  
VDV

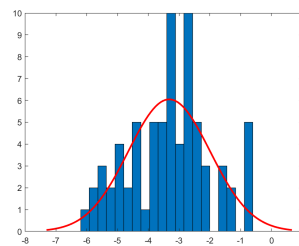


**Figure 4.8:**  
Histogram of  
2F Multi Span  
2 H VDV

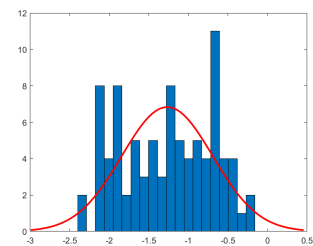


**Figure 4.9:**  
Histogram of  
3F Multi Span  
H VDV

Contour shapes in Figures 4.10 to 4.15 show the distribution of VDV and  $a_{rms}$  in an alternating sequence. Plotted values can be found in annex C and distribution for all plots can be compared to mode shapes in section 4.1.

The clean mode shapes found in Table 4.2 are reflected in the VDV contour, less so for  $a_{rms}$  contour. For 1F Public Area H, the VDV contour in Figure 4.10 indicates three different anti-nodes with the largest concentration of acceleration. In comparison, the  $a_{rms}$  contour in Figure 4.11 is harder to interpret. It has no clearly defined edge but shares two anti-nodes with the VDV contour. The even distribution is apparent when comparing the VDV contour to the statistical analysis. The centre of the floor is experiencing the highest VDV, as one approaches the edges smaller values are measured.

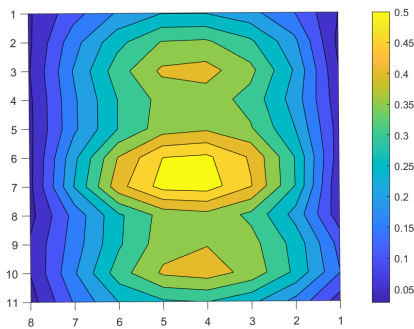


**Figure 4.10:** 1F Public Area VDV-contour

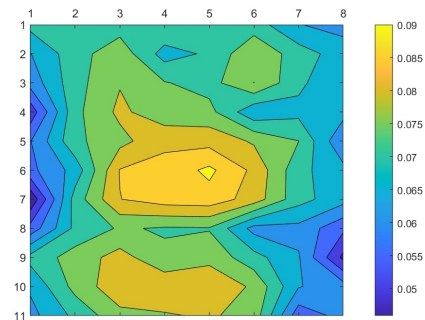


**Figure 4.11:** 1F Public Area H  $a_{rms}$ -contour

Contour shapes in Figures 4.12 and 4.13 for 2F Multi Span 2 H share the same characteristics as 1F Public Area H. The partition walls clearly affect the distribution, as discussed in section 4.2. Mode shapes and VDV contours mostly line up, but the contour moves down to a much higher degree. As no motion could be detected at the bottom when inspecting the fundamental mode shape, this is likely acceleration from higher modes. The island of motion in 2F Multi Span 2 H mode shapes can also be seen in the top right.

The  $a_{rms}$  contour is hard to understand and measures some acceleration along the edges. This acceleration around the edges can be seen in all contours. Weckendorf found that vibration transfer between areas occurs at higher frequencies, around 60 Hz (Weckendorf et al., 2014). VDV is calculated with weighted  $a_{rms}$  where such high frequencies are given a low weight. The weighting of acceleration at specific frequencies is likely why VDV do not go all the way to the walls but unweighted  $a_{rms}$  do. An interaction between the walls and the floor might produce an additional acceleration at higher frequencies.

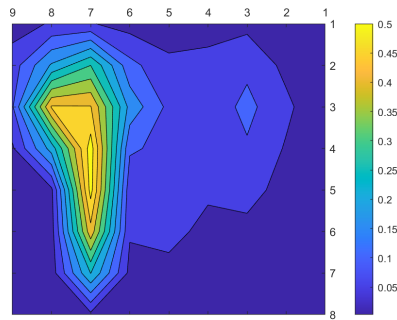


**Figure 4.12:** 2F Multi Span 2 H VDV-contour

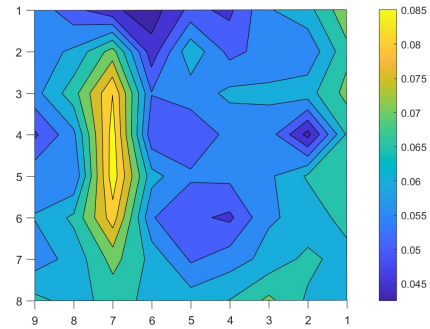


**Figure 4.13:** 2F Multi Span 2 H  $a_{rms}$ -contour

3F Multi Span H contours in Figure 4.14 and 4.15 corroborate the previous discussion, VDV is providing a contour that resembles the actual mode shape much more than  $a_{rms}$  can. The two contour shapes share the same large area of acceleration on the left side, but Figure 4.15 has a confusing distribution elsewhere. The partition wall and increased acceleration can be seen on the right side of both contours, but VDV is much more straightforward.

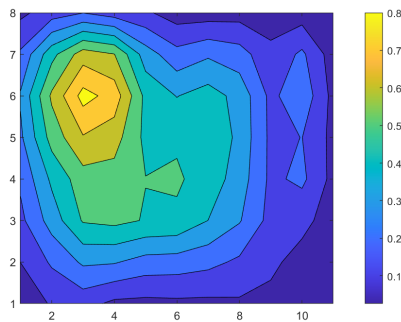


**Figure 4.14:** 3F Multi Span H VDV-contour

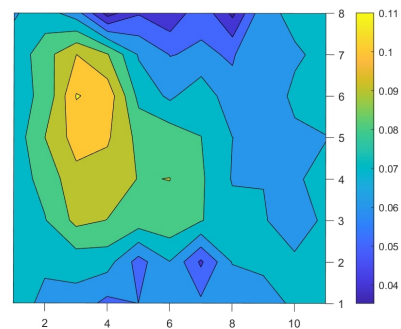


**Figure 4.15:** 3F Multi Span  $a_{rms}$ -contour

Contour maps always have the same shape, with the highest value at the fundamental mode's anti-node. They also have an elongated shape limited to the span containing the anti-node. It could be theorised that contour maps present a superposition, with the fundamental mode and mode (2,2) in Figure 2.3 being the largest contributors. Mode shapes from single-span tests indicate that after the fundamental mode, transversal modes follow. The transversal modes go perpendicular to the outer layer of the CLT and top to bottom in the contour figures.

Figure 4.15 indicates a possible error during testing not seen in VDV. The classroom door is in the bottom right corner, meaning that before and after each test participants would walk from the corridor into the classroom. Every floor was given time to settle before starting a new test, but it might have been too short. The same effect can be

observed in all  $a_{rms}$  contours but is less clear. It is unlikely to provide a significant error and it could be theorised it is the door opening itself that creates the effect.

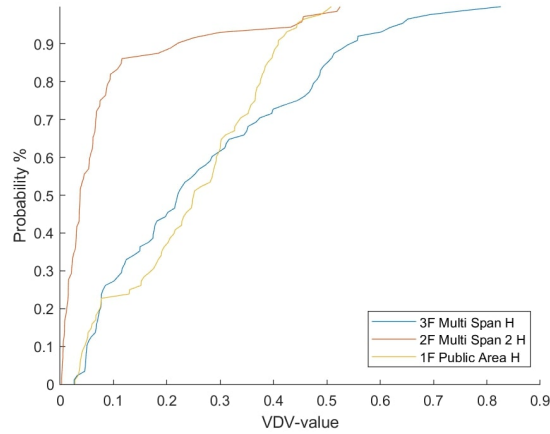


**Figure 4.16:** Empirical distribution of VDV

The empirical distribution function evaluates how likely a point on the floor is to experience a value lower than the specified VDV. The graphs in Figure 4.16 reflect the rest of the analysis in this section. 2F Multi Span 2 H has a high likelihood of having low values but shares a peak VDV with 1F Public Area H. Other areas have a more even distribution, and 3F Multi Span H has the highest peak.

## 4.5 Evaluation of analytical results

Several spans were calculated to determine the accuracy of Eq (3.2) in determining the fundamental natural frequency for CLT (CEN, 2010). An additional span was also calculated on either side of the measured spans. Table 4.17 shows the measured lowest frequency for a span and the calculated value.

**Table 4.17:** Measured fundamental frequency compared with values calculated with cEC5

	Span [m]	Measured [Hz]	Equation 3.2 [Hz]	$\Delta F_1$ [Hz]
CLT 160 mm	4	-	11.27	-
	5	7.9	7.21	0.69
	6	6.2	5.01	1.19
	7	-	3.68	-
CLT 200 mm	5	-	9.37	-
	6	8.2	6.50	1.7
	7	-	4.78	-

All spans measured had a fundamental frequency above the calculated utilising cEC5, this corroborates Hamm et al. (Hamm et al., 2010). No set value for underestimation

was determined. The number of tests ought to be higher to appropriately use statistical tools on the data. For 160mm CLT with 5 and 6 meters span, the equivalent span lengths are 4.78m and 5.39m. CLT 200mm with a 6m span has an equivalent span of 5.34m. The 6m spans are massively over-performing recommended values, especially 160mm since the weight of the cabinets is not added to the equation. Underestimation, while safest also leads to the overuse of resources.

The reason for this underperformance is uncertain. Improvement to the calculation that would further decrease fundamental frequency is the addition of dead-loads and further reduction of strength as found by the FEM-model section 4.20. cEC5 assumes all edges are supported, but the mode shapes only indicate a certain level of support on all sides. Similar to Hamm et al. beam supports were found to be closer to a rotational spring, which should reduce the stiffness (Hamm et al., 2010). Including transversal stiffness in Eqs (2.35a) and (2.35b) could increase the calculated fundamental frequency.

cEC5 is primarily based on Ohlsson's work on joisted timber floors and employs an equivalent bending stiffness perpendicular to beams (Ohlsson, 1982)(CEN, 2010). The code uses the *gamma-method* in Annex B to calculate the equivalent bending stiffness. However, since it is not intended for CLT plates, so proHolz was utilised instead.

**Table 4.18:** Measured fundamental frequency compared with values calculated with prEC5

Span [m]	Width [m]	Heel drop [Hz]	Equation (3.3) [Hz]	$\Delta F_1$
6 with 160mm CLT	12	6.2	5.06	1.14
2x5 with 160mm CLT	8	7.9	7.26	0.63
6 with 200mm CLT	11.5	8.2	6.75	1.45

The revised Eurocode 5 Figure (2.12) has factors accounting for transversal stiffness and floor width,  $k_{e,1}$  and  $k_{e,2}$ . As the equation accounts for more parameters, a more accurate calculation was expected. Based on the findings presented in Table 4.18, it appears that there were only minor improvements. The 6m span has only improved slightly, even when  $k_{e,2}$  were above 1 for all tests. The improvement in predicting 5m span is also not seen, even when it is calculated as a double span instead of a single span. Revised Eurocode 5 still underestimate floor performance, and the improvement by including additional parameters is insignificant. Due to this thesis's small data set, it was impossible to conduct extensive statistical analysis. It is important to note that the accuracy of the codes may improve if more data is obtained and other buildings are measured. The current measurements are based on only one building, and it is possible that this building is an outlier.



**Table 4.19:** Measured rms-acceleration compared with values calculated with prEC5

Span [m]	Width [m]	$\zeta$	Heel drop [ $m/s^2$ ]	Walk [ $m/s^2$ ]	Equation (3.4) [ $m/s^2$ ]	$\Delta a_{rms}$		Performance
						Heel drop	Walking	
5 with 160mm CLT	8	0.04	0.1085	0.0740	0.0738	0.0347	0.0002	Level IV
6 with 160mm CLT	12	0.04	0.0880	-	0.0410	0.047	-	Level IV
6 with 200mm CLT	11.5	0.04	0.0757	0.0680	0.0397	0.0360	0.0283	Level III

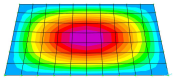
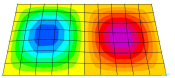
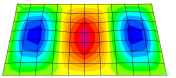
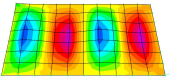
prEC5 also includes an  $a_{rms}$  step in the verification process; see Figure 2.11. Table 4.19 compares the  $a_{rms}$  produced by either walking or heel drop to calculated values. The code is based on a person walking, but heel drops are also included. Since the span lengths are mostly similar, the data set is too small to determine any statistical differences accurately. The data suggests that the code's  $a_{rms}$  predictions are lower than the actual measurements. The consequence of this is that the code overestimates the performance of the floor. Specially 6m with 200mm CLT shows a significant difference between measured and calculated  $a_{rms}$ .

## 4.6 SAP2000 FEM-model

A FEM model was created and adjusted in SAP2000; results from the simulation are presented in Tables 4.20 and 4.21. The sequence of mode shapes are corresponding and higher modes are all transversal like the results in Table 4.2. The simulated floors had a much higher frequency relative to field experiments.

Further calibration of the model is needed before it can be used as an accurate representation. Lowering stiffness should be prioritised as the simulated model likely overestimate it. The simulated slab is assumed to be one continuous plate, but from the BIM model it is known that its four plates connected with a spline connection. Possible solutions are to create spring connections between the plates or calibrate an equivalent stiffness. Similar FEM models have been developed previously (Ussher et al., 2018)

**Table 4.20:** Simulated floor model in SAP2000

	Mode 1	Mode 2	Mode 3	Mode 4
Model				
Freq. SAP200 [Hz]	11.64	14.15	18.28	23.73
Freq. Artemis [Hz]	8.24	9.49	13.754	18.317
Freq. difference [Hz]	3.4	4.66	4.526	5.413

MAC-values, frequency and the total absolute difference between each iteration of the simulation are provided in Table 4.21. Test nr. 0 assumed a 10  $kN/mm$  stiffness on all joints, further test had adjusted stiffness on all individual joints. The absolute difference between the tests decreased rapidly from test 0 to test 1. Subsequent tests showed a

slower decrease but continued to approach convergence. After the first adjustment, the frequency remained stable and was not significantly affected.

MAC for mode 1 was highest with test 0 and fell for each adjustment of springs by a small amount. The reason why the starting value provided the best MAC is unknown since it was picked at random. All tests where joints were simulated as springs performed better than with hinged or fixed support. High MAC for modes higher than the first would require a calibration tool to adjust stiffness. As it stands, the model is far from being functional. The method of finding spring stiffness proved possibly successful, and providing it with the total displacement for all modes would most likely be even better. While the absolute total difference indicates the difference in movement, it cannot determine if points converge to their real-life twin. More accurate sensitivity analyses for FEM updating are available and would give better indications (Mordini et al., 2007).

**Table 4.21:** Results from iterative adjusting of joint stiffness.

Test nr	Mode 1 MAC	Mode 2 MAC	Mode 3 MAC	Mode 4 MAC	Frequency [Hz]	Total absolute difference [mm]
0	0.9339	0.6276	0.1918	0.0019	10.26	-38.9424
1	0.9300	0.6143	0.1857	0.0017	11.62	-0.9865
2	0.9283	0.6142	0.1792	0.0019	11.64	-1.0091
3	0.9283	0.6142	0.1795	0.0018	11.64	0.1167
4	0.9283	0.6142	0.1795	0.0017	11.64	0.1092
5	0.9283	0.6144	0.1799	0.0017	11.64	0.1041
6	0.9283	0.6144	0.1799	0.0017	11.64	0.1002
7	0.9283	0.6143	0.1799	0.0017	11.64	0.0977
8	0.9283	0.6144	0.1799	0.0017	11.64	0.0958
9	0.9283	0.6143	0.1794	0.0021	11.64	0.0944
10	0.9283	0.6144	0.1799	0.0021	11.64	0.0931
Hinged support	0.9213	0.6095	0.1552	0.0015	11.71	-
Fixed support	0.8776	0.5453	0.1235	0.0115	19.56	-



# 5. General disucssion

General discussion differs from chapter 4 with that the discussion applies to all results, and is not specific to one. The structure follows the same one used in chapter 3 and chapter 4.

## 5.1 Modal Characteristics

### 5.1.1 Detected modes of vibration



**Figure 5.1:** Example of the resolution of the sensor grid

When comparing the modes found in similar experiments conducted on ex-situ floors, it was discovered that the number of modes found in-situ was relatively low. (Weckendorf et al., 2016) (Kawrza et al., 2021). The highest number of modes found was four in 1F Public Area H. As the number of local properties increased and complex floor plans were introduced, the number of modes quickly decreased. The test set-up replicated what was used in Weckendorf et al. 2016 using a Nyquist frequency of 100 Hz, meaning measurements were taken at 200 Hz. Introducing floor systems into superstructures drastically reduces the number of identified higher modes. Several factors

could be attributed to this, including partition walls and the clamping effect from non-bearing elements. Increased complexity was also observed in Jarnerö's work on in-situ CLT floors. He noted that complexity stemmed from changed support conditions and localised damping from screws and elastic interlayers. The resolution used for all tests in this thesis was relatively high; see Figure 5.1. It is not certain that a finer grid would result in more discovered modes.

All measured floors behave like four sides supported (S-S-S-S), even when built as two sides supported (S-F-S-F). The facade walls likely provide a clamping effect on one side, and the partition wall provides support on the other. Corroborating Ussher's work on multiple strips of CLT, the whole floor is engaged in the motion (Ussher et al., 2022). The spline connection in Figure 3.12 is enough to create a continuous plate. The middle beam in a multi-span test acts as a sub-beam, while beams plus partition walls are fixed boundaries. Research has been done on sub-beams by Weckendorf et al., but it is hard to compare research when the discrepancy in detected mode is so high (Weckendorf et al., 2016). Observing 1F and 3F Public Area H and all single-span tests indicate that the transverse mode appears after the fundamental mode. No longitudinal mode could ambiguously be detected.

### 5.1.2 Damping

No discussion of damping values were included about damping in section 4 since the property is so hard to accurately predict. Too many factors contribute to the final result that comparing test to test is inherently unreliable. Table 5.1 provides an overview of the max, min and mean found with the different OMA tools.

**Table 5.1:** Modal damping values found through testing

Analytical Tool	EFDD	SSI-Merged
Max $\zeta$	5.477%	6.929 %
Min $\zeta$	2.738 %	3.197 %
Mean $\zeta$	3.54 %	4.75 %

After comparing the measured damping values to the recommendations in cEC5, it has been determined that all floors have a damping value above the recommended 1% for joisted timber floors. Updated prEC5 contains four recommended modal damping ratios depending on the floor construction method. For CLT slabs with a floating floor layer, it recommends 4 %. On some floors, both EFDD and SSI-Merged demonstrate damping levels below the recommended value, while in other areas, they exceed it. The mean of EFDD is below the recommended value, while SSI is significantly above it.

Working on a conservative principle, the fact that revised Eurocode 5 recommends

damping higher than measured could allow an unacceptable design to go through. The thesis found very few modes, making any modal damping predictions unreliable. The evidence suggests that the recommended values are too high. High assumed modal damping could contribute to overestimation seen in Table 4.19. Damping found from the experiments is lower than the 6 % Jarnerö found in his in-situ experiments (Jarnerö et al., 2015).

## 5.2 Influence of secondary structure

All mode shapes found in section 4.1 were impacted by partition walls. The interaction was further explored in section 4.2, showing the fundamental mode overlaid on the floor plan. Only the existence of the effect where documented in this thesis, no exact amount could be determined. Most building codes like cEC5, prEC5 and CSA086-19 utilise span length with no regard given to partition walls. Research on joisted timber floors supported this, indicating non-bearing structures could be ignored (Weckendorf et al., 2014). Results in this thesis show that not accounting for partition walls can lead to an incorrect assessment of fundamental mode shape. Contributions from partition walls are positive for all tests, indicating they provide higher additional stiffness than mass (Ohlsson, 1982). Ignoring them for building codes would therefore lead to a conservative design.

For standards based on measuring acceleration like BS 6472 and ISO 2631, partition walls must be accounted for if critical areas are to be tested (ISO, 2007)(BSI, 2008). As seen in Figure 4.16, the placement of a sensor would highly influence the measured value. It would be challenging to predict critical spots if the placement of partition walls is unknown.

The deflection was not directly measured and was only derived from acceleration. Determination of the buckling of the floor would require additional testing and an accurate FEM model. While fundamental frequency was higher than calculated with cEC5 and prEC5, it is possible that deflection were higher. Timber beams provide less stiff support than steel beams, allowing more movement (Weckendorf et al., 2016). As the whole floor is engaged in fundamental mode shape, using span length to determine deflection might be an underestimation.

Incorporating partition walls into the design code could damage the flexibility and adaptability of the building should usage change. The entire life cycle of the building should be considered, and extending the life of buildings is one of the most impactful steps to save emissions(Kamara et al., 2020).

### 5.3 Time history response

The strength of acceleration measured by reference sensors over roving sensors is that the same excitation was felt at two spread-out points. Using reference sensors eliminates a possible error of inconsistent performance of heel drops and isolates the floor's performance.

Walking produced similar  $a_{rms}$  for all sensors and only slightly increased with adding an extra person. When performing heel drops, there was a discrepancy between Ref.1 and Ref.2 in areas with higher complexity. The discrepancy is likely because walking occurred around the floor, and heel drops were stationary. The difference became more pronounced since motion, as seen in Figure 4.2 would only reach one reference.

The acceleration reached during heel drops was consistently higher than that of walking. The force-to-weight ratio is drastically higher for jumping than walking (Wheeler, 1982). Heel drops similarity to jumping is the likely cause of the difference. An example of heel drops being performed can be seen in Figure 5.2. The relationship between peak and rms acceleration was never  $\sqrt{2}$  and would consistently be much higher. prEC5 and AISC11 both utilise a relationship of  $\frac{a_{peak}}{a_{rms}} = \sqrt{2}$  to transform between the two forms. From Figure 2.4 this symbolises a square single. The reason for the much higher ratio found is not known but would influence that factor used in Figure 2.11. Eq (3.4) brought out from the figure shows the  $\sqrt{2}$  in the denominator, stated use is converting peak acceleration to rms-acceleration (CEN, 2023). The minimum ratio between measured  $a_{peak}$  and  $a_{rms}$  is 1.56, while the maximum ratio is 11.41. On average, the mean ratio is 4.77. With such a wide range there might not be a single that could transform between peak and rms acceleration.

Guidance on perceivable vibrations is given in ISO 10137 and shown in Figure 2.9. All measured floors had  $a_{rms}$  above  $0.0679 \text{ m/s}^2$  measured by reference sensors. The baseline for a floor with an 8 Hz fundamental frequency is  $0.005 \text{ m/s}^2$ , increasing slightly for higher frequencies. Adjusting the baseline with a factor of 4, suitable for a school, give a limit of  $0.02 \text{ m/s}^2$ . All floors are over the recommended value, confirming the vibration problem experienced by occupants.

The scale developed by Chui would not be applicable for any floors measured (Chui, 1987). The scale developed with field tests has a starting value of

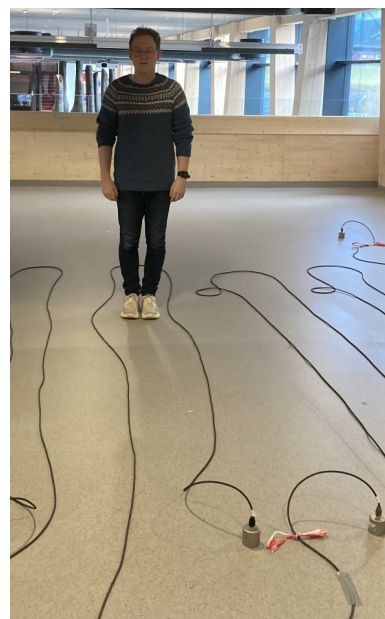


**Figure 5.2:** Heel drops being performed at 1F Public Area

0.100  $m/s^2$ , something only achieved in the most severe cases. No floor would be categorised as even slightly perceptible when using Figure 2.7. The scale was developed on joisted timber floors but is only connected to a single parameter. Alvis showed that a single parameter alone is not enough to predict performance accurately (Alvis et al., 2001)

## 5.4 The distribution of VDV

Statistical distribution of VDV across the three different floors is discussed in section 4.4. A comparison of VDV and  $a_{rms}$  contours shows that VDV resembles the found low-frequency mode shapes more than  $a_{rms}$ .

The weighting of  $a_{rms}$  performed with ISO 2631-1 seems to remove a higher frequency acceleration stemming from partition walls. Consequently, the lower frequency mode shapes found more closely align with contour shapes. If each subsequent mode decreases in importance, then weighted rms-acceleration can be seen as preferred to unweighted. Important to note that there exists considerable acceleration at higher frequencies on the floor. VDV being to the power of four, also evens out the contour shapes by separating high values from low, making it better at finding critical areas.

## 5.5 Building codes

Both the current and revised Eurocode 5 have a lower calculated fundamental frequency than measured in field tests. The calibration of cEC5 Eq (3.2) was done specifically for joisted timber floors, whereas prEC5 is intended to work for a broader range, including CLT. The difference can be relatively large at 1.7 Hz and never lower than 0.68 Hz. A conservative estimation is often desired for a building code but could lead to excess engineering and wasted materials.

While not ideal that the provided equations in sections 2.4.4 and 2.4.5 are underestimating the performance, it would be worse if they provided a much higher frequency than measured. The revised Eurocode 5, unlike the current, provide calculated  $a_{rms}$  that were compared with in-field acceleration. The code consistently predicted a lower value than the actual measurement in all the tests conducted. This underestimation was observed for both walking and heel drop tests. The formula for calculating the rms-acceleration uses an assumed walking frequency, therefore difference for heel drop was expected. Underestimation of  $a_{rms}$  goes against the conservative principle and can prove a problem since an unacceptable design could be approved. The amount of data gathered on the



subject in this thesis is too small to draw a concrete statistical conclusion. However, if future tests corroborate an adjustment should be made

## 5.6 FEM-modelling

A simple FEM model of the floor proved accurate for the first mode with a MAC of 0.9339, but MAC for higher modes fell quickly. In future modelling, adding a spring connection between each plate would be advised to decrease the frequency. A calibration program should be included if the model were to be used to provide analytical value in a study. Minor adjustments to the bending stiffness could be made to increase the MAC for higher modes.

The estimation of joint stiffness was successful and could be further developed. The difference between real and simulated displacement seems to converge for each additional cycle. The adjustment could be even more accurate if the displacement of all modes were included instead of only the first mode displacement. A calibration program could include this as an additional parameter when adjusting stiffness. From the results in Table 2.36 the MAC remained mostly stable as spring stiffness was adjusted, at least for the first mode. The program could adjust the spring stiffness and CLT stiffness in an alternate pattern until a decided convergence value was reached.

Seen in constants A and B of Eq 2.17, and noted in the literature, knowing the boundary conditions is vital for accurate modal updating models (Kawrza et al., 2021). The properties of the surface support have been shown to influence all modes, but especially higher modes (Weckendorf et al., 2016). Accurately predicting stiffness is a challenging problem, since wood displays different properties with changes in the surrounding environment (Hoffmeyer, 1990)(Gülzow et al., 2011).

## 6. Conclusions and further work

Conclusions based on gathered field data, analysis results and discussions are:

1. Partition walls are essential in deciding the distribution of motion and modal characteristics of CLT floors. No negative effects were found with the presence of partition walls, and they can generally be considered as a positive contribution.
2. Relative to ex-situ, the in-situ environments provided far fewer modes due to the complexity of floor plans, boundary conditions and environmental factors.
3. Fundamental mode shapes were not contained to a single span and would actuate the whole floor in a room.
4. When two spans exist in a room, the three beams work together to create a system. The edge beams near partition walls act as boundary conditions, while the middle beam functions as a sub-beam.
5. Plotted VDV contour better represents the superposition of low-frequency mode shapes than  $a_{rms}$  contour. Since VDV represent low-frequency mode shapes, it follows that the distribution of VDV is affected by partition walls.
6. Current Eurocode 5 and revised Eurocode 5 underestimate all span's fundamental frequency. Revised Eurocode 5 underestimates the root-mean-square acceleration.
7. The addition of another person walking during testing increases the  $a_{peak}$  more relative to the  $a_{rms}$ . Heel drops will always produce a significantly higher  $a_{peak}$ , but the difference in  $a_{rms}$  is dependent on the complexity of the mode shapes.
8. The mean modal damping ratio found with EFDD was lower than the recommended value, while for SSI-Merged the mean was higher. Both EFDD and SSI found floors with modal damping well below the recommended value.
9. The relationship between  $a_{peak}$  and  $a_{rms}$  was shown to not conform to the transformation ratio  $\sqrt{2}$  used by revised Eurocode 5 and ASIC 11, indicating signal waves with other shapes than sinusoidal and square

Suggestions for further research are:

- Further development of a FEM model such that simulations can be performed with high accuracy. Attention should be given to developing methods to approximate support surfaces and connections.
- Quantify the influence of partition walls so they can be reliably used in the design phase.
- Perform similar tests across a broader range of buildings to eliminate the inherent unreliability of only testing a single building.
- Investigate the deflected shape and quantify the influence of partition walls on the maximum deflected shape.
- Developing a more robust transformation between  $a_{rms}$  and  $a_{peak}$  build upon real-world environments.
- Recommended modal damping ratios in prEC5 should be further investigated to ensure they are robust.
- VDV contour maps ability to represent low-frequency mode shapes should be explored with walking tests since this thesis only utilised heel drip. Modal analysis should also be performed to see how mode shapes contribute to the contour.

# References

- AISC (2016). *Design Guide 11. Vibrations of Steel-Framed Structural Systems Due to Human Activity Second Edition*.
- Alvis, S. R., Plaut, R. H., and Setareh, M. (2001). An Experimental and analytical investigation of floor vibrations. Master's thesis. Virginia Polytechnic Institute and State University.
- Animas, H., Pacheco Martínez, J., and Ortiz, J. (Feb. 2016). Translation of SAP2000 Models to Equivalent-Models for Finite Element Command-Based Softwares. *Ideas en Ciencia*: 37–48.
- Aranha, C. (Oct. 2016). Experimental and Numerical Assessment of the Seismic Behaviour of Log and CrossLaminated Timber Systems. PhD thesis. University of Minho.
- Bazli, M., Heitzmann, M., and Ashrafi, H. (2022). Long-span timber flooring systems: A systematic review from structural performance and design considerations to constructability and sustainability aspects. *Journal of Building Engineering* 48: 103981. DOI: <https://doi.org/10.1016/j.jobe.2021.103981>.
- Beskyroun, S., Navabian, N., Wotherspoon, L., and Ma, Q. (2020). Dynamic behaviour of a 13-story reinforced concrete building under ambient vibration, forced vibration, and earthquake excitation. *Journal of Building Engineering* 28: 101066. DOI: <https://doi.org/10.1016/j.jobe.2019.101066>.
- BIPM (2019). The International System of Units 9th Ed EN.
- Brandner, R. (2013). Production and Technology of Cross Laminated Timber (CLT): A state-of-the-art Report. English. In: *Focus Solid Timber Solutions - European Conference on Cross Laminated Timber (CLT)*. Conference date: 21-05-2013 Through 22-05-2013. University of Bath: 3–36.
- Brandner, R., Flatscher, G., Ringhofer, A., Schickhofer, G., and Thiel, A. (May 2016). Cross laminated timber (CLT): overview and development. *Holz als Roh- und Werkstoff* 74. DOI: [10.1007/s00107-015-0999-5](https://doi.org/10.1007/s00107-015-0999-5).
- Brandt, A. and Ahlin, K. (May 2010). Sampling and Time-Domain Analysis. *Sound vibration* 44: 13–17.
- Brincker, R., Zhang, L., and Andersen, P. (Jan. 2000). Modal identification from ambient responses using frequency domain decomposition. *Proceedings of the International Modal Analysis Conference - IMAC 1*.
- Brincker, R. and Andersen, P. (2006). Understanding Stochastic Subspace Identification. English. In: *Conference Proceedings : IMAC-XXIV : A Conference Exposition on Structural Dynamics*. null ; Conference date: 30-01-2006 Through 02-02-2006. United States: Society for Experimental Mechanics.
- BSI (2008). *BS 6472-1:2008. Guide to evaluation of human exposure to vibration in buildings Vibration sources other than blasting*.

- CEN (2010). *Eurocode 5: Design of timber structures - Part 1-1: General - Common rules and rules for buildings. NS-EN 1995-1-1:2004*. translate by committee SN/K 064.
- CEN (2023). *CEN/TC 250/SC 5 "Eurocode 5: Design of timber structures"*. version: prEN 1995-1-1 v2023-04-19.
- Chopra, A. (2019). *Dynamics of Structures: Theory and Applications to Earthquake Engineering* 5th Ed. Prentice Hall international series in civil engineering and engineering mechanics.
- Chui, Y. H. (1987). *Vibrational Performance of Wooden Floors in Domestic Dwellings*. as cited in Weckendorf, 2009. PhD thesis. Brighton Polytechnic.
- Computers and Structures, I. (Nov. 2017). *CSI SAP2000 Ultimate v.24.0.0. CSI Analysis reference manual for SAP2000, ETABS, SAFE and CSiBridge*.
- Crépel, P. (2005). *Chapter 11 - Jean Le Rond D'Alembert, Traité de dynamique (1743, 1758)*. Ed. by I. Grattan-Guinness, R. Cooke, L. Corry, P. Crépel, and N. Guicciardini. Amsterdam: Elsevier Science: 159–167. DOI: <https://doi.org/10.1016/B978-044450871-3/50092-9>.
- Dibk (2023). *TEK 17 § 11-8. Brannceller Tiltak mot antennelse, utvikling og spredning av brann og røyk*. in Norwegian. Accessed: 2023-05-09. URL: <https://dibk.no/regelverk/byggteknisk-forskrift-tek17/11/iii/11-8>.
- DIN (Dec. 2008). *DIN 1052. 2008-12: Entwurf, Berechnung und Bemessung von Holzbauwerken – Allgemeine Bemessungsregeln und Bemessungsregeln für den Hochbau*. as cited in Hamm, Richter, and Winter, 2010.
- Døssing, O. (Mar. 1988). *Structural Testing Part II: Modal Analysis and Simulation*.
- Dovetail (2013). *Carbon in Wood Products - The Basics*.
- Duarte, M. L. and Pereira, M. (Jan. 2006). Vision Influence on Whole-Body Human Vibration Comfort Levels. *Shock and Vibration* 13: 367–377. DOI: [10.1155/2006/950682](https://doi.org/10.1155/2006/950682).
- Ebrahimpour, A. and Sack, R. L. (2005). A review of vibration serviceability criteria for floor structures. *Computers Structures* 83 (28). A Selection of Papers from Civil-Comp 2003 and AICivil-Comp 2003: 2488–2494. DOI: <https://doi.org/10.1016/j.compstruc.2005.03.023>.
- EC (May 2010). *M/466 - EN. Programming mandate addressed to CEN in the field of the structural Eurocodes*. Ref. Ares(2010)280222 - 26/05/2010.
- EC (Dec. 2012). *M/515 - EN. Mandate for amending existing Eurocodes and extending the scope of structural Eurocodes*. Ref. Ares(2012)1516834 - 18/12/2012.
- EC (2023). *Timeline for the Eurocodes second generation*. <https://eurocodes.jrc.ec.europa.eu/2nd-generation-evolution/timeline-eurocodes-second-generation>. Accessed: 2023-04-27.
- Ewins, D. (1984). *Modal Testing: Theory and Practice*. Engineering dynamics series. Wiley.
- Gil-Martín, L. M., Carbonell-Márquez, J. F., Hernández-Montes, E., Aschheim, M., and Pasadas-Fernández, M. (2012). Dynamic magnification factors of SDOF oscillators under harmonic loading. *Applied Mathematics Letters* 25 (1): 38–42. DOI: <https://doi.org/10.1016/j.aml.2011.07.005>.
- Glišović, I. and Stevanovic, B. (Jan. 2010). Vibrational behaviour of timber floors. In: vol. 4: 2785–2793.
- Gülzow, A., Richter, K., and Steiger, R. (May 2011). Influence of wood moisture content on bending and shear stiffness of cross laminated timber panels. *European Journal of Wood and Wood Products* 69 (2): 193–197. DOI: [10.1007/s00107-010-0416-z](https://doi.org/10.1007/s00107-010-0416-z).

- Habibullah, A. (2023). *Home - SAP2000 - Computers and Structures, Inc. Technical Knowledge Base*. <https://wiki.csiamerica.com/display/sap2000/Home>. Accessed: 2023-04-14.
- Hamm, P., Richter, A., and Winter, S. (Jan. 2010). Vibrational behaviour of timber floors. In: *Proceeding 11th World Conference on Timber Engineering 2010*: 20–24.
- Han, S. W., Lee, M.-J., Moon, K. H., Sang, W., and Han, S. (Aug. 2009). Acceleration Thresholds of Vertical Floor Vibrations According to Human Perception Levels in Korea. *Advances in Structural Engineering* 12. DOI: [10.1260/136943309789508537](https://doi.org/10.1260/136943309789508537).
- Hildebrandt, J., Hagemann, N., and Thrän, D. (Oct. 2017). The contribution of wood-based construction materials for leveraging a low carbon building sector in europe. *Sustainable Cities and Society* 34: 405–418. DOI: [10.1016/j.scs.2017.06.013](https://doi.org/10.1016/j.scs.2017.06.013).
- Hoffmeyer, P. (1990). Failure of wood as influenced by moisture and duration of load. PhD thesis. State University of New York College of Environmental Science and Forestry.
- Homb, A. (2005). Low frequency sound and vibrations from impacts on timber floor constructions. PhD thesis. Norwegian University of Science and Technology.
- IPCC (2022). Summary for Policymakers. In: *Climate Change 2022: Impacts, Adaptation, and Vulnerability. Contribution of Working Group II to the Sixth Assessment Report of the Intergovernmental Panel on Climate Change*. Ed. by H. O. Pörtner, D. C. Roberts, M. Tignor, E. S. Poloczanska, K. Mintenbeck, A. Alegría, M. Craig, S. Langsdorf, S. Lösschke, V. Möller, A. Okem, and B. Rama. In Press. Cambridge, UK: Cambridge University Press: In Press.
- ISO (1997). *ISO 2631-1:1997. Mechanical vibration and shock - Evaluation of human exposure to whole-body vibration - Part 1: General requirements*.
- ISO (2003). *ISO 2631-2:2003. Mechanical vibration and shock — Evaluation of human exposure to whole-body vibration — Part 2: Vibration in buildings (1 Hz to 80 Hz)*.
- ISO (2007). *ISO 10137. Bases for design of structures - Serviceability of buildings and walkways against vibrations*.
- ISO (2017). *ISO 8041-1:2017 Human response to vibration — Measuring instrumentation — Part 1: General purpose vibration meters*.
- Jacobsen, N.-J., Andersen, P., and Brincker, R. (Jan. 2007). Using enhanced frequency domain decomposition as a robust technique to harmonic excitation in operational modal analysis. In: *Proceedings of the International Operational Modal Analysis Conference (IOMAC 2007)*. Vol. 4.
- Jarnerö, K., Brandt, A., and Olsson, A. (Jan. 2015). Vibration properties of a timber floor assessed in laboratory and during construction. *Engineering Structures* 82: 44–54. DOI: [10.1016/j.engstruct.2014.10.019](https://doi.org/10.1016/j.engstruct.2014.10.019).
- Kamara, J. M., Heidrich, O., Tafaro, V. E., Maltese, S., Dejacco, M. C., and Re Cecconi, F. (Aug. 2020). Change Factors and the Adaptability of Buildings. *Sustainability* 12 (16): 6585. DOI: [10.3390/su12166585](https://doi.org/10.3390/su12166585).
- Kawrza, M., Furtmüller, T., Adam, C., and Maderebner, R. (Mar. 2021). Parameter identification for a point-supported cross laminated timber slab based on experimental and numerical modal analysis. *European Journal of Wood and Wood Products* 79 (2): 317–333. DOI: [10.1007/s00107-020-01641-7](https://doi.org/10.1007/s00107-020-01641-7).
- Leissa, A. (1969). *Vibration of Plates*. NASA SP. Scientific, Technical Information Division, National Aeronautics, and Space Administration.
- Lenzen, K. H. (1933). Vibration of Steel Joist-Concrete Slab Floors. *AISC Engineering Journal* 3: 133–136.

- Ljunggren, F. (2006). Floor Vibration-Dynamic Properties and Subjective Perception. PhD thesis. Luleå University of Technology.
- Ljunggren, F., Wang, J., and Ågren, A. (2007). Human vibration perception from single- and dual-frequency components. *Journal of Sound and Vibration* 300(1): 13–24. DOI: <https://doi.org/10.1016/j.jsv.2006.06.072>.
- Markus Wallner-Nova Josef Koppelhuber, K. P. (2014). *Cross-Laminated Timber Structural Design*. proHolz Austria.
- Markus Wallner-Nova Josef Koppelhuber, K. P. (2018). *Cross-Laminated Timber Structural Design vol.II*.
- Mårtensson, A. and Crocetti, R. (2022). *Design of timber structures Volume 1 3th Ed*. Swedish wood.
- Mathworks (2023a). *Box-Cox transformation*. <https://se.mathworks.com/help/finance/boxcox.html>. Accessed: 2023-04-19.
- Mathworks (2023b). *Empirical cumulative distribution function*. <https://se.mathworks.com/help/stats/ecdf.html>. Accessed: 2023-04-19.
- Mathworks (2023c). *Filled 2-D contour plot*. <https://se.mathworks.com/help/matlab/ref/contourf.html>. Accessed: 2023-04-19.
- Mathworks (2023d). *Histogram with a distribution fit*. <https://se.mathworks.com/help/stats/histfit.html>. Accessed: 2023-04-19.
- Mohammad, M., Douglas, B., Rammer, D., and Pryor, S. (Feb. 2013). Chapter 5: Connection in Cross-Laminated Timber Buildings. In: *CLT Handbook U.S edition*. U.S. Department of Agriculture, Forest Service, Forest Products Laboratory, Binational Softwood Lumber Council (BSLC): 45.
- Mordini, A., Savov, K., and Wenzel, H. (2007). The Finite Element Model Updating: A Powerful Tool for Structural Health Monitoring. *Structural Engineering International* 17(4): 352–358. DOI: [10.2749/101686607782359010](https://doi.org/10.2749/101686607782359010).
- Oh, J.-W., Park, K.-S., Kim, H. S., Kim, I., Pang, S.-J., Ahn, K.-S., and Oh, J.-K. (2023). Comparative CO2 emissions of concrete and timber slabs with equivalent structural performance. *Energy and Buildings* 281: 112768. DOI: <https://doi.org/10.1016/j.enbuild.2022.112768>.
- Ohlsson, S. (1982). Floor Vibrations and Human Discomfort. PhD thesis. Chalmers University of Technology.
- Pain, H. (Jan. 2005). *The Physics of Vibrations and Waves (6th Ed)*. John Wiley Sons Ltd.
- Park, G., Lee, K. M., and Koo, S. (July 2021). Uniqueness of gait kinematics in a cohort study. *Scientific Reports* 11(1): 15248. DOI: [10.1038/s41598-021-94815-z](https://doi.org/10.1038/s41598-021-94815-z).
- Pasca, D. P., Aloisio, A., Fragiaco, M., and Tomasi, R. (Sept. 2021). Dynamic Characterization of Timber Floor Subassemblies: Sensitivity Analysis and Modeling Issues. *Journal of Structural Engineering* 147. DOI: [10.1061/\(ASCE\)ST.1943-541X.0003179](https://doi.org/10.1061/(ASCE)ST.1943-541X.0003179).
- Pastor, M., Binda, M., and Harčarik, T. (2012). Modal Assurance Criterion. *Procedia Engineering* 48. Modelling of Mechanical and Mechatronics Systems: 543–548. DOI: <https://doi.org/10.1016/j.proeng.2012.09.551>.
- Pavic, A. and Reynolds, P. (Jan. 2002). Vibration serviceability of long-span concrete building floors. Part 1: review of background information. *The Shock and Vibration Digest* 34.
- Rainieri, C. and Fabbrocino, G. (2014). Operational modal analysis of civil engineering structures. *Springer, New York* 142: 143.

- Reiher, H. and Meiste, F. (1931). Die Empfindlichkeit des Menschen gegen Erschütterungen. *Forschung auf dem Gebiete des Ingenieurwesens* 2(11). as cited in Weckendorf, 2009: 381–386.
- Reiher, H. and Meister, F. (1932). Die Empfindlichkeit des Menschen gegen Stöße. *Forschung auf dem Gebiete des Ingenieurwesens* 3(4). as cited in Weckendorf, 2009: 177–180.
- Saidin, S. S., Kudus, S. A., Jamadin, A., Anuar, M. A., Amin, N. M., Ibrahim, Z., Zakaria, A. B., and Sugiura, K. (2022). Operational modal analysis and finite element model updating of ultra-high-performance concrete bridge based on ambient vibration test. *Case Studies in Construction Materials* 16: e01117. DOI: <https://doi.org/10.1016/j.cscm.2022.e01117>.
- Schirén, W. and Swahn, T. (Sept. 2019). Vibrations in residential timber floors-A comparison between the current and the revised Eurocode 5. Master’s thesis. Linnaeus University.
- Sintef (2022). *Splitkon Teknisk Godkjenning*. <https://splitkon.no/wp-content/uploads/2022/02/20712g.pdf>. Accessed: 2023-04-19, in Norwegian.
- Smith, A., Hicks, S., Devine, P., and Britain, S. (Jan. 2007). *Design of Floors for Vibration: A New Approach*. DOI: [10.13140/RG.2.2.29342.95048](https://doi.org/10.13140/RG.2.2.29342.95048).
- Solutions, S. V. (2023a). *Curve-fit Frequency Domain Decomposition*. <https://svibs.com/curve-fit-frequency-domain-decomposition/>. Accessed: 2023-04-11.
- Solutions, S. V. (2023b). *Enhanced Frequency Domain Decomposition*. <https://svibs.com/enhanced-frequency-domain-decomposition/>. Accessed: 2023-04-11.
- Solutions, S. V. (2023c). *Technical Paper on the Stochastic Subspace Identification Techniques*. [http://www.svibs.com/resources/ARTEMIS\\_Modal\\_Help\\_v3/SSI\\_ssi.htm](http://www.svibs.com/resources/ARTEMIS_Modal_Help_v3/SSI_ssi.htm). Accessed: 2023-04-11.
- Solutions, S. V. (2023d). *Unweighted Principal Component (SSI)*. [http://www.svibs.com/resources/ARTEMIS\\_Modal\\_Help\\_v3/SSI\\_Unweighted\\_Principal\\_Component.htm](http://www.svibs.com/resources/ARTEMIS_Modal_Help_v3/SSI_Unweighted_Principal_Component.htm). Accessed: 2023-04-11.
- Standards Norway (July 2010). *National Annex NA - Eurocode 5: Design of timber structures - Part 1-1: General - Common rules and rules for buildings*. SN/K 064.
- Trunmo, T. (2021). *Ås vgs*. <https://www.bygg.no/as-vgs/1476712!/>. Accessed: 2023-04-14, in Norwegian.
- Ussher, E., Arjomandi, K., Weckendorf, J., and Smith, I. (2017). Predicting effects of design variables on modal responses of CLT floors. *Structures* 11: 40–48. DOI: <https://doi.org/10.1016/j.istruc.2017.04.006>.
- Ussher, E., Arjomandi, K., and Smith, I. (June 2018). Estimating Filtering Frequency for Vibration Serviceability Design Analysis of CLT Floor. In: *6th International Structural Specialty Conference*. Paper no. ST-123. Canadian Society for Civil Engineering.
- Ussher, E., Arjomandi, K., and Smith, I. (2022). Status of vibration serviceability design methods for lightweight timber floors. *Journal of Building Engineering* 50: 104111. DOI: <https://doi.org/10.1016/j.jobe.2022.104111>.
- Weckendorf, J. (2009). Dynamic response of structural timber flooring systems. PhD thesis. Edinburgh Napier University.
- Weckendorf, J., Hafeez, G., Doudak, G., and Smith, I. (Dec. 2014). Floor Vibration Serviceability Problems in Wood Light-Frame Buildings. *Journal of Performance of Constructed Facilities* 28 (6). DOI: [10.1061/\(asce\)cf.1943-5509.0000538](https://doi.org/10.1061/(asce)cf.1943-5509.0000538).
- Weckendorf, J., Ussher, E., and Smith, I. (2016). Dynamic response of CLT plate systems in the context of timber and hybrid construction. *Composite Structures* 157: 412–423. DOI: <https://doi.org/10.1016/j.compstruct.2016.08.033>.



- Wheeler, J. E. (1982). PREDICTION AND CONTROL OF PEDESTRIAN-INDUCED VIBRATION IN FOOTBRIDGES. *Journal of the Structural Division* 108: 2045–2065.
- Wood Works (Feb. 2023). *US Mass Timber Floor Vibration Design Guide 1th Rev.Ed.* Wood Works – Wood Products Council.
- Yanik, Y., Türker, T., Yildirim, Ö., and Dede, T. (2020). Identification Material Properties By Modal Calibration Method Based On Ambient Vibration Tests. *Uludağ University Journal of The Faculty of Engineering* 25: 573–590.

# Appendix A. Sensor grids with partition walls and cabinets

This Annex seeks to provide the reader with an overview over sensor placement and organisation. In total ten sensors were used in testing, eight were moved around to cover the hole floor and two were stationary as reference.

Every figure in Annex A follows the same guidelines:

- Reference sensors are denoted with coordinates marked in yellow. Reference symbol marked filled with black means it's reference 1, and not filled means reference 2.
- Each row denoted one configuration measured before moving sensors to the next row. Every row has its own unique symbol helping the reader to see the direction.
- Sensor 3 to 10 is always moved in increasing number along the row.
- For simulation and modelling purposes the edges are included even if no sensor was placed there, these are marked.

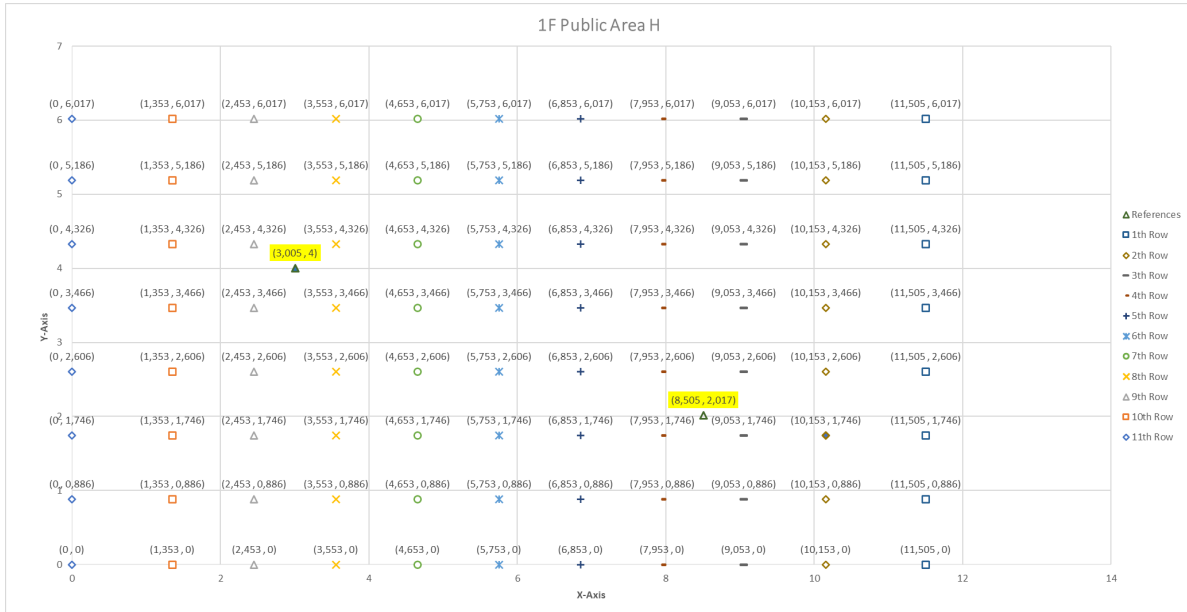


Figure A.1: Test setup for 1F Public Area



Figure A.2: Test setup for 2F Multi Span

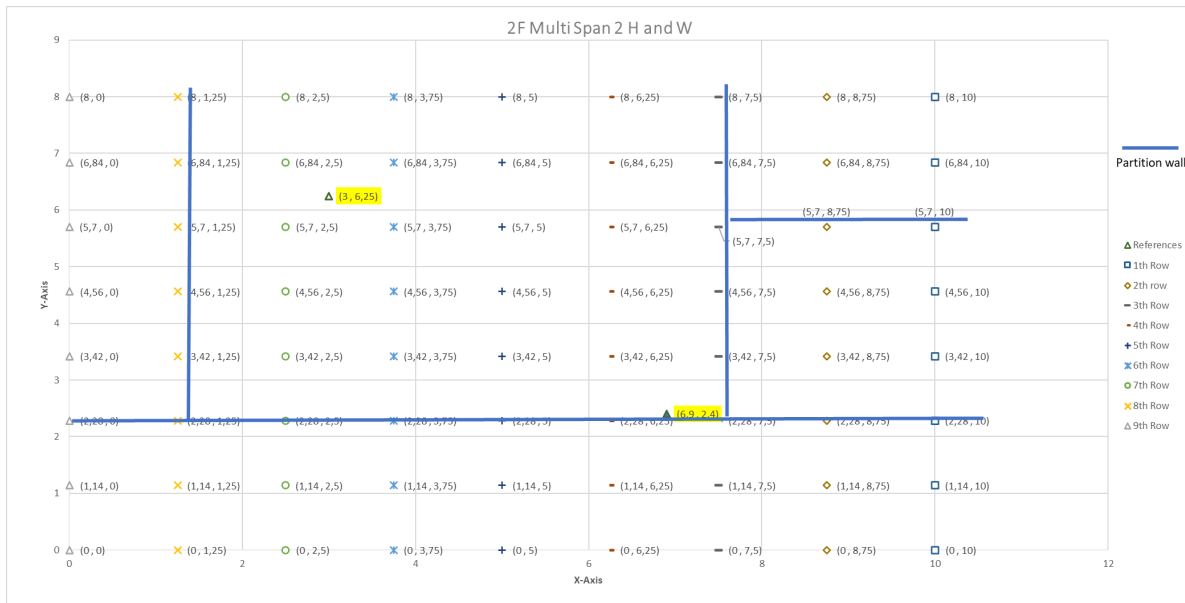


Figure A.3: Test setup for 2F Multi Span 2

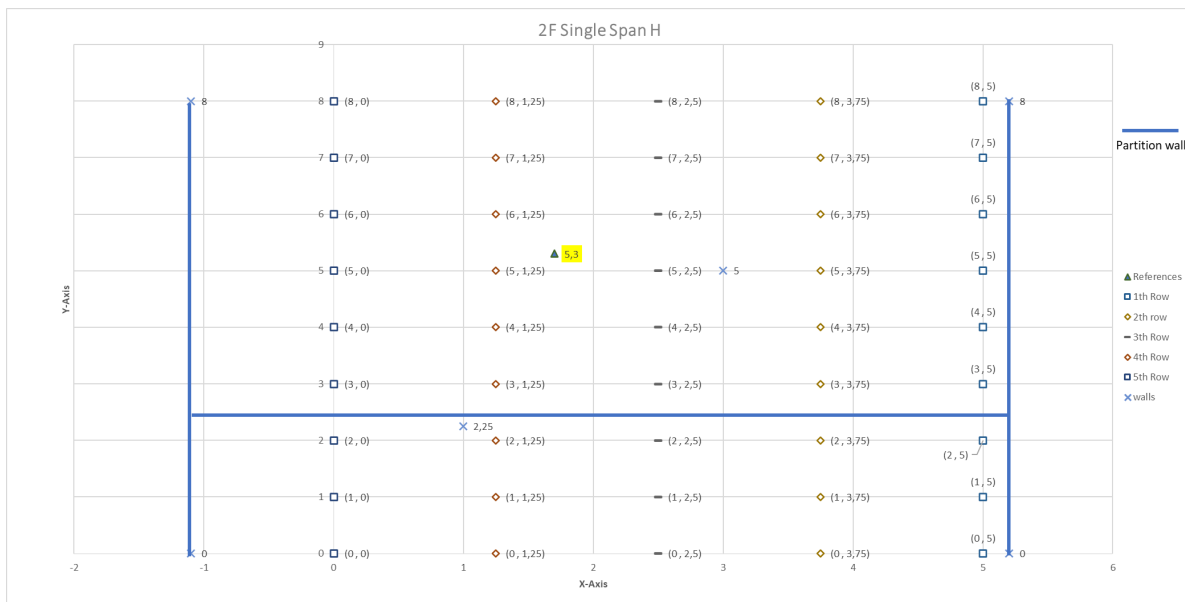


Figure A.4: Test setup for 2F Single Span

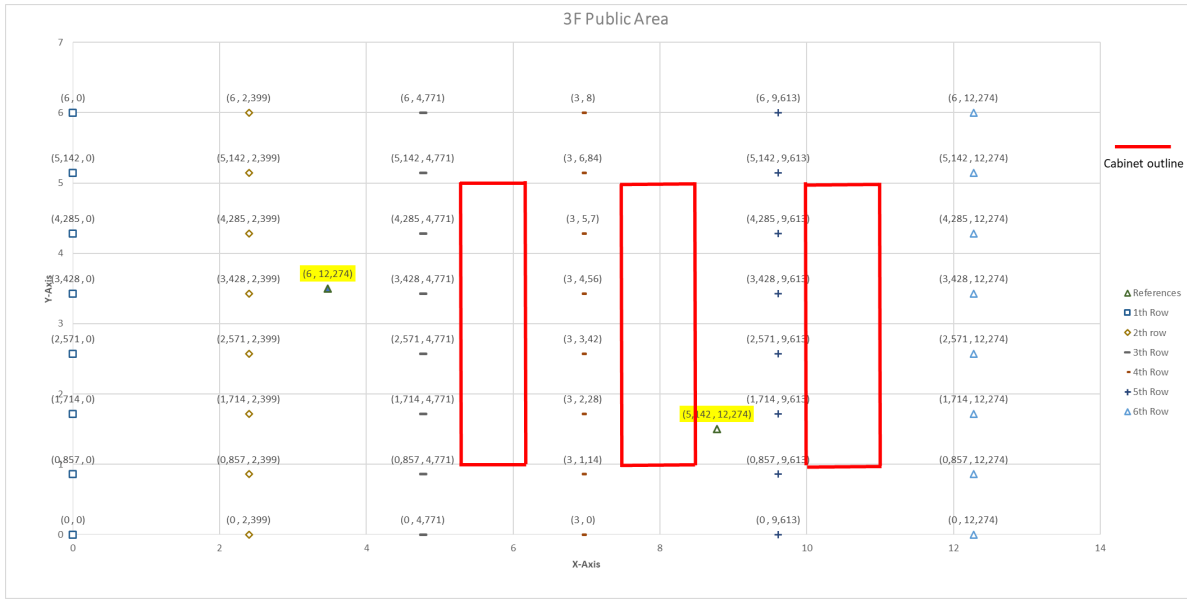


Figure A.5: Test setup for 3F Public Area

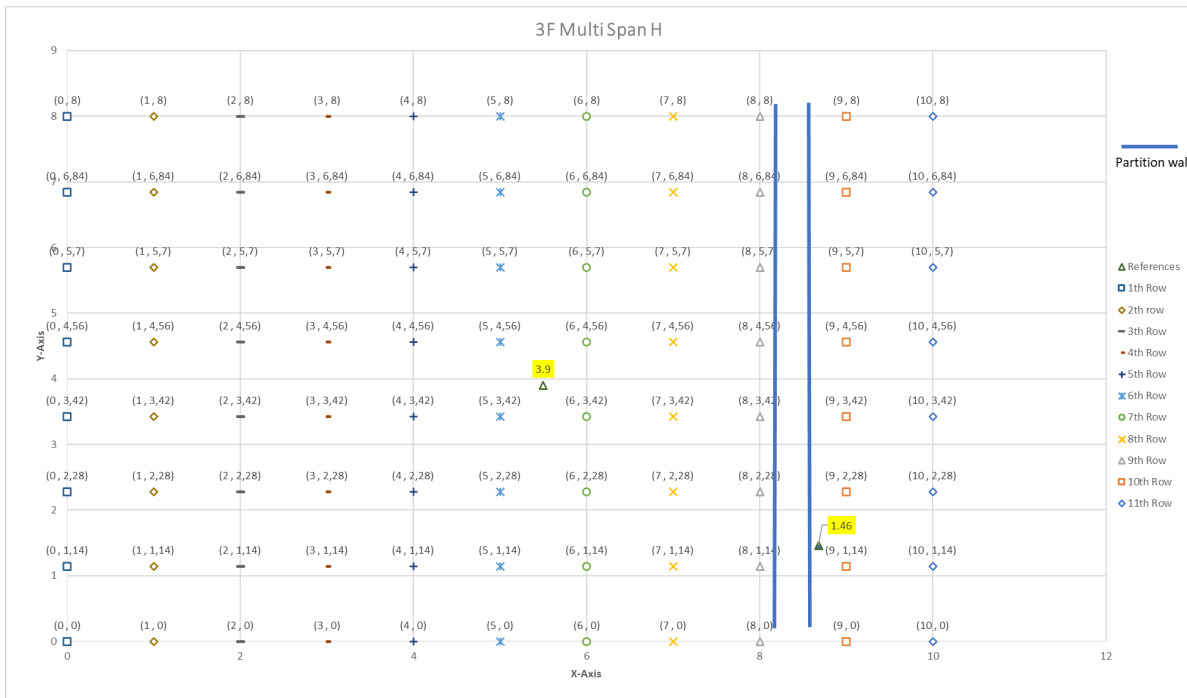


Figure A.6: Test setup for 3F Multi Span



Figure A.7: Test setup for 3F Classroom



Figure A.8: Test setup for 3F Single Span

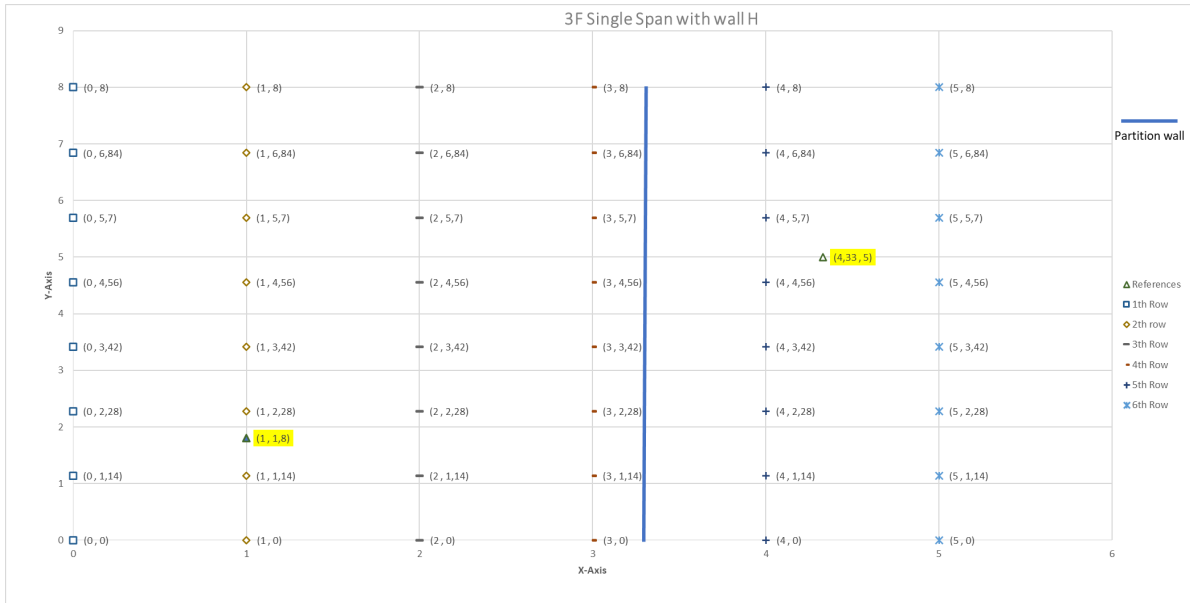


Figure A.9: Test setup for 3F Single Span Wall

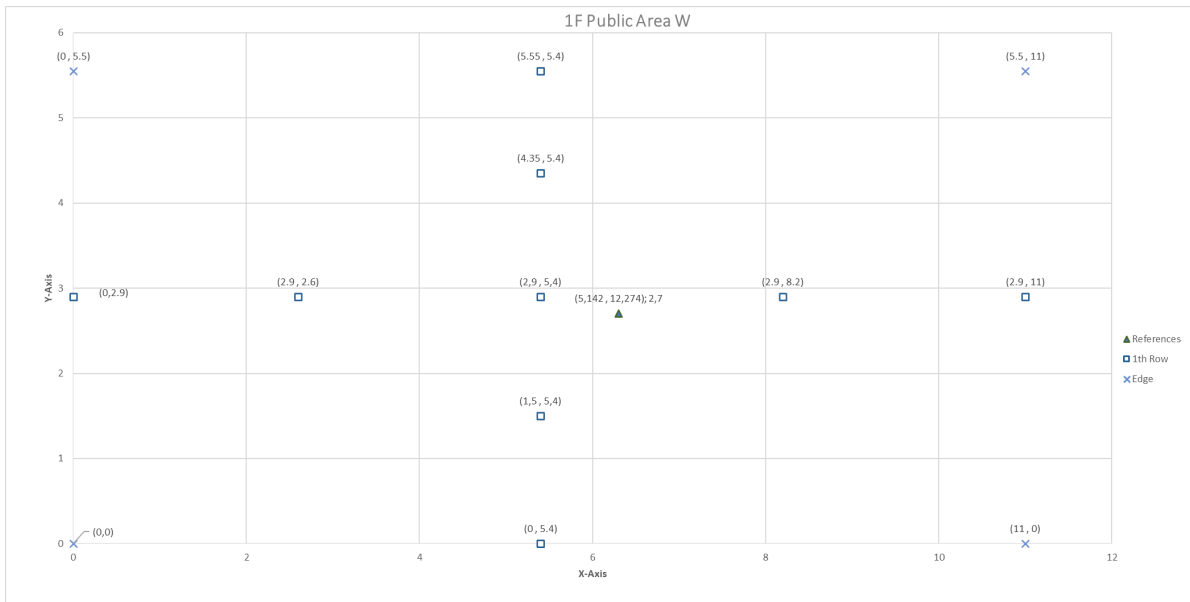


Figure A.10: Test setup for 1F Public Area Walk

# Appendix B. Specifications for technical equipment

## **ACCELEROMETER, ICP®, SEISMIC Model 393B12**

Seismic, high sensitivity, ceramic shear ICP® accel., 10 V/g, 0.15 to 1k Hz, 2-pin top conn.

- Sensitivity: ( $\pm 10\%$ )10000 mV/g (1019.4 mV/(m/s<sup>2</sup>))
- Broadband Resolution: 0.000008 g rms (0.00008 m/s<sup>2</sup> rms)
- Measurement Range: 0.5 g pk (4.9 m/s<sup>2</sup> pk)
- Frequency Range: ( $\pm 5\%$ )0.15 to 1000 Hz
- Electrical Connector: 2-Pin MIL-C-5015
- Weight: 7.4 oz (210 gm)

**Datalogger, MX1601B universal amplifier** 16-channel amplifier of the QuantumX family

It supports the following transducer technologies:

- Current-fed piezoelectric transducers (IEPE, ICP)
- Voltage ( $\pm 100$  mV,  $\pm 10$  and  $\pm 60$  V)
- Current (0/4 ... 20 mA, 2-/3- or 4-wire)

Precise

- Accurate measurement attributed to the 0.03 accuracy class
- Integrated delta-sigma-analog-to-digital converter (24 bit)
- Digital low-pass filters (Bessel, Butterworth, linear phase)
- Sample rates of up to 20 kS/s per channel and a signal bandwidth of up to 3 kHz



- Interference-free signal path due to electrically isolated channels
- Working standard calibration certificate according to ISO 10012 stored in the module
- DAkkS certificate (ISO 17025) from HBM on request

### **PCB PIEZOTRONICS 482C05 FOUR-CHANNEL, ICP SENSOR SIGNAL CONDITIONER**

Model features:

- Measurements 0 Hz to 100 kHz with AC/DC coupling selection per channel
- Auto zero function to negate DC bias when DC coupling enabled
- Positive peak performance measurements with clamped output in AC coupled mode
- Incremental gain from x0.1 to x200

## Appendix C. All results calculated for section 4.4

RMS (m/s <sup>2</sup> )	Row 1	Row 2	Row 3	Row 4	Row 5	Row 6	Row 7	Row 8	Row 9	Row 10	Row 11
Sensor 1	0,071583	0,064837	0,061917	0,051819	0,059796	0,058641	0,045912	0,056825	0,071679	0,065819	0,063352
Sensor 2	0,073925	0,073039	0,073164	0,073648	0,073845	0,066851	0,072255	0,071261	0,077227	0,076645	0,071247
Sensor 3	0,07272	0,078073	0,079633	0,081182	0,078354	0,085245	0,084877	0,07559	0,082	0,083584	0,078461
Sensor 4	0,074801	0,0679	0,075306	0,076672	0,083842	0,086748	0,087482	0,074463	0,076033	0,083899	0,079484
Sensor 5	0,073654	0,070811	0,073134	0,076567	0,083222	0,091124	0,088027	0,074639	0,078452	0,084067	0,080649
Sensor 6	0,072449	0,079339	0,080024	0,066158	0,079349	0,083858	0,082711	0,063208	0,071889	0,079114	0,078004
Sensor 7	0,065201	0,07238	0,071158	0,06852	0,075073	0,071514	0,07182	0,063542	0,065449	0,0653	0,056877
Sensor 8	0,063215	0,067511	0,065196	0,066703	0,060369	0,066449	0,066856	0,056037	0,048805	0,062246	0,061717
PEAK (m/s <sup>2</sup> )	Row 1	Row 2	Row 3	Row 4	Row 5	Row 6	Row 7	Row 8	Row 9	Row 10	Row 11
Sensor 1	0,1555	0,1157	0,1166	0,1638	0,2075	0,1858	0,1554	0,1514	0,259	0,3096	0,1971
Sensor 2	0,3239	0,3344	0,3335	0,3658	0,4599	0,5298	0,5834	0,4537	0,4184	0,4735	0,3522
Sensor 3	0,4263	0,4657	0,5062	0,4744	0,5571	0,727	0,7956	0,6214	0,4984	0,582	0,4688
Sensor 4	0,4851	0,5341	0,5772	0,5066	0,5621	0,7784	0,8557	0,6594	0,502	0,6304	0,5302
Sensor 5	0,4912	0,5509	0,5666	0,4995	0,5003	0,7305	0,7997	0,5942	0,475	0,6176	0,5321
Sensor 6	0,4265	0,4851	0,5078	0,4221	0,396	0,5995	0,6796	0,4449	0,3582	0,5113	0,4819
Sensor 7	0,2948	0,3469	0,3596	0,3054	0,282	0,3911	0,4432	0,284	0,2182	0,3247	0,3256
Sensor 8	0,1448	0,1402	0,1464	0,1231	0,111	0,1186	0,1273	0,1052	0,1075	0,1302	0,116
VDV (m/s <sup>-1.75</sup> )	Row 1	Row 2	Row 3	Row 4	Row 5	Row 6	Row 7	Row 8	Row 9	Row 10	Row 11
Sensor 1	0,0492	0,03676	0,0521	0,06694	0,07712	0,07187	0,07642	0,06699	0,13	0,1515	0,0757
Sensor 2	0,1519	0,213	0,2457	0,2277	0,2503	0,2975	0,2284	0,2314	0,2809	0,2878	0,1837
Sensor 3	0,2159	0,3098	0,3652	0,3327	0,3546	0,4434	0,3992	0,3385	0,3668	0,3826	0,2638
Sensor 4	0,2477	0,3577	0,4192	0,3762	0,3899	0,5096	0,4579	0,3844	0,3973	0,4247	0,3022
Sensor 5	0,2481	0,3522	0,409	0,3661	0,3746	0,4994	0,4878	0,3688	0,3787	0,4087	0,2926
Sensor 6	0,2058	0,2844	0,3269	0,3001	0,3003	0,4024	0,4443	0,2901	0,293	0,3274	0,2518
Sensor 7	0,1292	0,1798	0,2023	0,1906	0,1894	0,2367	0,2878	0,1672	0,1755	0,1951	0,1571
Sensor 8	0,04256	0,03996	0,04638	0,03892	0,03732	0,03569	0,05948	0,03356	0,05812	0,05181	0,02764

Figure C.1: Acceleration values for 1F Public Area H

RMS (m/s <sup>2</sup> )	Row 1	Row 2	Row 3	Row 4	Row 5	Row 6	Row 7	Row 8	Row 9
Sensor 1	0,058523	0,051755	0,045912	0,042471	0,051398	0,048837	0,059538	0,063178	0,073586
Sensor 2	0,057453	0,060911	0,072255	0,046884	0,063813	0,053366	0,057144	0,056123	0,06851
Sensor 3	0,058123	0,06784	0,084877	0,055211	0,057134	0,061173	0,060946	0,06293	0,071663
Sensor 4	0,049071	0,058679	0,087482	0,051357	0,051728	0,056235	0,057706	0,043234	0,0656
Sensor 5	0,058627	0,055113	0,088027	0,061888	0,055681	0,056342	0,059004	0,065686	0,068135
Sensor 6	0,060157	0,066074	0,082711	0,055332	0,051201	0,048968	0,059435	0,061396	0,067468
Sensor 7	0,057494	0,061737	0,07182	0,063444	0,054252	0,057659	0,06164	0,0664	0,062601
Sensor 8	0,066498	0,0631	0,066856	0,063745	0,062667	0,065191	0,071226	0,064104	0,061732
PEAK (m/s <sup>2</sup> )	Row 1	Row 2	Row 3	Row 4	Row 5	Row 6	Row 7	Row 8	Row 9
Sensor 1	0,1595	0,2508	0,1554	0,1306	0,1136	0,1056	0,1266	0,09083	0,08108
Sensor 2	0,2969	0,6962	0,5834	0,3376	0,2178	0,1814	0,2233	0,1245	0,08217
Sensor 3	0,2954	1,13	0,7956	0,4341	0,2602	0,181	0,286	0,1861	0,09413
Sensor 4	0,1575	0,5323	0,8557	0,2406	0,2254	0,1614	0,2658	0,1467	0,08704
Sensor 5	0,1192	0,1402	0,7997	0,209	0,2175	0,1583	0,2009	0,1382	0,08548
Sensor 6	0,114	0,1242	0,6796	0,1799	0,2145	0,1225	0,1403	0,1078	0,08246
Sensor 7	0,1049	0,1168	0,4432	0,1398	0,1467	0,09239	0,09222	0,08815	0,07068
Sensor 8	0,09306	0,1035	0,1273	0,09444	0,08209	0,07374	0,08663	0,07364	0,06738
VDV (m/s <sup>-1.75</sup> )	Row 1	Row 2	Row 3	Row 4	Row 5	Row 6	Row 7	Row 8	Row 9
Sensor 1	0,0289	0,05444	0,05322	0,0294	0,0227	0,02999	0,0369	0,01507	0,003177
Sensor 2	0,07438	0,2066	0,2995	0,1159	0,06137	0,06564	0,08812	0,03721	0,005569
Sensor 3	0,09402	0,456	0,4532	0,1832	0,08661	0,06773	0,1141	0,06068	0,008316
Sensor 4	0,04304	0,2217	0,5256	0,1073	0,08491	0,06149	0,0936	0,0452	0,007215
Sensor 5	0,02321	0,03984	0,5188	0,06619	0,07462	0,05765	0,06811	0,03123	0,00569
Sensor 6	0,02146	0,03015	0,4324	0,05502	0,06488	0,03649	0,03585	0,02054	0,004994
Sensor 7	0,0159	0,02569	0,2513	0,03578	0,0355	0,01426	0,01496	0,01179	0,003768
Sensor 8	0,01019	0,01533	0,03746	0,01308	0,007929	0,0041	0,007847	0,005002	0,002774

Figure C.2: Acceleration values for 2F Multi Span v2 H

RMS (m/s <sup>2</sup> )	Row 1	Row 2	Row 3	Row 4	Row 5	Row 6	Row 7	Row 8	Row 9	Row 10	Row 11
Sensor 1	0,069169	0,07418	0,064369	0,035183	0,049017	0,042091	0,057328	0,037527	0,06854	0,071296	0,07251
Sensor 2	0,073404	0,085841	0,09997	0,090475	0,068816	0,059604	0,061449	0,059074	0,068995	0,06941	0,071179
Sensor 3	0,07744	0,081517	0,110603	0,106487	0,077029	0,067985	0,077605	0,062552	0,067334	0,070886	0,071501
Sensor 4	0,073904	0,090059	0,104387	0,101332	0,087119	0,086269	0,080076	0,070063	0,067792	0,069187	0,069893
Sensor 5	0,074758	0,083463	0,096756	0,095507	0,089629	0,090126	0,081449	0,069361	0,069565	0,069563	0,07113
Sensor 6	0,075497	0,079386	0,09279	0,0898	0,085788	0,087489	0,0806	0,073326	0,071331	0,061779	0,073048
Sensor 7	0,072975	0,071339	0,07423	0,074427	0,05597	0,069757	0,048268	0,070378	0,071925	0,072764	0,073636
Sensor 8	0,074016	0,068004	0,066066	0,05715	0,060039	0,061616	0,062262	0,063833	0,066003	0,071512	0,074862
PEAK (m/s <sup>2</sup> )	Row 1	Row 2	Row 3	Row 4	Row 5	Row 6	Row 7	Row 8	Row 9	Row 10	Row 11
Sensor 1	0,197	0,3166	0,3721	0,2898	0,2409	0,09934	0,1658	0,1424	0,1573	0,1771	0,1202
Sensor 2	0,379	0,6288	0,8213	0,7852	0,4521	0,408	0,5771	0,5247	0,3178	0,6066	0,1708
Sensor 3	0,5421	0,7775	1,046	0,9742	0,6006	0,6628	0,7972	0,7161	0,4059	0,688	0,213
Sensor 4	0,5093	0,7272	0,8724	0,739	0,6657	0,7624	0,8097	0,6658	0,3526	0,4945	0,2053
Sensor 5	0,3983	0,5592	0,635	0,6814	0,6973	0,7825	0,7081	0,5907	0,306	0,529	0,1841
Sensor 6	0,3213	0,5185	0,7412	0,7325	0,792	0,8599	0,6803	0,5059	0,2688	0,3123	0,1732
Sensor 7	0,2324	0,4373	0,5852	0,5487	0,4094	0,4555	0,4149	0,2954	0,2129	0,2221	0,1463
Sensor 8	0,1557	0,2846	0,3266	0,1976	0,1586	0,1628	0,1513	0,1688	0,1701	0,163	0,1225
VDV (m/s <sup>-1.75</sup> )	Row 1	Row 2	Row 3	Row 4	Row 5	Row 6	Row 7	Row 8	Row 9	Row 10	Row 11
Sensor 1	0,07708	0,1495	0,1973	0,1492	0,1164	0,04819	0,04948	0,05799	0,0531	0,05006	0,02609
Sensor 2	0,2161	0,467	0,6517	0,6025	0,3501	0,2337	0,2848	0,2449	0,1237	0,22	0,0487
Sensor 3	0,3112	0,6181	0,8366	0,7604	0,4717	0,3965	0,4443	0,3671	0,174	0,2723	0,06753
Sensor 4	0,2813	0,5394	0,692	0,6421	0,4746	0,4865	0,4878	0,3744	0,1765	0,2016	0,07044
Sensor 5	0,2185	0,4202	0,557	0,5583	0,5019	0,5132	0,4579	0,3521	0,1776	0,2233	0,06809
Sensor 6	0,1743	0,3444	0,5096	0,5271	0,4933	0,4821	0,3992	0,3086	0,1653	0,1208	0,0656
Sensor 7	0,1006	0,2148	0,3165	0,3086	0,2598	0,2533	0,2284	0,1815	0,115	0,07332	0,04582
Sensor 8	0,04763	0,1079	0,13747	0,07684	0,07177	0,07735	0,07643	0,08477	0,08045	0,04683	0,03163

Figure C.3: Acceleration values for 3F Multi Span H





**Norges miljø- og biovitenskapelige universitet**  
Noregs miljø- og biovitenskapelige universitet  
Norwegian University of Life Sciences

Postboks 5003  
NO-1432 Ås  
Norway